National Library of Canada
Bibliothèque nationale du Canada

Canadian Theses Service
Service des thèses canadiennes

Ottawa, Canada
K1A 0N4

NOTICE

The quality of this microform is heavily dependent upon the quality of the original thesis submitted for microfilming. Every effort has been made to ensure the highest quality of reproduction possible.

If pages are missing, contact the university which granted the degree.

Some pages may have indistinct print especially if the original pages were typed with a poor typewriter ribbon or if the university sent us an inferior photocopy.

Reproduction in full or in part of this microform is governed by the Canadian Copyright Act, R.S.C. 1970, c. C-30, and subsequent amendments.

AVIS

La qualité de cette microforme dépend grandement de la qualité de la thèse soumise au microfilmage. Nous avons tout fait pour assurer une qualité supérieure de reproduction.

S'il manque des pages, veuillez communiquer avec l'université qui a conféré le grade.

La qualité d'impression de certaines pages peut laisser à désirer, surtout si les pages originales ont été dactylographiées à l'aide d'un ruban usé ou si l'université nous a fait parvenir une photocopie de qualité inférieure.

La reproduction, même partielle, de cette microforme est soumise à la Loi canadienne sur le droit d'auteur, SRC 1970, c. C-30, et ses amendements subséquents.

NL-339 (r. 88/04) c

Canada

THE UNIVERSITY OF ALBERTA

THE SSIMT: A CMOS BASED MAGNETIC SENSOR

BY

TOM SMY

A THESIS
SUBMITTED TO THE FACULTY OF GRADUATE STUDIES AND
RESEARCH IN PARTIAL FULFILLMENT OF THE REQUIREMENTS FOR
THE DEGREE OF DOCTOR OF PHILOSOPHY

DEPARTMENT OF ELECTRICAL ENGINEERING

EDMONTON, ALBERTA
SPRING, 1990

National Library of Canada
Bibliothèque nationale du Canada

Canadian Theses Service
Service des thèses canadiennes

Ottawa, Canada
K1A 0N4

NOTICE

The quality of this microform is heavily dependent upon the quality of the original thesis submitted for microfilming. Every effort has been made to ensure the highest quality of reproduction possible.

If pages are missing, contact the university which granted the degree.

Some pages may have indistinct print especially if the original pages were typed with a poor typewriter ribbon or if the university sent us an inferior photocopy.

Reproduction in full or in part of this microform is governed by the Canadian Copyright Act, R.S.C. 1970, c. C-30, and subsequent amendments.

AVIS

La qualité de cette microforme dépend grandement de la qualité de la thèse soumise au microfilmage. Nous avons tout fait pour assurer une qualité supérieure de reproduction.

S'il manque des pages, veuillez communiquer avec l'université qui a conféré le grade.

La qualité d'impression de certaines pages peut laisser à désirer, surtout si les pages originales ont été dactylographiées à l'aide d'un ruban usé ou si l'université nous a fait parvenir une photocopie de qualité inférieure.

La reproduction, même partielle, de cette microforme est soumise à la Loi canadienne sur le droit d'auteur, SRC 1970, c. C-30, et ses amendements subséquents.

ISBN 0-315-60334-8

NL-339 (r. 88/04) c

Canada

THE UNIVERSITY OF ALBERTA

RELEASE FORM

NAME OF AUTHOR: TOM SMY

TITLE OF THESIS: THE SSIMT: A CMOS BASED MAGNETIC SENSOR

DEGREE: DOCTOR OF PHILOSOPHY

YEAR THIS DEGREE GRANTED: 1990

Permission is hereby granted the THE UNIVERSITY OF ALBERTA LIBRARY to reproduce single copies of this thesis and to lend or sell such copies for private, scholarly or scientific purposes only.

The author reserves other publication rights, and neither the thesis nor extensive extracts from it may be printed or otherwise reproduced without the author's written permission.

#2 8408 105st
Edmonton, Alberta
Canada

Date: October 31, 1989

THE UNIVERSITY OF ALBERTA

FACULTY OF GRADUATE STUDIES AND RESEARCH

The undersigned certify that they have read, and recommend to the Faculty of Graduate Studies and Research for acceptance, a thesis entitled *The SSIMT: A CMOS Based Magnetic Sensor,* submitted by Tom Smy, in partial fulfilment of the requirements for the degree of *Doctor of Philosophy.*

Supervisor

Date: October 31, 1989

Abstract

The experimental analysis and an analytical model of a novel microelectronic magnetic sensor are presented. Known as the Suppressed Sidewall Injection MagnetoTransistor (SSIMT) this device is manufactured in a standard CMOS technology and has produced the highest sensitivities reported for a linear magnetotransistor. The analytical model based, on the assumption of the dominance of carrier deflection as the operating mechanism, successfully predicts the bias dependance of the SSIMT and provides considerable insight into the physical cause of the very high measured sensitivities. Experimentally a large variety of devices are characterized and the SSIMT is operated under two different biasing conditions. The SSIMT is compared systematically to a simpler more traditional magnetotransistor in order to determine the effect of its unique structure, on the magnetic behavior of the collector currents. The structure of the SSIMT provides the opportunity of analyzing the relative roles, in the magnetic operation of the device, of simple current deflection and the modulation of the emitter injection by a Hall field in the base region. An experimental study of the two effects determines carrier deflection to the dominant mechanism of magnetic operation.

ACKNOWLEDGEMENTS

It is a pleasure to thank my supervisor, Dr. Lj. Ristic, who first introduced me to semiconductor devices. Without his constant help and encouragement this work would never have been completed. I would also like to thank Dr. Igor Filanovosky, whose careful reading of the text was of great assistance.

In addition, I would like to thank Ken Westra for keeping me sane and Graham McKinnon and Alan Mitchell for helpful discussions. I would also like to thank all the students and staff at AMC for putting up with my idiosyncrasies and making my stay a pleasure.

Finally, I wish to express my gratitude to AMC and NSERC for financial support.

Table of Contents

		page
1.0	Introduction	1
2.0	Microelectronic Magnetic Field Sensors	7
	2.1 Current flow in a semiconductor with an applied magnetic field	8
	2.2 Magnetic field sensors	8
	2.2.1 Hall plates	8
	2.2.2 MagFETs	13
	2.2.3 Magnetodiodes	14
	2.2.4 Magnetotransistors	15
	2.2.5 Carrier domain magnetic field sensors	18
3.0	Magnetotransistor Theory	25
	3.1 Carrier deflection	25
	3.1.1 Carrier deflection in a VMT	25
	3.1.2 Carrier deflection in an LMT	29
	3.2 The emitter modulation effect	33
	3.2.1 Hall voltage generation	34
	3.2.2 Collector current response	35
	3.3 Magnetoconcentration	36
	3.4 Numerical modeling of magnetotransistors	37
	3.5 Figures of merit	38
	3.5.1 Relative sensitivity	39
	3.5.2 Absolute sensitivity	41
	3.5.3 Signal to noise ratio	41

3.5.4 DC zero field offset 42

4.0 SSIMT Operation and device geometries 47

4.1 Basic SSIMT structure and operation 47

4.1.1 Biased stripes 48

4.1.2 Floating stripes 49

4.2 Device Models 51

4.2.1 LMT operation 51

4.2.2 SSIMT operation with stripes floating 55

4.2.3 SSIMT operation with stripes biased 58

4.2.3.1 Analytical model 61

4.2.3.2 Effect of Bias parameters on device sensitivity 65

4.2.3.2.1 Influence of V_r 66

4.2.3.2.2 Influence of V_S 69

4.2.3.2.3 Influence of I_B 71

5.0 Experimental results 80

5.1 Process and Geometrical variations 80

5.1.1 CMOS processes 80

5.1.2 Device geometries 81

5.1.2.1 Basic SSIMT structure 81

5.1.2.2 The LMT 81

5.1.2.3 Emitter geometries 81

5.1.2.4 Base width variation 81

5.2 LMT and SSIMT with stripes floating 83

5.2.1 Electrical Characteristics 84

	5.2.2 Magnetic Characteristics	84
	5.3 SSIMT with stripes biased	86
	5.3.1 Electrical Characteristics	88
	5.3.2 Magnetic Characteristics	89
	5.4 Device Geometry variations	91
	5.4.1 Emitter geometry variations	94
	5.5 DC zero field offset control	94
6.0	On the injection modulation effect	125
	6.1 The emitter modulation effect	126
	6.1.1 Hall voltage generation	126
	6.1.2 Collector current response	128
	6.2 Experimental Results	131
	6.2.1 Hall voltage generation	132
	6.2.2 Collector current response	133
7.0	Conclusion	137
References		140

List of Figures

Figure		page
Fig. 2-1	Ideal Hall plate.	20
Fig. 2-2	Hall plate in bipolar technology.	20
Fig. 2-3	Vertical Hall device.	21
Fig. 2-4	MOS Hall plate.	21
Fig. 2-5	Ideal Magnetodiode.	22
Fig. 2-6	CMOS based magnetodiode.	22
Fig. 2-7	VMT fabricated in a bipolar process.	23
Fig. 2-8	LMT fabricated in a CMOS process.	23
Fig. 2-9	LMT sensitive to a perpenicular magnetic field.	24
Fig. 3-1	Two collector npn VMT.	43
Fig. 3-2	Electron current flow in collector region of VMT.	43
Fig. 3-3	Electron current flow in base region of CMOS LMT.	44
Fig. 3-4	LMT a) top view b) crossection	45

Fig. 3-5	LMT analysed by Mitnikova et al.	46
Fig. 4-1	Basic SSIMT structure a) crossection b) planview.	73
Fig. 4-2	Circuit diagram for SSIMT with stripes biased.	74
Fig. 4-3	Circiut diagram for SSIMT with stripes floating.	74
Fig. 4-4	Electron flow for a) LMT b) SSIMT stripes floating c) SSIMT with stripes biased.	75
Fig. 4-5	a) Electron current flow in base region of the LMT. b) Electron current deflection due to an applied magnetic field B.	76
Fig. 4-6	Electron current flow in base region of the SSIMT with stripes floating	77
Fig. 4-7	a) Electron current flow in base region of SSIMT with stripes biased	77
Fig. 4-8	a) electron flow in base region responsible for collector current, b) magnetic response of this electron flow.	78
Fig. 4-9	a) L-shaped model of the flow of electrons responsible for the collector current, b)current deflection through	79

Hall angle of linear current flow.

Fig. 5-1 SSIMT emiter structure a) 30x100 μm b) 30x30 μm. 98

Fig. 5-2 SSIMT 50 μm base width. 99

Fig. 5-3 I_C as a function of I_B for the LMT with stripes floating V_C = 5 V. 1) V_S = 5 V. 2) V_S = 10 V. 3) V_S= 15 V. 100

Fig. 5-4 I_C as a function of I_B for the SSIMT with stripes floating V_C = 5 V. 1) V_S = 5 V. 2) V_S = 10 V. 3) V_S= 15 V. 100

Fig. 5-5 V_B as a function of I_B for both the LMT (dashed) and the SSIMT with stripes floating (solid) V_C = 5 V. 1) V_S = 5 V. 2) V_S = 10 V. 3) V_S= 15 V. 101

Fig. 5-6 I_S as a function of I_B for both the LMT (dashed) and the SSIMT with stripes floating (solid) V_C = 5 V. 1) V_S = 5 V. 2) V_S = 10 V. 3) V_S = 15 V. 101

Fig. 5-7 I_C as a function of V_S for both the LMT (dashed) and the SSIMT with stripes floating (solid) V_C = 5 V. 1) I_B = 1 mA. 2) I_B =2 mA. 3) I_B =3 mA. 102

Fig. 5-8	I_S as a function of V_S for both the LMT (dashed) and the SSIMT with stripes floating (solid) V_C = 5 V. 1) I_B = 1 mA. 2) I_B =2 mA. 3) I_B = 3 mA.	102
Fig 5-9	Current response, ΔI_C, as a function of B. a) LMT b) SSIMT with stripes floating: V_C = 5 V, I_B = 1 mA, V_S = 15 V.	103
Fig. 5-10	Absolute sensitivity versus I_B, V_C = 5 V a) LMT b) SSIMT. 1) V_S = 5 V, 2) V_S = 10 V, 3) V_S = 15 V.	104
Fig. 5-11	Relative sensitivity versus I_B, V_C = 5 V a) LMT V b) SSIMT. 1) V_S = 5 V, 2) V_S = 10 V, 3) V_S = 15 V. Relative sensitivity versus V_S, V_C = 5 c) LMT V d) SSIMT. Absolute sensitivity versus V_C, V_S = 10 e) LMT f) SSIMT. 1) I_B = 1 mA, 2) I_B = 2 mA 3) I_B = 3 mA.	105
Fig. 5-12	I_C as a function of V_C, V_S = 5 V, V_r = 0 V: 1) I_B =6 mA, 2) I_B = 8 mA, 2) I_B = 10 mA.	108
Fig. 5-13	I_C as a function of I_B, V_S = 5 V, V_C = 5 V: 1) V_r = 0.0 V, 2) V_r = -0.2 V, 2) V_r = -0.4 V.	108
Fig. 5-14	I_C as a function of V_r, V_S = 5 V, V_C = 5 V: 1) I_B =7 mA, 2) I_B = 8 mA, 2) I_B =9 mA.	109

Fig. 5-15 a) V_B as a function of I_B, b) I_S as a function of I_B, V_r = 0 V, V_C = 5 V: 1)V_S = 5 V, 2) V_S = 10 V, 3) V_S = 15 V. c) I_C as a function of V_S, V_r = 0 V, V_C = 5 V: 1) I_B =7 mA, 2) I_B = 8 mA, 2) I_B =9 mA. 109

Fig. 5-16 Collector current response as a function of the applied magnetic field. a) V_S = 5 V, V_r = -0.25 V, I_B = 8.5 mA, V_C = 5 V. b) V_S = 5 V, I_B = 7 mA, V_C = 5 V: 1) V_r = -198 mV, 2) V_r = -193 mV, 3) V_r = -150 mV. 111

Fig 5-17 Absolute sensitivity versus stripe potential, V_S = 5 V, I_B = 7 mA, V_C = 5 V, B = 30 mT. 112

Fig 5-18 Relative sensitivity versus stripe potential, V_S = 5 V, I_B = 7 mA, V_C = 5 V, B = 30 mT. Theory shown in solid. 112

Fig. 5-19 a) W_{eff} and $L_1 + L_2$ as a function of V_r. b) X_1 and X_2 as a function of V_r. Bias conditions as in Fig. 6-18. 113

Fig 5-20 Absolute sensitivity versus V_S , I_B = 7 mA, V_C = 5 V, B = 30 mT. 1) V_r = 0.0 mV, 2) V_r =-50 mV, 3) V_r =-100 mV. 114

Fig 5-21	Relative sensitivity versus V_S , I_B = 7 mA, V_C = 5 V, B = 30 mT. 1) V_r = 0.0 mV, 2) V_r =-50 mV, 3) V_r =-100 mV, 4) V_r = -180 mV. Theory shown in solid	114
Fig. 5-22	a) W_{eff} and $L_1 + L_2$ as a function of V_r. I_B = 7 mA, V_C = 5 V, V_r = -180 mV.	115
Fig 5-23	Absolute sensitivity versus I_B , V_S = 5 V, V_C = 5 V, B = 30 mT. 1) V_r = 0.0 mV, 2) V_r =-198 mV, 3) V_r =-460 mV	116
Fig 5-24	Relative sensitivity versus I_B , V_S = 5 V, V_C = 5 V, B = 30 mT. 1) V_r = 0.0 mV, 2) V_r =-198 mV, 3) V_r =-460 mV. Theory shown in solid.	116
Fig. 5-25	a) W_{eff} and $L_1 + L_2$ as a function of I_B. V_S = 5 V, V_C = 5 V, V_r = -198 mV.	117
Fig 5-26	a) Absolute sensitivity versus V_C . b) Relative sensitivity versus V_C. V_S = 5 V, V_r = 0 V, B = 30 mT, I_B = 8 mA.	118
Fig. 5-27	Electrical and magnetic characteristics of 5 μm SSIMT a) I_S versus I_B, b) V_B versus I_B, c) S_r versus I_B, d) S_a versus I_B, V_r = 0 V, V_C = 5 V,1) V_S = 5 V, 2) V_S = 10 V, 3) V_S = 15 V.	119

Fig. 5-28 I_{Bc} as a function of A_E V_S = 15 V, V_C = 5 V, I_B = 10 mA, V_r = 0.0 V 120

Fig. 5-29 S_a as a function of L_E, V_S = 15 V, V_C = 5 V, I_B = 10 mA, V_r = 0.0 V 1) square devices 2) devices for which W_E is a constant. 121

Fig. 5-30 ΔI_C as a function of B, V_S = 5, I_B = 1 mA, stripes floating, V_S = 5 V. L_E = 20, 40, 60, 80 and 100 μm. 122

Fig. 5-31 S_r as a function of A_E V_S = 15 V, V_C = 5 V, I_B = 10 mA, V_r = 0.0 V 123

Fig. 5-32 S_a as a function of A_E V_S = 15 V, V_C = 5 V, I_B = 10 mA, V_r = 0.0 V 123

Fig. 5-33 The offset as a function of V_r when both p^+ stripes are at the same potential. V_C = 5 V, V_S = 5 V. 124

Fig. 5-34 The potential difference as a function of V_r for offset elimination. V_C = 5 V, V_S = 5 V. 124

Fig. 6-1 R_H as a function of the injection level, a, b=3, $N_A = 10^{16}$ cm^{-3}, r = 1.2. 134

Fig. 6-2 Hall voltage distribution along emitter/base junction 134

Fig. 6-3 Hall voltage versus applied base current at a magnetic field of 500 mT, L_E = 100 μm, 1) substrate disconnected, 2) V_S = 5 V. 135

Fig. 6-4 Hall voltage versus magnetic field, I_B = 5 mA, L_E = 100 μm, 1) substrate disconnected, 2) V_S = 5 V. 135

Fig. 6-5 Hall voltage versus emitter length I_B = 5 mA, B = 500 mT, 1) substrate disconnected, 2) V_S = 5 V. 136

Fig. 6-6 ΔI_C as a function of B, I_B = 5 mA, L_E = 100 μm, 1) substrate disconnected, 2) V_S = 5 V. IM1 and IM2 correspond to equation 3.29 for conditions 1) and 2) respectivily 136

List of Symbols

Symbol	Name	Unit
$\vec{B}$	Magnetic induction vector	tesla
B_{off}	Effective zero field magnetic field offset	tesla
D_n	Electron diffusion coefficient	m^2/s
D_p	Hole diffusion coefficient	m^2/s
$\vec{E}$	Electric field vector	volts/meter
E_x	Electric field vector in x direction	volts/meter
E_y	Electric field vector in y direction	volts/meter
E_a	Accelerating electric field	volts/meter
E_L	Laterally accelerating electric field	volts/meter
G	Geometrical Hall factor	-
$\vec{H}$	Magnetic field vector	amp/meter
I_C	Collector current	amp
I_{C0}	Collector current at zero magnetic field	amp
ΔI_C	Collector current change due to a magnetic field	amp
I_S	Substrate current	amp
I_B	Base current	amp
I_E	Emitter current	amp
I_r	Current through p^+ stripes	amp
I_{Bc}	Critical base current	amp
$\vec{J}_n$	Electron current density vector	amp/m^2
J_{nx}	Electron current density in x direction	amp/m^2
J_{ny}	Electron current density in y direction	amp/m^2
J_{n0}	Electron current density at zero magnetic field	amp/m^2
J_s	Reverse biased junction saturation current	amp/m^2

k	Boltzmann constant	J/K
K_{MI}	Injection modulation coefficient	-
N_A	Acceptor doping concentration	m^{-3}
N_D	Donor doping concentration	m^{-3}
n	Electron carrier concentration	m^{-3}
p	Hole carrier concentration	m^{-3}
q	Elementary electronic charge	coulomb
r	Hall scattering Coefficient	-
R_H	Hall coefficient	$m^{-3}coulombs^{-1}$
S_r	Relative sensitivity	% / tesla
S_a	Absolute sensitivity	amp/tesla
S/N	Signal to noise ratio	-
V_H	Hall voltage	volts
V_C	Collector voltage	volts
V_E	Emitter voltage	volts
V_B	Base voltage	volts
V_r	p^+ stripe voltage	volts
V_S	Substrate voltage	volts
V_{rc}	Critical p^+ stripe voltage	volts
V_{Sc}	Critical substrate voltage	volts
V_t	Thermal voltage	volts
W_{eff}	Effective width of lateral electron flow	meter
Z	Emitter crowding parameter	-
α	Injection coefficient	-
$ß_v$	DC current gain of the vertical transistor	-
$ß_l$	DC current gain of the lateral transistor	-
μ_n	Electron drift mobility	$meter^2/volt\text{-}sec$

μ_p	Hole drift mobility	meter^2/volt-sec
μ_n^*	Electron Hall mobility	meter^2/volt-sec
μ_p^*	Hole drift mobility	meter^2/volt-sec
μ_0	Magnetic permeability of free space	amp/meter-tesla
μ_r	Relative magnetic permeability	-
σ_n	electrical conductivity in n region	$(\Omega - m)^{-1}$
σ_p	electrical conductivity in p region	$(\Omega - m)^{-1}$
$\emptyset_H$	Hall angle	radians
ρ	resistivity	volt-meter/amp

1.0 Introduction

The rapid decrease in feature size for digital microelectronics technologies has produced an astounding increase in the signal processing power available to the design engineer. In particular, real time signal processing and complex control applications are possible which could not have even been contemplated 10 years ago.

Generally, any real time electronic system consists of 3 distinct sections:

1) an input section consisting of an interface device, either, human interface devices (such as electronic keyboards) or, sensors providing a signal relating to a particular state of the environment of interest, examples of this are magnetic field sensors and electro-mechanical devices such as position sensors;

2) A signal processing stage often consisting of an analog to digital stage to convert incoming data, a central digital processor and a digital to analog stage to allow for an output interface;

3) An output stage consisting of either information output devices (typically a cathode ray tube or equivalent), or actuators such as stepper motors.

The application of modern VLSI technologies to the fabrication of the processing section of an electronic system has produced a substantial drop in the cost of this stage. Therefore, the cost of an electronic system is often dominated by the cost of the input and output stages. A typical control system will consist of a

number of large expensive sensors providing information to an inexpensive mass produced signal processing unit.

This discrepancy in relative costs has provided the impetus for research into the use of microelectronic fabrication techniques in the production of a variety of sensors. Micromachining techniques are being used to produce mechanical sensors and a variety of chemical sensors have been produced. Microelectronic temperature and optical sensors are well developed. An obvious area of interest and application is microelectronic magnetic sensors and it is with a particular type of magnetic sensor that this thesis will deal.

A large variety of magnetic field sensors (MFS) have been fabricated using microelectronic technologies (see [1,2] and ref. therein). These vary widely both in operation and in fabrication. Basically, all standard integrated circuit fabrication technologies have been exploited from standard complementary metal oxide silicon (CMOS) processes to a variety of bipolar technologies. Devices have also been fabricated in a number of unusual materials such as InSb.

All microelectronic magnetic sensors have as their fundamental operating principle the action of the Lorentz force on the carriers flowing in the device [1,2]. The Lorentz force is given by,

$$\vec{F} = q\vec{v} \times \vec{B} \qquad (1.1)$$

where q is the charge on a carrier flowing through a region of the device, $\vec{v}$ is the velocity of the carrier and $\vec{B}$ the magnetic induction present in the region. The magnetic induction, $\vec{B}$, is related to the applied magnetic field, $\vec{H}$, by the relation

$\vec{B} = \mu_r \mu_0 \vec{H}$, where μ_r is the relative permeability of the device region and μ_o the permeability of free space. The Lorentz force manifests itself in a variety of effects in semiconductor devices. These include carrier deflection, Hall field generation, injection modulation effects and magnetoconcentration [1,2]. These effects are present to a greater or lesser degree in a particular device determined by the device structure and biasing configuration. A number of these effects are a function of the mobility of the carriers in certain regions of the device. This has promoted the use of materials such as InSb and GaAs. Of interest is the relationship between $\vec{B}$ and $\vec{H}$. It can be seen from equation (1.1) and this relationship that a sensor fabricated out of a material with a large μ_r would have a large sensitivity. Unfortunately, all semiconductors have relative permeability of approximately 1 and metals, that do have a large μ_r, are unsuitable for magnetic sensor use, due to their high conductivities.

The use of an established semiconductor technology to fabricate an MFS does, however, have other advantages despite the small μ_r. An extremely wide variety of devices, varying from simple Hall plates to complex active devices such as magnetotransistors can be fabricated by the use of regions doped with acceptor and donor atoms to form n and p doped areas.

Particular interest has been focussed on the fabrication of MFS using standard semiconductor technologies such as CMOS. This interest is due to a number of reasons. A standard process has the advantage of being a known technology with well understood device characteristics. In addition the process is presumably reliable, and predictable, facilitating sensor development. Finally, the

sensor, its bias electronics and any signal processing can be integrated on the same chip allowing for inexpensive batch fabrication of the final product [3].

A number of devices have been fabricated using standard processes. These include field effect transistors (MagFET), bipolar transistors and Hall plates in MOS technologies and Hall plates and bipolar devices in bipolar technologies. Perhaps the most promising of all the devices fabricated in standard technologies is the magnetotransistor (MT), a bipolar transistor optimized for magnetic operation [1,2].

This work will deal with the characterization, modelling and optimization of a magnetotransistor fabricated in CMOS technology. Known as the Suppressed Sidewall Injection MagnetoTransistor (SSIMT) this device has displayed extremely high sensitivities [4,5]. In addition, to the characterization of the device, the device will be used to provide a means of analyzing the relative roles of the responsible mechanisms of operation [6]. Due to the geometric and operational complexity numerical simulation of device operation is unpractical. Therefore, in order to allow for an understanding of the SSIMT a simple analytical model of the device will be presented and compared to experiment [4]. The purpose of this model will be to promote an intuitive understanding of the device operation in order to allow for an intelligent development of the device.

The contents of the following sections of the work will now be described. The second chapter will be a basic revision, of first, the fundamental effects present in a semiconductor with an applied magnetic field and, secondly, of the various devices produced to respond to this effect. Typical devices such as Hall plates [7,8], Magnetodiodes [9], MagFETs [10,11] and Magnetotransistors

[12,13] will be described. Simple explanations of their operation will be provided and an indication of their range of sensitivity given.

Chapter 3.0 will present a description of the previous research on magnetotransistors. The chapter will deal first with the analytical work presented in the literature. This section will be broken up into parts dealing with each proposed mechanism of operation for the magnetotransistor. The three principles dealt with are carrier deflection, the emitter modulation effect and magnetoconcentration. An overview of the current state of numerical modelling of microelectronic MFS will also be given. Finally, in this chapter, a discussion of the figures of merit used to characterize microelectronic magnetotransistors will be presented. This discussion will deal with both relative and absolute sensitivities and other concerns such as zero field offset.

The basic SSIMT structure and operation will be presented in chapter 4.0. The method of fabrication of the device will be outlined. A qualitative description of the both the electrical and magnetic operation of the device will be presented. The various biasing options of the device will be discussed. In the second section of this chapter a quantitative model of the SSIMT will be presented. The device's operation will be analyzed under two fundamentally different biasing arrangements and compared to the operation of a simpler more basic magnetotransistor structure.

The experimental characterization of the device is presented in chapter 5.0. First the electrical and magnetic behavior of the basic SSIMT and a simple lateral magnetotransistor is given. Experimental confirmation of the theory developed in chapter 4.0 is then presented. A large variety of devices differing in geometry, and

process technology, were fabricated and experimental results from a number of different devices will be presented to elucidate the SSIMT operation.

In chapter 6.0 a theoretical and experimental study of the role of carrier deflection and emitter injection modulation in the SSIMT will be presented. The unique SSIMT geometry presents the opportunity of measuring the Hall field produced in the base region of the device and then determining the role of this field in SSIMT operation.

Chapter 7.0 is the conclusion of the work and will deal with the implications of both the theoretical model and the experimental results. Results from an application of the SSIMT will be outlined. Lastly, a proposal for further work will be given.

2.0 Microelectronic Magnetic Field Sensors

2.1 Current flow in a semiconductor with an applied magnetic field.

The action of the Lorentz force on the current flow within a semiconductor device can best be illuminated by the simple case of a homogeneous, isotopic sample of a n-doped material with no temperature variation [1]. Incorporation of the Lorentz force expression into the zero field diffusion approximation of the Boltzmann transport equation

$$\vec{J}_n(0) = \sigma_n \vec{E} + qD_n \nabla n \qquad (2.1)$$

leads to the general expression for electron flow in the presence of a magnetic field

$$\vec{J}_n(\vec{B}) = \vec{J}_n(0) - \mu_n^*(\vec{J}_n(\vec{B}) \times \vec{B}) \qquad (2.2)$$

where $J_n(0)$ is the zero field current flow, μ_n^* the Hall mobility of electrons, σ_n the zero field electrical conductivity, q the fundamental electric charge and D_n the electron diffusion coefficient. This expression is difficult to manipulate due to the cross product on the right hand side. However, a weak field approximation of $J_n(B)$ can be obtained for $(\mu_n^*|\vec{B}|)^2 << 1$

$$\vec{J}_n(\vec{B}) = \frac{[\vec{J}_n(0)+\mu_n^*(\vec{B} \times \vec{J}_n(0))+(\mu_n^*)^2(\vec{B}\cdot\vec{J}_n(0))\vec{B}]}{1 + (\mu_n^*|\vec{B}|)^2} \qquad (2.3)$$

This equation, along with the corresponding equation for hole current density, describes the isothermal current dependance on the magnetic field. It only considers first order temperature effects taking into account the temperature

variation of carrier concentrations and the diffusion and conductivity coefficients. Second order effects are neglected. To solve for the current flow within a semiconductor device it is needed to solve equation (2.3) and its complementary equation for holes, with the pertinent continuity equations and Poisson equation.

In order to obtain a physical feel for the effect of a magnetic field on current flow, in a semiconductor, equation (2.3) can be further simplified. If current flow due to diffusion is neglected, true for a simple Hall plate with ohmic contacts, and if we also assume that $\vec{B}$ is perpendicular to the applied electric field then equation (2.3) becomes

$$J_n(B) = \sigma_{nB} [\vec{E} + \mu_n^* (\vec{B} \times \vec{E})] \qquad (2.4)$$

where $\sigma_{nB} = \sigma_n [1 + (\mu_n^* \vec{B})^2]^{-1}$. Defining $B = B_z$ and $\vec{E} = E_x i + E_y j$ we obtain for the individual current components:

$$J_{nx} = \sigma_{nB} (E_x - \mu_n^* B_z E_y) \qquad (2.5)$$

$$J_{ny} = \sigma_{nB} (E_y - \mu_n^* B_z E_x) \qquad (2.6)$$

At this point it is needed to assign a particular geometry for the semiconductor sample in question. Two extreme geometries are enlightening. For the case of a long thin Hall plate ($l >> w$) with a current passing through the length of the sample it can be assumed that the current flow across the width of the sample is small, ie $J_{ny} \approx 0$ .We can now solve equations (2.5) and (2.6). Obtaining the Hall field E_y

$$E_y = -\mu_n^* B_z E_x \qquad (2.7)$$

$$= -\frac{\mu_n^*}{\sigma_n} J_{nx} B_z$$

Defining the Hall coefficient as $R_H = -\mu_n^* / \sigma_n$ equation (2.7) becomes,

$$E_y = - R_H J_{nx} B_z \qquad (2.8)$$

The net result of the applied magnetic field is the rotation of the equipotential lines across the width of the Hall plate by the tangent of the Hall angle

$$\tan \varnothing_H = E_y / E_x = \sigma_n R_H B_z \qquad (2.9)$$

The second easily solvable geometry is a short thick slab where w>>l in this case we can assume there is no confinement of the carrier flow and therefore no generation of a Hall field ($E_y = 0$). Equations (2.6) and (2.7) can now be solved and we obtain the result that the current flow in the sample is deflected by the tangent of the Hall angle

$$\tan \varnothing_H = -J_{ny} / J_{nx} = - \mu_n^* B_z \qquad (2.10)$$

As the electrons flow from x=0 to x=l in the sample they travel a greater distance due to their deflection by the magnetic field. This results in a larger effective resistance of the semiconductor plate and a lower effective conductivity σ_{nB}

$$\sigma_{nB} = \frac{\sigma_n}{1 + (\mu_n^* B_z)^2} \qquad (2.11)$$

This effect is known as the geometric magnetoresistance effect [1].

2.2 Microelectronic Magnetic Field Sensors

A large variety of microelectronic magnetic field sensors have been proposed, varying widely in operation and geometry. In this section we shall review a number of typical sensors manufactured using microelectronic processes.

2.2.1 Hall Plates

The Hall plate is the simplest of all the proposed microelectronic magnetic sensors. Easily implemented by integrated circuit technologies, the Hall plate consists of a slab of semiconductor of length l width w and thickness t. A current I is passed along the length of the slab and the sensor is oriented such that the magnetic signal to be measured is perpendicular to the slab. One voltage contact is placed on each side of the slab. Ideally these contacts would be negligibly small, however, due to technological reasons this is not the case and they are of a finite width s (see Fig. 2-1).

As current can not pass across the sides of the plate and the slab is of a finite width the application of a magnetic field perpendicular to the plate produces a rotation of the equipotential lines within the plate by the tangent of the Hall angle. This rotation gives rise to a potential difference V_H between the two voltage

contacts. For the ideal plate described in the previous section (l>>w) this voltage can be determined from equations (2.8), (2.9) and (2.10),

$$V_H = \frac{R_H I B}{t} \tag{2.12}$$

where I is the current passed through the plate.

In the previous section the plate was considered n-type, the minority hole current flow was ignored and R_H was determined to be $-\mu_n/\sigma_n$. If both the carrier types, minority and majority, need to be taken into consideration the situation is more complicated and the Hall coefficient becomes [14]

$$R_H = \frac{-[r(\frac{\mu_n}{\mu_p})^2 n - r_p p]}{q[(\frac{\mu_n}{\mu_p}) + p]^2} \tag{2.13}$$

With $r_n = \mu_n^*/\mu_n$ and $r_p = \mu_p^*/\mu_p$. As can be seen R_H shows a strong dependance on the relative levels of the carrier concentration n and p. In fact, if $p = r_n/r_p(\mu_n/\mu_p)^2 n$ then $R_H = 0$

In a real Hall plate the presence of current and sensor contacts cause a degradation of the Hall voltage predicted by the expression calculated for the ideal Hall plate [15]. This effect is usually taken into account by the incorporation of a geometrical factor G and we obtain for the Hall voltage

$$V_H = \frac{R_H I B}{t} G(l/w, s/w, y/l, \emptyset_H) \qquad (2.14)$$

where $G \equiv V_H / V_\infty$ and V_∞ is the Hall voltage obtained as $w/l \Rightarrow 0$.

Both bipolar and CMOS technologies have been used to fabricate Hall plate sensors [7,16]. Fig. 2-2 shows a simple implementation in bipolar technology [13]. The plate is formed using the n-epilayer, current and voltage contacts being implemented using n^+ and p^+ diffusions respectively.

Two quite different implementations are fabricated in MOS technologies. One, known as the vertical Hall device (VHD), is unusual, both with regards to its geometry and its sensitivity to the B field parallel to the chip surface [8,17]. Shown in Fig. 2-3, a central current contact is formed using a n^+ source/drain diffusion in the n-substrate. Current flows from this central contact through the substrate to two n^+ outside contacts. Between each outside current contact and the central contact is placed an n^+ voltage contact. This device, despite its unusual geometry, functions as a simple Hall plate, however, with somewhat difficulty to quantify geometric factors such as l, w and t.

A device proposed by Takamiya et al [20] incorporates a transistor amplifier directly into the Hall plate structure. Manufactured in bipolar technology a Hall plate is formed out of a n-epilayer, as with the previous example, and a current is passed through the device by the use of two base contacts. However, instead of using two n^+ diffusions as voltage contacts, two emitters are formed using p^+ diffusions. Two collectors are then fabricated using p^+ diffusions at the edge of the base region. The electrical operation of this device is quite straight

forward. The current passed from one base contact to the other results in the two emitter junctions being forward biased. Holes are injected into the base region by each emitter and then collected by the nearest collector. In the presence of a magnetic field the electron current, the flow of majority carriers, produce a Hall voltage in the base region. A potential difference is present between the two base regions in the vicinity of each emitter. This results in one emitter being more forward biased then the other and there is a resulting asymmetrical injection of holes into the base region. This asymmetrical injection causes a current difference, $I_{C2} - I_{C1}$.

2.2.2 MagFETs

A more conventional use of the CMOS technology, than the fabrication of the VHD, is the MagFET [10,18,19]. In this device a Hall plate is formed by applying a voltage to the gate region between a source and a drain. An inversion layer forms at the silicon surface under the gate, effectively producing a very thin conductive plate between the source and the drain (see Fig. 2-4). The source and the drain are used as current contacts and small n^+ diffusions are placed at the edges of the gate region to act as voltage contacts. These contacts are then used to measure the Hall field produced by a magnetic field perpendicular to the chip surface.

A variation on this device, also known as a MagFET, is the split or triple drain MagFET. This device is nearly identical to the Hall plate MagFET described above, however, the voltage contacts are removed and the drain is split into two or three portions. Under zero field conditions the device is symmetrical and the drain currents are balanced. In the presence of a magnetic field, however, the symmetry

of the current flow is disturbed and a current difference can be measured between the relevant drain currents.

2.2.3 Magnetodiodes

It was shown by Suhl et al [21] that for large applied magnetic fields the conductivity of a bar of semiconductor is a stronger function of the magnetic field then could be explained by magnetoresistance. This strong dependance in conductivity was attributed to local variation of the carrier concentrations within the semiconductor sample. With an appropriate choice of magnetic field the electron and hole distributions within the semiconductor will be concentrated along the surface of the sample. This will result in an increase of the carrier recombination due to surface effects and therefore a reduction in the average conductivity of the bar as a whole.

This "magnetoconcentration" effect has been exploited in a device known as the magnetodiode. The basic magnetodiode structure is shown in Fig. 2-5. It consists of a small p^+ region used as an anode and a larger n^- region as a cathode [1]. The diode is operated under forward bias and a current is passed from the cathode to the anode across the p^+/n junction. The unique feature of the diode is that it has two different recombination rates on the top and bottom surfaces of the n^- region (in early devices this was done by grinding one surface and polishing the other [22]). Under the presence of a magnetic field both the holes and the electrons will be concentrated against either the top or bottom surface of the diode. The different recombination rates of the two surfaces will result in the V-I curve of the diode being a function of the applied magnetic field.

The first magnetodiode manufactured in an IC technology was proposed by Lutes et al [23]. This device was manufactured in a Silicon on Sapphire technology and used a Si/SiO_2 interface as the top recombination surface and Si/Sapphire surface as the bottom. A magnetodiode compatible with a CMOS process was investigated by Popovic et al [24]. This device was conceived slightly differently. The basic structure (shown in Fig. 2-6) consists of a bipolar transistor formed using a p-well as the base region, the substrate as a collector, an n^+ diffusion as an emitter and a p^+ diffusion as base contact. In the operation of the device a current was passed through the p-well from the base contact to the emitter which was grounded. The substrate/p-well junction was reverse biased and acts effectively as a high recombination surface for the minority carriers in the base, the SiO_2/p-well surface at the top of the device acts as a low recombination surface. In this device the sensitivity of the V_B - I_B curve to the magnetic field was determined.

2.2.4 Magnetotransistors

A number of devices known as magnetotransistors have been fabricated [1,2]. The magnetotransistor is a bipolar transistor, either npn or pnp, optimized so that its response to a magnetic field is maximized. The operation and geometries of magnetotransistors differ greatly. Traditionally, magnetotransistors have been categorized by the direction of the flow of current responsible for the magnetic operation of the device. If the flow of the magnetically dependant current is lateral, parallel to the chip surface, the device is known as a lateral magnetotransistor (LMT). Conversely, if the dominant current flow is vertical, perpendicular to the chip surface, the device is called a vertical magnetotransistor (VMT).

The magnetic operation of both VMTs and LMTs is complicated and three basic principles have been proposed [1,2]:

1) carrier deflection - the deflection of either minority or majority carriers through the Hall angle within a region of the device;

2) emitter modulation - the presence of a Hall voltage, in the base region of the device, causes an asymmetrical injection of minority carriers into the base of the device;

3) magnetoconcentration - the concentration of carriers within a particular region of the device causes a local modulation of the conductivity in this region.

A more detailed description of each of these effects will be given in the following chapter.

A typical VMT is shown in Fig. 2-7. The device was fabricated in a bipolar technology and consists of a central emitter, a thin base region with two base contacts and a single collector region with two contacts [12]. The operation of the device is dominated by carrier deflection and is as follows. Electrons are injected from the emitter into the base across the forward biased emitter junction. These electrons are then collected at the base/collector junction immediately below the emitter. The electrons then flow away from the chip surface down towards the two n^+ buried layers. These buried layers provide a low resistance path for the electrons to flow to the two contacts C_1 and C_2. In the absence of a magnetic field I_{C2} will equal I_{C1}. However, if a B field is applied parallel to the chip surface, the

electrons flowing through the collector region between the emitter and buried layers are deflected. This deflection results in a difference between I_{C1} and I_{C2}, ΔI_C, that is proportional to the magnetic field.

An example of a simple LMT in which the carrier deflection of the minority carriers in the base is the dominant mechanism is shown in Fig. 2-8 [25]. The device was fabricated in a standard CMOS process. A p-well was used to form the base region of the device, p^+ diffusions are used as base contacts and n^+ source/drain diffusions formed the emitter and collector. An ohmic substrate connection is provided by the use of n^+ diffusion.

The electrical operation of this device can conceptually be broken up into two bipolar transistors. A vertical npn transistor formed from the emitter, base and substrate, and a lateral npn transistor consisting of the emitter, base and collector. In the operation of the device both the collector/base junction and the substrate/base junction are reverse biased. The emitter/base junction is forward biased and electrons are injected across this junction into the base. These electrons then flow either to the collector, and form the collector current, or to the substrate where they form the substrate current. In order to improve the ratio of the substrate current to the collector current a second base contact (B^-) is placed to the left of the emitter, this contact is grounded and the flow of holes from the base contact B^+ to the contact B^- establishes an accelerating electric field which sweeps the injected electrons towards the collector. If a magnetic field is applied parallel to the chip surface a deflection of these electrons will occur as they flow towards the collector. For a magnetic field as shown in Fig. 2-8 this will result in the electrons being deflected away from the chip surface and towards the

substrate. A resulting decrease in I_C and increase in I_S will be apparent and this change in current will be a linear function of the magnetic field.

A similar LMT [26], but sensitive to a magnetic field perpendicular to the chip surface, is shown in Fig. 2-9. The electrical operation is very similar to the device in Fig. 2-8. However, two collectors are fabricated, instead of one. Once again electrons are injected from the emitter and swept towards the collectors by an accelerating electric field. In the absence of a magnetic field $I_{C1} = I_{C2}$ because of the device's symmetry. If a B field is applied perpendicular to the chip surface, a change in the current $\Delta I_C = I_{C2} - I_{C1}$ will be realized due to the deflection of electrons towards one collector and away from the other.

2.2.5 Carrier domain microelectronic magnetic sensors

The device shown in Fig. 2.7 can be operated in such a way as to produce a carrier domain within the device [27]. A carrier domain is a region in which the majority and minority carriers are not in equilibrium and $n \approx p$ due to the charge neutrality equation. In order to achieve this condition the p^- substrate is forward biased with respect to the n^- collector region, while in the previous case this junction is reverse biased. The result of this is to inject holes into the n^- region between the n^+ buried layers. The interaction of this flow of holes with the electrons being collected at the p/n^- junction results in a potential distribution in the n^- region which will produce a current filament (formed from both holes and electrons) flowing between the p^- substrate and the p base region. The position of this filament is affected by the presence of a magnetic field parallel to the chip surface. Any displacement of the carrier domain results in a measurable change in

the bias currents of the device. A number of carrier domain devices have been built (see [1] and ref. therein).

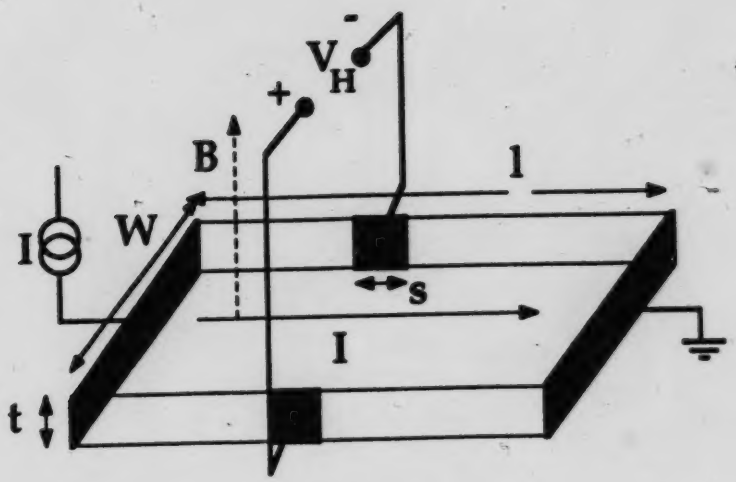

Fig. 2-1 Ideal Hall plate

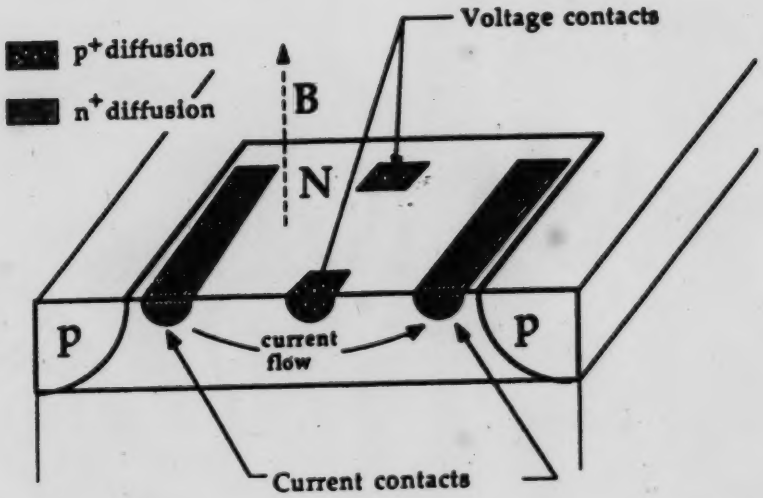

Fig. 2-2 Hall plate in bipolar technology

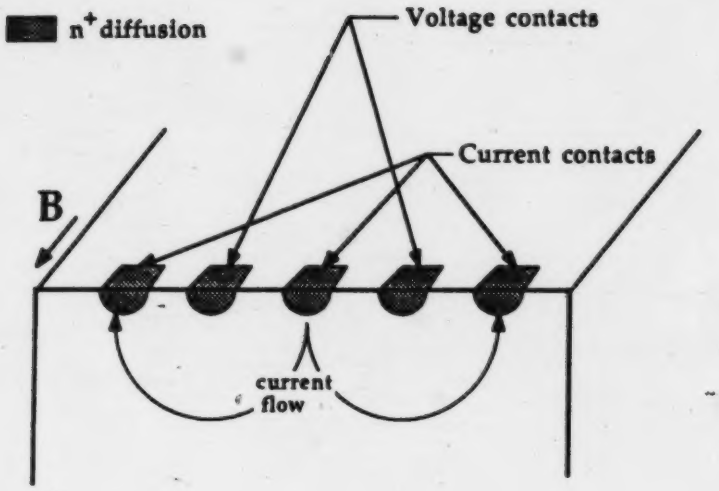

Fig. 2-3 Vertical Hall device

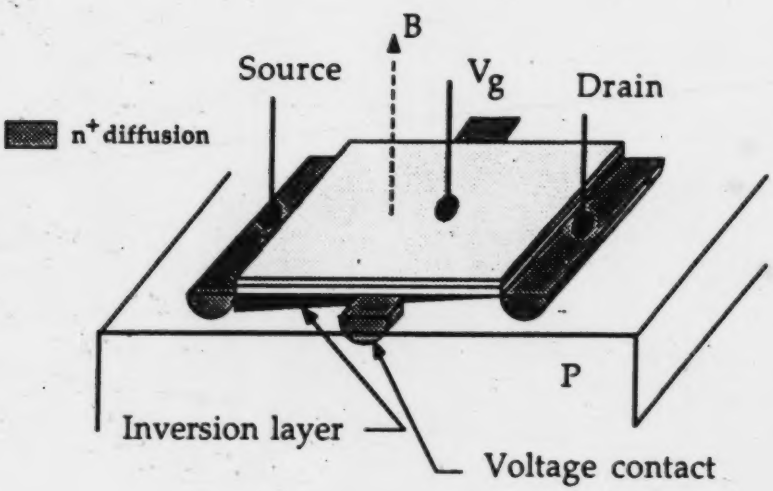

Fig. 2-4 MOS Hall plate

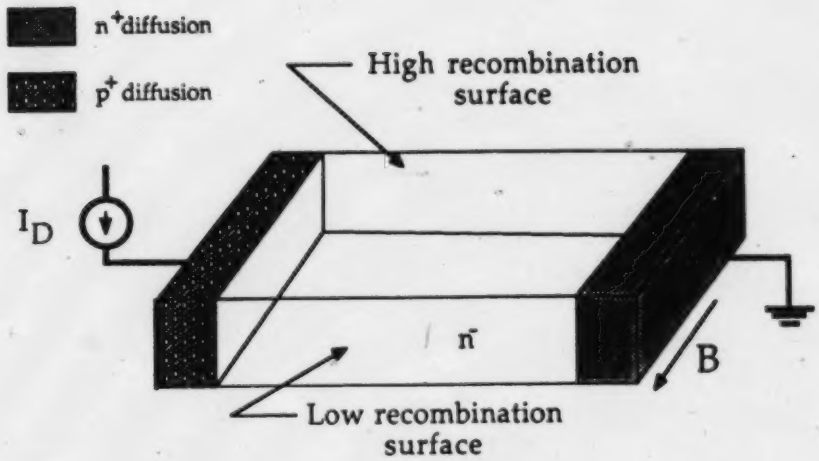

Fig. 2-5 Ideal Magnetodiode

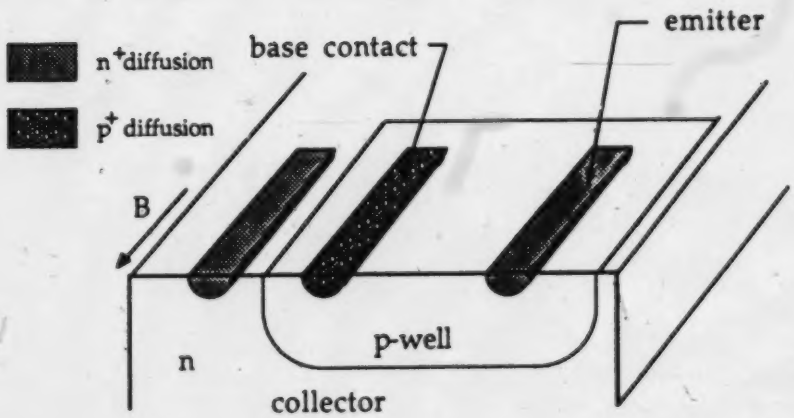

Fig. 2-6 CMOS based magnetodiode

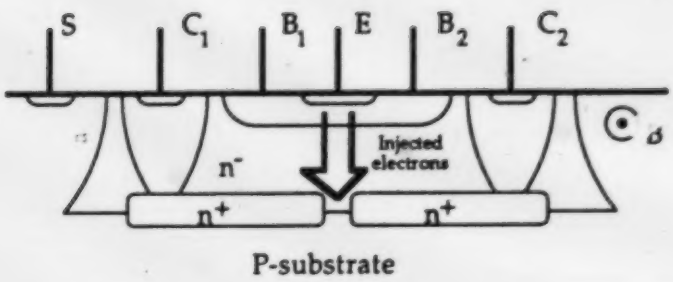

Fig. 2-7 VMT fabricated in a bipolar process [12]

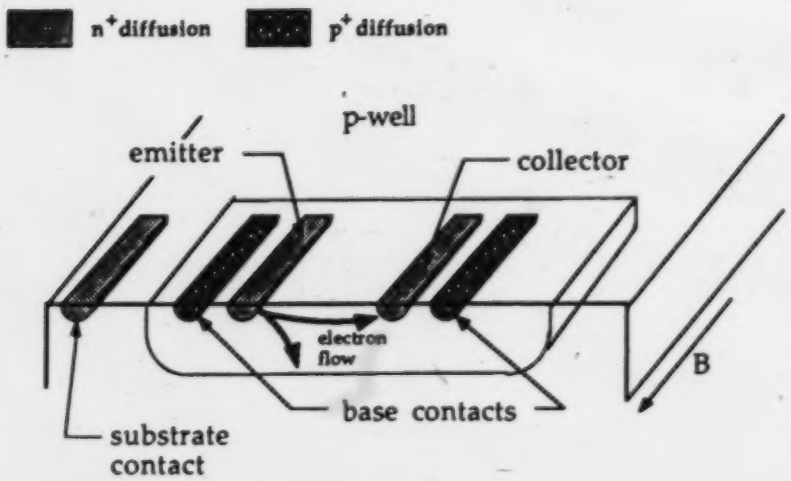

Fig. 2-8 LMT fabricated in a CMOS process [25]

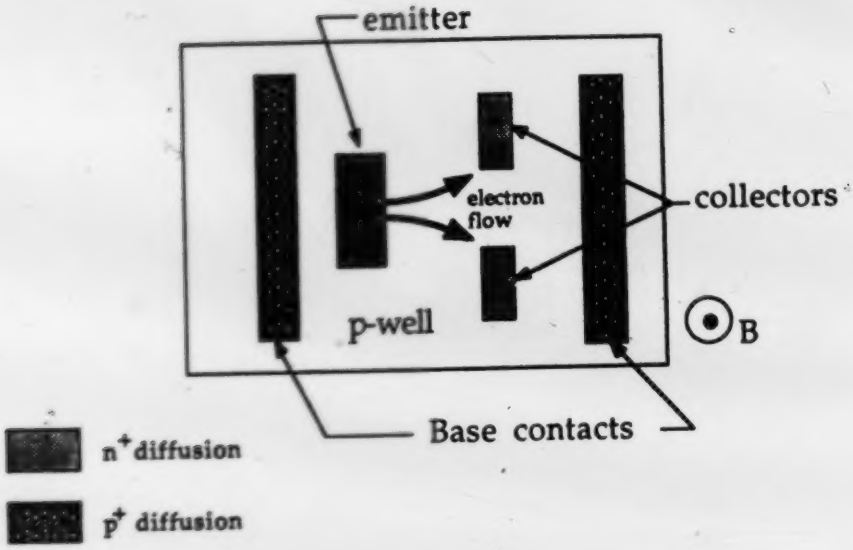

Fig. 2-9 LMT sensitive to a perpendicular magnetic field

3.0 Magnetotransistor Theory

As mentioned previously, the fundamental effect on which all magnetic field sensors are based is the Lorentz force. The operation of the Lorentz force in a magnetotransistor (MT) manifests itself in three basic forms, current deflection, emitter modulation and magnetoconcentration. Current deflection is the deflection of carriers in the neutral base or collector region of the device [12]. The emitter modulation model proposes that a Hall voltage is produced along the emitter/base junction, which in turn causes an asymmetric injection of minority carriers [13]. Magnetoconcentration is the asymmetrical concentration of carriers within the device, causing a local modulation of the conductivity [28]. Of these three effects the last two involve a non-linear magnetic response. Previously reported MTs that display a linear response to the magnetic field have had relative sensitivities (change in collector current / change in magnetic field normalized by the total collector current) varying from 1 %/T to 150 %/T [25]. An MT displaying non-linear behavior has been reported with a sensitivity of 400 %/T [29]. However, this sensitivity was reported for large fields of 1 Tesla and very small collector currents of 20 nA.

3.1 Carrier Deflection

3.1.1 Carrier Deflection in a VMT

A theoretical analysis based on carrier deflection of the device shown in Fig. 3-1 was proposed by Zieren and Duyndam in 1982 [12]. The basic operation of the device, as described in the previous section, is that electrons are injected from the emitter across the forward biased emitter/base junction. They flow down

through the base to the base/collector junction where they are collected. From this junction they flow through the collector region down away from the chip surface to the buried layers below. The n^+ buried layers then provide a high conductivity region for the electrons to flow to the collector contacts C_1 and C_2. In the absence of a magnetic field I_{C1} will equal I_{C2} due to symmetry. However, a magnetic field applied in the z direction will result in a deflection of the electron flow in the collector region through the Hall angle, causing a reduction in one collector current and corresponding increase in the other.

The theoretical analysis of this structure by Zieren et al [12] assumed that this current deflection was the dominant magnetic effect. In addition, to this assumption, the authors made the following four simplifications:

1) There is a hypothetical dividing line centered between the two n^+ buried layers, to the right of this line electrons are assumed to flow into the n^+ buried layer on the right and will form the collector current I_{C2}, conversely any electrons to the left of this line will form I_{C1}.

2) The electrons collected at the base/collector junction flow directly down along the center line towards the buried layers with no current spreading. The authors therefore treat the electron flow in the collector region of the device as a current beam.

3) The emitter current density distribution can be described in the presence of current crowding effects by the parameter Z, where Z is defined by

$$Z \tan Z = \frac{I_E(1-\alpha)}{8 V_t} \frac{\rho_B}{W_B} \frac{W_E}{L_E} \qquad (3.1)$$

and $V_t = kT/q$, ρ_B is the average base resistivity, W_B the base width, W_E the emitter width, L_E the emitter length, α the common base current gain, and I_E the DC emitter current. The current density along the emitter junction J_{Ex} can then be described in terms of Z.

4) Magnetothermal effects are ignored.

A depiction of the assumed electron flow in the collector region, based on these assumptions, is shown Fig. 3-2. The electron flow is assumed to be a "beam" of current of width W_E and length L. The current density of the beam is J_{Ex}. The relative change in the collector currents due to an applied magnetic field can be shown to be

$$\frac{\Delta I_C}{I_C} = \frac{I_{C2} - I_{C1}}{I_{C1} + I_{C2}} = \frac{\tan(kZ)}{\tan(Z)} \qquad (3.2)$$

with

$$k = \frac{2 L \mu_n^* B}{W_E} \qquad (3.3)$$

where B is the magnitude of the applied magnetic field

If we assume the simple case of a uniform current density (Z = 0) we obtain for the collector current response

$$\Delta I_C = k B I_C \qquad (3.4)$$

We can see from equation (3.4) that the change in current is linear with respect to the magnetic field if there is no current crowding due to a potential drop along the emitter junction.

We can define a relative sensitivity for the device of

$$S_r = \frac{\Delta I_C}{I_C}\frac{1}{B} \qquad (3.5)$$

and we obtain (for the simple case of uniform current)

$$S_r = \frac{2 L \mu_n^*}{W_E} \qquad (3.6)$$

Experimental results obtained from this device were presented in [12]. Sensitivities were approximately 2.5 times smaller then the calculated values. This discrepancy was attributed to the spreading of the current "beam" due to the physical separation of the buried layers in real devices. Sensitivities of 3 %/T were measured.

3.1.2 Carrier deflection in an LMT

Carrier deflection was proposed by Popovic and Widmar as an explanation for the operation of a single collector npn lateral MT fabricated in standard CMOS. The device shown in Fig. 3-3 consists of an n^+ emitter and collector placed in a p-well base region separated by a length L. A p^+ base contact is placed at either end of the p-well. The emitter and base contact adjacent to it are grounded and the other base contact is biased with a constant current source. This current forward biases the emitter/base junction and produces a laterally accelerating field E_a in the base region between the emitter and collector. This electric field is due to the flow of holes from the base contact B^+ to the grounded base contact B^-.

In order to determine the magnetic sensitivity of the device Popovic and Widmar analyzed the flow of minority carriers in the base region of the device. Electrons are injected into the base from the emitter. A portion of these electrons, injected from the right sidewall of the emitter and the section of the bottom of the emitter adjacent to this sidewall, is swept towards the collector by the lateral electric field, E_a. However, the remaining portion of the injected electrons is collected by the reverse biased p-well/n-substrate junction.

To simplify the analysis the following model of the electron flow in the base was used. A plane y = -Y is assumed to divide the base region between the emitter and the collector, such that all minority current density lines reaching the plane x = L above this plane contribute to the collector current and all beneath it the substrate current (see Fig. 3-3). It was assumed that the hole current in the base region between the collector is due only to the accelerating field. We can then calculate the hole current densities in this region

$$J_{pox} = q\mu_p p E_s \tag{3.7a}$$

$$J_{py} = 0 \tag{3.7b}$$

These conditions will produce a Hall field due to the flow of holes

$$E_{py}^{H} = \mu_p^* B_z E_s \tag{3.8}$$

where μ_p^* is the Hall mobility of the holes in the base and B_z the applied magnetic field. The authors neglected the Hall field produced by the flow of electrons, as n << p for the base region of the device, and assume the effect of the magnetic field on the diffusion component of the minority current flow is small.

Simple expressions for the electron current flow in the base are obtained by the assumption that the electron current flow, with an applied field, can be obtained by a simple rotation of the zero field current flow through the Hall angle with an additional electric field component due to the Hall field generated by the flow of holes through the base. We can then derive

$$J_{nx} = J_{nox} + \mu_n^* B_z J_{noy} \tag{3.9a}$$

$$J_{ny} = J_{noy} - \mu_n^* B_z J_{nox} \tag{3.9b}$$

with

$$J_{nox} = \mu_n q n E_a + q D_n \frac{\partial n}{\partial x} \tag{3.10a}$$

$$J_{noy} = \mu_n q n (E_b + E_{py}^H) + q D_n \frac{\partial n}{\partial y} \qquad (3.10b)$$

where E_b is the built in electric field due to the nonuniform doping of the p-well base region.

The substrate current I_S can be expressed in terms of the y component of the electron current density

$$I_S = \left[\int_0^L \int_0^z J_{ny} dx \right]_{y=-Y} \qquad (3.11)$$

where the integral is taken over the plane y = -Y which divides the base region. A change in this current due to a small magnetic field can be expressed as

$$\partial I_S = \left[\int_0^L \int_0^z \partial J_{ny} dx \right]_{y=-Y} \qquad (3.12)$$

As it was assumed that an applied magnetic field will produce a redistribution of the electron current, such that electrons once flowing to the collector will now flow to the substrate, and we have

$$\partial I_S = -\partial I_C = -\left[\int_0^L \int_0^z \partial J_{ny} dx \right]_{y=-Y} \qquad (3.13)$$

The authors made the assumption that the magnetic field has no effect on the electron diffusion current and using equations (3.8) and (3.9) we obtain for ∂J_{ny}

$$\partial J_{ny} = \left(\frac{J_{nox}}{B_z} - \mu_n^* J_{nox}\right) \partial B_z \qquad (3.14a)$$

or

$$\partial J_{ny} = \mu_p^* q \mu_n n E_a - \mu_n^* \left(q \mu_n n E_a + q D_n \frac{\partial n}{\partial x}\right) \qquad (3.14b)$$

In order to obtain the relative sensitivity of the device it is needed to to obtain an expression for the collector current at zero magnetic field. It can be expressed as

$$I_C^{(0)} = \left[\int_{-Y}^{0}\int_{0}^{z} J_{ny}\, dy\, dz\right]_{x=L} \qquad (3.16)$$

To obtain tractable expressions the authors assumed that J_{nox} is a constant over the region of integration in equations (3.13) and (3.16). We then obtain for the relative sensitivity

$$S_r = \frac{L}{Y} \frac{\mu_p^* q \mu_n n E_a - \mu_n^* \left(q \mu_n n E_a + q D_n \frac{\partial n}{\partial x}\right)}{\mu_n q n E_a + q D_n \frac{\partial n}{\partial x}} \qquad (3.17)$$

Two obvious simple cases of this expression are apparent. One if the drift component of J_{nox} is dominant, ie $\mu_n n E_a >> D_n \partial n/\partial x$, in which case Sr becomes

$$S_r = \frac{-\mu_n^* L}{Y} \qquad (3.18)$$

Conversely if diffusion is dominant ($D_n \partial n/\partial x << \mu_n n E_a$) we have

$$S_r = (\mu_p^* - \mu_n^*) \frac{L}{Y} \qquad (3.19)$$

It remains in both these equations to calculate the parameter Y. This parameter was fitted to experimental results to be 6 μm, a reasonable value given a p-well depth of 15 μm. The sensitivity is obviously a direct linear function of the length L and this was confirmed by experiment with a typical sensitivity of 100 %/T for L = 50 μm.

3.2 Emitter modulation effect

In 1982 Vinal and Masnari proposed the modulation of the emitter injection of minority carriers as the dominant mechanism of operation for two LMTs [13,30,31]. The mechanism immediately became the center of some controversy as to its relative role in the operation of MTs [32,33], with other researchers suggesting carrier deflection and magnetoconcentration as more important effects.

A typical LMT structure is shown in Fig. 3-4. An analysis of the device presuming emitter injection as the dominant mechanism of operation is presented in the following section. The first section deals first with the Hall voltage

generated in the base region beneath the emitter and the second with the magnetic response of the collector current due to this Hall field.

3.2.1 Hall voltage generation

Following the approach used by Vinal and Masnari in [30] the collector current variation due to the magnetic field can be determined. The generation of a Hall voltage in the base region along the emitter is assumed to be similar to that produced in a Hall plate (the Hall voltage in the n^+ emitter region is assumed negligible due to the high electron concentration in this region). This Hall voltage will cause an asymmetrical biasing of the emitter base junction, with one side of the junction being more forward biased then the other. This will in turn cause a higher level of injection of carriers on the more forward biased side, with the result of the collector current being increased.

The basic equation for the Hall voltage produced by current flow through a semiconductor Hall plate is [15]

$$V_H = K R_H I B \tag{3.20}$$

where K is a geometric constant, R_H is the Hall coefficient, I the current through the device and B the magnetic induction perpendicular to the Hall plate. This equation can be adapted to the base region of the LMT near the emitter [34]. Under these conditions the current I is replaced then by the emitter current I_E and B by B_x

$$V_H = K R_H I_E B_x \tag{3.21}$$

The actual Hall voltage produce in the base region is a function of both the geometry and operating conditions of the device. The variation with geometry is contained in the constant K. For the case of the LMT in Fig. 3-4 it is difficult to evaluate K due to the complicated geometry of the base region of the device. It is obvious that V_H will vary directly with changes in the emitter current of the device, but it was also noted by Popovic and Baltes [34] that R_H is also highly dependant on the injection level at which the device is operating. The Hall coefficient is defined as [14, 35]

$$R_H = \frac{r}{q}\left(\frac{p - nb^2}{(p + nb)^2}\right) \tag{3.22}$$

where r is the Hall scattering coefficient, q the fundamental electron charge, and n and p are the electron and hole carrier concentrations respectively, and b the ratio of the electron mobility to the hole mobility in the base.

3.2.2 Collector current response

In order, to calculate the collector current change due to an applied magnetic field, the authors assume that the presence of the Hall field V_H will cause an additional biasing of the base/emitter junction by V_H. If the zero field collector current is represented in the form

$$I_C(0) = I_S e^{\left(\frac{qV_{BE}}{nkT}\right)} \tag{3.23}$$

then the collector current with a magnetic field present is given the assumptions above [34]

$$I_C(0) = I_S e^{\left(\frac{q(V_{BE}+V_H)}{nkT}\right)} \qquad (3.24)$$

Defining the sensitivity of the device as the ratio of these two currents we find that the sensitivity is

$$S_r = e^{\left(\frac{qV_H}{nkT}\right)} \qquad (3.25)$$

Both of these expressions indicate a nonlinear dependence on the magnetic field.

3.3 The magnetoconcentration effect

In 1978 Mitnikova et al. [22] proposed a combination of carrier deflection and magnetoconcentration effect as the basic principles responsible for the magnetic operation of a lateral transistor (shown in Fig. 3-5). This MT displayed a markedly nonlinear response to the magnetic field when operated under high injection conditions. The collector current could be expressed in the form [22]

$$\Delta I_C = K_{CD} B + f(B) \qquad (3.26)$$

where the term $K_{CD} B$ takes into account the change in the collector current due to carrier deflection. The second term f(B) was determined to be a nonlinear even function of B, the magnetic field. This term can not be explained by emitter modulation as it would produce a collector current response that is a symmetrical

and odd function of the magnetic field. The local concentration of carriers in the base region of the device does, however, explain the nonlinearity.

As holes flow from the emitter to the collector through the base region (and likewise electrons from the base contact to the emitter) the presence of positive B field will deflect both carriers to the chip surface between the emitter and collector. Under condition of high injection and large magnetic fields, there will be a concentration of carriers in this region causing a decrease of the resistivity of the base region between the emitter and the collector. This resistance change will provide a low resistance path for holes flowing from the emitter to the collector and in conjunction with the carrier deflection effect will increase the change in the collector current. Conversely, if B is negative the carriers will be concentrated in a region deep with in the base region well away from the chip surface. This would have the tendency to widen the flow of electrons from the emitter to the collector and degrade the effectiveness of the carrier deflection effect.

3.4 Numerical modeling of magnetotransistors

The mechanisms of operation described in the previous sections of this chapter were simple intuitive models of the device behavior, based on an understanding of how the fundamental electromagnetic equations manifest themselves in the current flow and carrier distributions within a device. However, due to the complex interaction of galvanomagnetic effects and bipolar action a simple model might be misleading.

Ideally, a full understanding and an exact prediction of device behavior could be obtained by the solution of the carrier continuity equations and the Poisson equation. Due to the inherent complexity of the carrier transport in a semiconductor

and the geometric complexity of microelectronic devices an analytical approach to the solution of these equations is unsuitable. However, a numerical solution of the relevant equations has been done [38-41].

An investigation of the carrier transport and potential distribution in a variety of MTs is presented in ref. [40,41]. The basic approach of the model was the use of a finite element technique to solve the steady-state galvanomagnetic equations. Nathan et al used a combination of numerical techniques and experimental results to analyze the operating mechanisms of a LMT with two collector contacts (similar in design to the device in Fig. 3-1). The basic conclusion of this paper was that the Hall field produced along the emitter/base junction was too small to generate a significant amount of asymmetrical emitter injection [40]. The authors conclude that carrier deflection is the dominant mechanism of operation of similar MTs with any nonlinearities being due to magneto-concentration.

Due to the large size and high current densities present in the devices dealt with in this thesis a numerical solution of their operation seems at this present time infeasible. Because of this simple analytical or empirical models of device operation, confirmed by experimental results, are the only tool the researcher has at his disposal in the intelligent development of such devices.

3.5 Figures of Merit

In the previous sections of this chapter the concept of sensitivity has arisen. It is useful when developing a sensor to have a number of measurable parameters that can be used to compare different devices. Magnetotransistors have traditionally been characterized with respect to relative sensitivity, absolute

sensitivity, signal to noise ratio and zero field offset [1,2]. Due to the complexity of MT operation a large number of differing definitions for both types of sensitivity have been used.

3.5.1 Relative sensitivity

The relative sensitivity of a magnetic sensor is usually defined as the derivative of the signal with respect to the magnetic field normalized by the magnitude of the signal

$$S_r = \frac{\partial X}{\partial B}\frac{1}{X_0} \tag{3.27}$$

where X is the magnetically sensitive signal and X_0 the zero field value of this quantity. For microelectronic magnetic sensors X is usually a current.

For the case of a simple two collector MT the relative sensitivity is often approximated by the expression

$$S_r = \frac{I_{C2}(B) - I_{C1}(B)}{I_{C1}(0) + I_{C1}(0)}\frac{1}{B} \tag{3.28}$$

where $I_{C1,2}(0)$ are the zero field collector currents and $I_{C1,2}(B)$ the collector currents with an applied magnetic field B present. This equation is sufficient if B is small and the collector currents a linear function of B. However, the usefulness of this equation becomes suspect if this is not the case.

Nonlinear MTs present difficulties with respect to the use of equation (3.28). If I_C is a nonlinear function of B then the expression for S_r will also be nonlinear, and S_r must be defined at a particular field in order to allow for comparison. Most sensitivities have been reported for a B field of 1 Tesla, this field is however very large [28,34]. Using an equation similar to (3.28), but for single collector devices, nonlinear LMTs have been presented as having very high sensitivities, however, all of these devices had very small collector currents (order of 1 μA) and the sensitivity was given for B = 1 T. If a more appropriate approximation of (3.27) is used

$$S_r = \frac{I_C(B) - I_C(0)}{I_C(B)} \frac{1}{B} \qquad (3.29)$$

then the measured sensitivity drops by several orders of magnitude, due to $I_c(B)$ being much larger than $I_c(0)$.

For the more complex LMTs there may be considerable current flow through the device in addition to the the collector current [5,25]. This is due the action of parasitic transistors and the low current gain of the LMT. Under these condition the use of the $I_C(0)$ in equation (3.27) as the normalizing factor can be misleading and the equation can instead be normalized with respect to the emitter current [5].

3.5.2 Absolute sensitivity

The absolute sensitivity of a device is defined as simply the ratio of the change in signal to the change in magnetic field [1,2]. For the case of collector current variation in an MT we have

$$S_a = \frac{\partial V_C}{\partial B} \tag{3.29}$$

where V_c is linearly related to the collector current through the collector load resistor.

For a nonlinear device S_a must, like S_r, be defined at a particular field. The only basic variation in the definition of S_a for MTs is the choice of a collector current as the measured quantity and the substitution of I_C for V_C in equation (3.29). If possible the use of I_C is preferred as it avoids the ambiguity of the choice of the value of the load resistor. In this thesis the absolute sensitivity is defined in terms of the collector current directly and is

$$S_a = \frac{\partial I_C}{\partial B} \tag{3.30}$$

3.5.3 Signal to noise ratio

The minimum resolvable magnitude of an AC magnetic field is determined by the signal to noise ratio of the device and is defined as

$$S/N = \frac{S_a}{\langle N \rangle} \qquad (3.31)$$

where <N> is the noise voltage or noise current as determined by the units of the absolute sensitivity.

At low frequency the dominant noise mechanism is 1/f noise and at high frequency shot noise and thermal noise dominate [42-44].

5.3.4 DC zero field offset

The minimum detectable DC magnetic field is determined by either, the zero field offset of the sensor, or if this quantity can be nulled the drift of this offset. Given a two collector MT the signal $\Delta I_{C0} = I_{C2}(0) - I_{C1}(0)$ is indistinguishable from an applied magnetic field of the magnitude $B_{off} = \Delta I_{C0} / S_a$. This B_{off} is therefore an indication of the DC resolution of the magnetic sensor.

The main causes of offset in microelectronic devices are imperfections in the process technology including mask misalignment [45], and strain introduced by packaging and aging [46]. Thus, one of the approaches for offset reduction is based on the improvement of process technology, but because of technological limitations it is not possible to eliminate offset completely. Other offset-reduction methods are calibration [47], which demands the presence of a known value of the measurand, compensation [48], which demands the use of two sensors where one of them is used as a reference, and the sensitivity variation offset reduction method [49,50], where the difference between the response of the sensitivity and the offset signal to a sinusoidal excitation is used to reduce the offset.

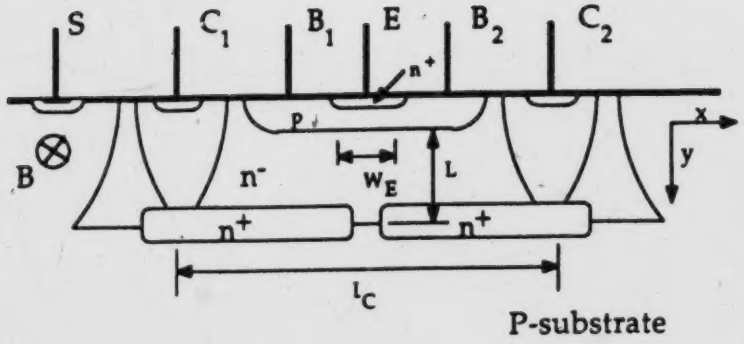

Fig. 3-1 Two collector npn VMT [12]

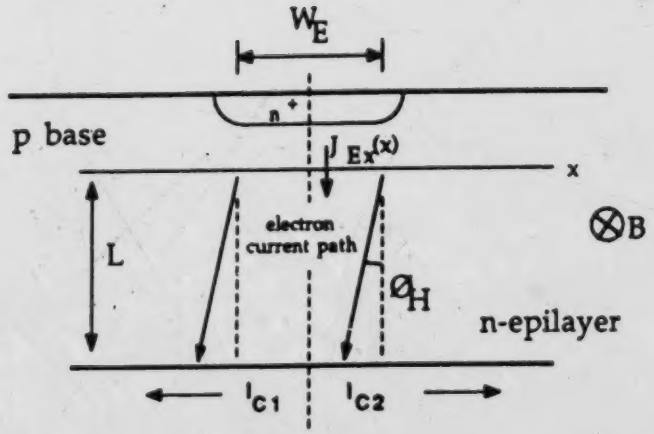

Fig. 3-2 Electron current flow in collector region of VMT [12]

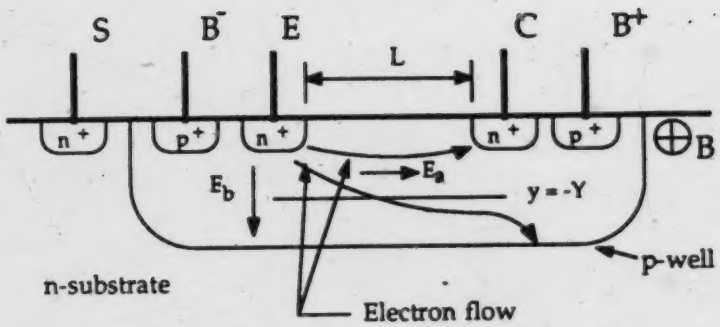

Fig. 3-3 Electron current flow in base region of CMOS LMT [25]

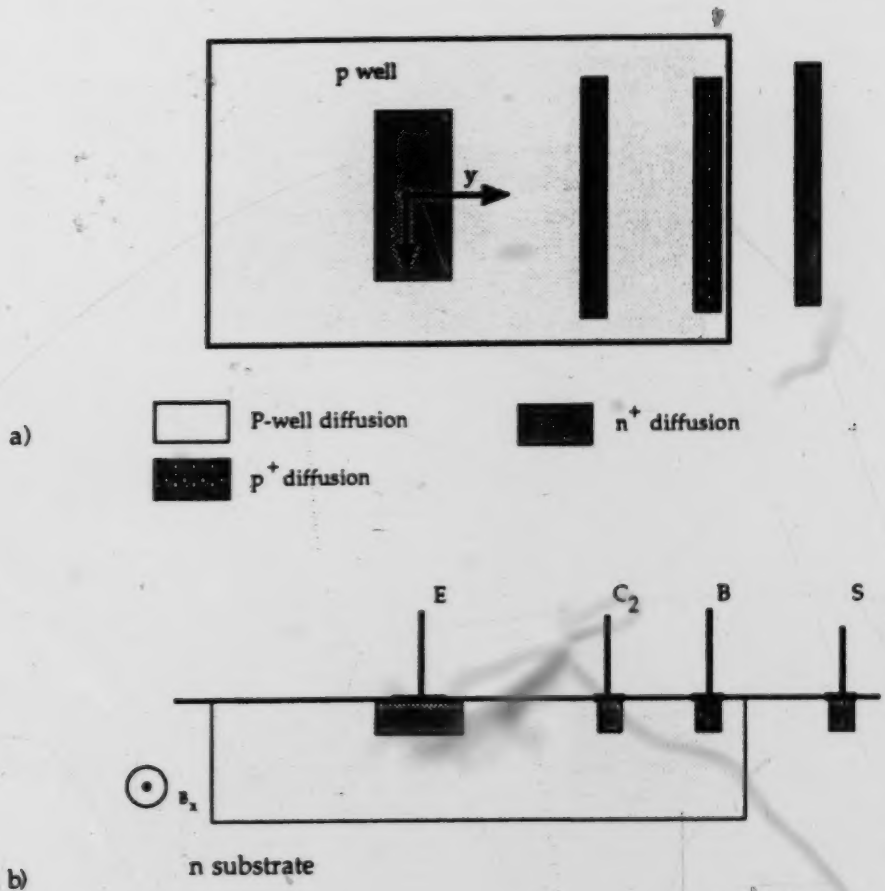

Fig. 3-4 LMT a) top view b) crossection

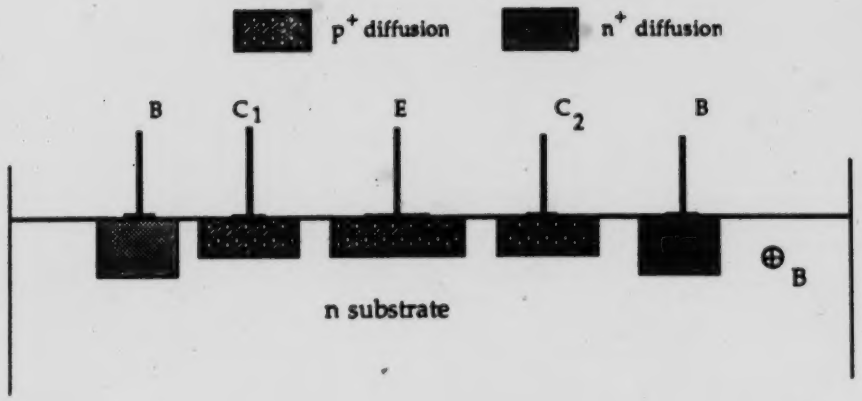

Fig. 3-5 LMT analysed by Mitnikova et al [22].

4.0 SSIMT Operation

4.1 Basic SSIMT structure

The basic SSIMT (suppressed sidewall injection magnetotransistor) is shown in Fig. 4-1 The novel feature of the device is the two p^+ stripes placed along the edges of the emitter, parallel to the collectors. All of the SSIMT variants were fabricated using a standard CMOS process.

The initial device structure was fabricated in a standard 4 μm CMOS process. The base region was formed by a p-well. The emitter and both collectors were realized using the standard doping procedure for the source and drain of a n-channel MOS transistor. The p^+ stripes at the side of the emitter and the base contacts B_1 were formed using the standard doping procedure for a p-channel MOS Transistor. The p-well diffusion depth is 10 μm, collector and emitter diffusion depths are 1.5 μm. The p-well doping is 10^{16} cm^{-3}.

The biasing circuit of the SSIMT is shown in Fig. 4-2. The values of I_b, V_S, V_C, V_{r1} and V_{r2} determine the operating point of the device. In the operation of the device two distinct bias configurations are used, one with the stripes biased to a voltage V_r and the other when the stripes are unbiased. We refer to these two bias configurations as "stripes biased" and "stripes floating". In normal operation slightly different values for V_{r1} and V_{r2} are used for offset elimination, and we define, $V_r = (V_{r1} + V_{r2}) / 2$, for convenience.

4.1.1 Biased stripes

The basic electrical operation of the device with biased stripes (stripe grounded or biased slightly negative with respect to the emitter) is as follows. The emitter base junction is forward biased by the applied base current and electrons are injected into the neutral base region. This injected current is then collected by either the two collectors or the substrate, which is in effect a third collector. Therefore the device can be thought of as a two npn transistors, a vertical one formed by the emitter, base and substrate and a differential lateral transistor formed by the emitter, base and collectors.

The p^+ stripes play a twofold role. First, they suppress carrier injection from the emitter in the lateral direction towards the collectors. If the p^+ stripes are biased with a voltage V_r and V_r is less then or equal to the potential of the emitter V_E this effect is obvious. The suppression of laterally flowing electrons is a consequence of the reverse biasing of the junction between the p^+ stripe and the emitter, in fact a small portion of the bottom of the emitter next to each stripe will also be reverse biased. The width of this reverse biased portion will increase with increasing negative V_r. At the same time carrier injection from the emitter is confined to the vertical direction, due to the formation of a potential hill (for electrons) around the p^+ stripes. The second effect of biasing the p^+ stripes is the creation of a lateral electric field, E_l, in the neutral base region. This field is due to the difference in potential between the base contacts B_1 and B_2. When the device is operated normally with $V_r < V_E < V_{B1}$, this field will be orientated in such a way as to sweep the injected electrons laterally towards the collectors, (Fig. 4-1a). The application of a larger negative potential to the stripes amplifies the effect of the p^+ stripes pushing the minority current further into the device and then

establishing a lateral flow of current out to the collectors. In the absence of a magnetic field, the collector currents I_{C10} and I_{C20} are equal because of the devices symmetry, and the device is balanced.

For the SSIMT it can be expected due to the long emitter that only a small portion of the emitter is responsible for the injected electrons which comprise the collector currents. This portion consists of two small segments of the emitter adjacent to the p^+ stripes. The remaining portion of the emitter bottom injects electrons that are collected by the substrate and form the substrate current.

The application of a magnetic field, $B = B_z$, parallel to both the chip surface and the collectors, will produce an imbalance in the two collector currents I_{C1} and I_{C2} due to the following "double-deflection" effect. The Lorentz force acts on all three current components I_S, I_{C1}, and I_{C2}. The I_S component is deflected in the y direction, increasing I_{C2} and decreasing I_{C1}. Moreover, the current components I_{C1} and I_{C2} are deflected in the "+ x" and "- x" directions respectively, causing a further increase of I_{C2} and a decrease of I_{C1}. These two deflections will combine to cause one collector current to increase at the expense of the substrate current and the other to decrease with a corresponding gain in the substrate current. The net effect on the substrate current should be zero.

4.1.2 Floating stripes

In the discussion above the p^+ stripes placed at the edges of the emitter were biased either to ground or to a small negative voltage, in order to suppress the injection of electrons out of the emitter sidewalls. A second biasing arrangement is possible in which the p^+ stripes are left unbiased and float at a voltage determined by the potential distribution inside the base region of the

device. This arrangement still provides suppression of the laterally injected electrons, due to the larger built in voltage across the n^+/p^+ junction relative to the n^+/p-well junction. This bias arrangement is shown in Fig. 4-3. The electrical operation of the device will be very similar to the operation of the device with the stripes biased. However, there will be no current flow through the p^+ stripes and no potential hill in the base region around the p^+ stripes. This will produce a less effective shaping of the electron flow in the base to the collectors, resulting in a reduced sensitivity.

The operation of the device in this manner has one major advantage. As a magnetic sensor it's use and implementation will be simpler due to the need for two less voltage sources. In order to achieve this simplicity we will sacrifice sensitivity.

The role of the p^+ stripes is crucial in the determination of the sensitivity of the SSIMT and this sensitivity is in turn determined by the flow of the minority current in the base region. In Fig. 4-4 the electron flow within base regions of a simple LMT (an SSIMT with out stripes) and the SSIMT for both stripes floating and biased is shown. This clearly shows the effect of the stripes. For the LMT the electron flow from the emitter to the collector is a wide diffuse flow and primarily composed of the electrons injected from the sidewall of the emitter. In Fig 4-4b the effect of the stripes when unbiased can be seen and the injection from the sidewall is suppressed, resulting in a more focussed flow of current. The biasing of the stripes slightly negative (Fig. 4-4c) produces a potential hill for electrons on the stripe and the injected electrons are forced deeper into the device with a resulting narrower and more concentrated electron flow to the collectors.

4.2 Device Models

The section 4.1 outlined qualitatively the basic operation of the SSIMT under a number of different biasing configurations. In the section 4.2 quantitative models of the device operation will be developed. These models will presume the dominance of carrier deflection as the mechanism of magnetic operation. Models will be developed for the following three cases. First a simple model of the LMT will be presented. Secondly a model of the operation of the SSIMT with stripes floating will be presented and finally a full and detailed description of the operation of the SSIMT with biased stripes will be given.

4.2.1 LMT operation

An obviously interesting variation in the SSIMT geometry was that of a simple LMT (an SSIMT without the p^+ stripes) of exactly identical dimensions. This device would allow, by a simple comparison of sensitivities and electrical characteristics, for the determination of the role of the p^+ stripes in the operation of the SSIMT.

The electrical operation of the LMT is identical with that of the SSIMT with the exception that electrons are injected from the sidewall of the emitter. The LMT can be thought of as two npn transistors, a vertical one formed by the emitter-base-substrate and a lateral one formed by the emitter base collectors. An analysis of an LMT structure was done in [25]. Using a similar approach we can derive an analytical model of the collector current flow within the base region.

As with the SSIMT only a small portion of the emitter of the LMT is responsible for the injected electrons which comprises the collector currents. This portion consists of the vertical edges of the emitter parallel to the collectors and a small segment of the bottom of the emitter adjacent to these edges. The remaining portion of the emitter bottom injects the electrons that produce the substrate current.

In order to analyze the flow of electrons in the device it is needed to define the plane X'. This plane, shown in Fig 4-5, divides the base region of the device into two regions, above this plane injected electrons are collected by the collector and beneath it by the substrate We can now calculate the total collector current by integrating the electron current density in the y direction over the region defined by plane X', the chip surface and the emitter width W_E

$$I_{C2} = \int_{-\frac{W_E}{2}}^{\frac{W_E}{2}} \int_0^{X'} J_{ny}(y = W_B, x, z)\, dx\, dz \qquad (4.1)$$

where J_{ny} is the electron current density in the y direction and W_B is the base width. If we now assume that J_{ny} is a constant in the area of integration we obtain for the collector current

$$I_{C2} \simeq J_{yn0} X' W_E \qquad (4.2)$$

where J_{ny0} is the average collector current density.

The effect of a magnetic field on the operation of the LMT is to alter the current flow described above. The flow of electrons in the base region undergo a deflection as they drift from the emitter to the collector. The current flowing towards C_1 is deflected down towards the substrate and the electron current flowing towards C_2 is deflected up towards the chip surface. Due to these deflections I_{C1} is reduced by ΔI_C as electrons are pushed down past the plane X' and I_{C2} is increased by ΔI_C as electrons are deflected up over the plane X'. A signal, $2\Delta I_C$, proportional to the magnetic field can then be measured. The net result on the substrate current should be zero as the increase in current from I_{C1} is offset by the loss to I_{C2}.

To calculate this current change we note that the electron current near the plane X' is the current responsible for the magnetic response of the device. Assuming constant current density in the region near X', the amount of deflected current is equal to, the current density of the electrons at the plane X' moving in the y direction multiplied by the area of the region defined by the Hall angle, the distance between the emitter and the collector W_B and the emitter width W_B (see Fig. 4-5b).

The change in current of I_{C2} can then be calculated as

$$\Delta I_{C2} = \tan \Ø_H \, W_B J_{ny}(X') \, W_E \qquad (4.3)$$

where $\Ø_H$ is the Hall angle. We have that $\tan\Ø_H$ can be expressed as $\tan\Ø_H = \mu_n^* B$ [1,25] where μ_n^* is the Hall electron mobility and B the magnetic field in the z direction

$$\Delta I_{C2} = \mu_n^* B W_B J_{ny}(X') W_E \qquad (4.4)$$

We now define the relative sensitivity following [25] as

$$S_r = \frac{\Delta I_{C2}}{I_{C2}} \frac{1}{B} \qquad (4.5)$$

and with (4.2) and (4.4) we obtain

$$S_r = \frac{\mu_n^* W_B}{X'} \qquad (4.6)$$

The effect of varying I_B on the relative sensitivity is felt through a change in the position of the plane X'. At very low values of I_B the current flow to the collector is mainly due to diffusion, this results in a wide weak current flow and X' is large and the sensitivity low. As I_B is increased, however, E_L becomes significant and the drift component of the electron flow to the collector starts to dominate. We expect that initially the change from current flow due to diffusion to one primarily due to drift will result in a sharper better shaped flow of electrons to the collector and X' will decreases, causing S_r rise. As I_B is further increased the potential in the base increases, the collector current becomes large and X' again increases. The net result of this is that the sensitivity can be expected to first increase to a peak and then decrease as I_B increased further.

4.2.2 SSIMT operation with stripes floating

The operation of the second structure, the SSIMT with the stripes unbiased is similar to that of the LMT. The operation of the vertical transistor is little changed from that of the LMT. However, the additional p^+ stripes have a substantial effect on the flow of the minority current to the collectors.

The basic effect of the additional p^+ stripes is to suppress the injected current flow from the vertical sides of the emitter. This can readily be understood as a consequence of the different built in voltage produced across the emitter junction. At the edge of the emitter we have a p^+/n^+ junction this produces a larger built in voltage V_{Bi}^+ , than the n^+/p on the bottom of the emitter. The electron current density across the emitter junction can be expressed in the form [14]

$$J_{ni} = J_{ni0}\, e^{\frac{q(V_j - V_{Bi})}{kT}} = J_{ni0}\, e^{\frac{-qV_{Bi}}{kT}}\, e^{\frac{qV_j}{kT}} \qquad (4.7)$$

where $J_{ni0}\, e^{-V_{Bi}/kT}$ is the reverse bias saturation current, V_{Bi} the built in voltage of the junction and V_j the voltage across the junction. Assuming a step junction we can express the built in voltage in terms of the base and emitter doping [14]

$$V_{Bi} = \frac{kT}{q} \ln\left(\frac{N_A N_D}{n_i^2}\right) \qquad (4.8)$$

with N_D being the doping of the base region, N_A the doping of the n^+ emitter and n_i the intrinsic concentration. Due to the high conductivity of the p^+ region we can assume that the potential of the base region at the emitter/base junction near the

stripe is equal to that of the p^+ stripe. If this is the case we can obtain an expression for the attenuation of the laterally injected current. We define this attenuation A as the ratio of the laterally injected electron current density injected into the p^+ stripe over the electron density injected from the bottom of the emitter near the stripe. Using equation (4.7) we have

$$A = \frac{J_{ni}^+}{J_{ni}} \approx \frac{e^{\frac{qV_{Bi}}{kT}}}{e^{\frac{qV_{Bi}^+}{kT}}} \tag{4.9}$$

where J_n^+ and V_{Bi}^+ are the injected electron current density and built in voltage across the n^+/p^+ junction and J_n and V_{Bi} are the same quantities across the n^+/p junction. Using equation (4.8) we can then obtain for the attenuation

$$A = \frac{N_A}{N_A^+} \tag{4.10}$$

where N_A and N_A^+ are the doping levels in the p-well and p^+ stripe respectively. Using the values for doping given above, we obtain for A a figure of 10^{-4} which indicates that the p^+ stripes suppresses the laterally injected current very effectively. The net effect then of the stripes is to force the electron current flow responsible for the collector current deeper into the device (see Fig 4-6). In order to analyze the device's response to a magnetic field it is needed to introduce a second plane X_1 in addition to the plane X' defined for the LMT. The plane X_1 is placed such that a majority of the electron flow which forms the collector current flows between it and the plane X_2 (which was previously designated X' for the

case of the LMT). We can now define an effective width, $W_{eff} = X_2 - X_1$ of this current flow and express the collector current in terms of this width

$$I_{C2} = \int_{-\frac{W_E}{2}}^{\frac{W_E}{2}} \int_{X_1}^{X_2} J_{ny}(y = W_B, x, z)\, dx\, dz \qquad (4.11)$$

Assuming a constant current density we have.

$$I_{C2} = W_{eff} J_{ny0} W_E \qquad (4.12)$$

The basic effect of a magnetic field on this device is the same as that for the LMT. As before I_{C1} is reduced through the deflection of carriers towards the substrate and I_{C2} is increased through the deflection of carriers from the substrate to the collector. The change in the collector current can be expressed in terms of the applied field and the electron current density in the y direction $J_{ny}(X_2)$ at the plane X_2

$$\Delta I_{C2} = \mu_n^* B W_B J_{ny}(X_2) W_E \qquad (4.13)$$

and using the same definition of sensitivity as before we have

$$S_r = \frac{\mu_n^* W_B}{W_{eff}} \qquad (4.14)$$

It can be seen when equation (4.6) is compared to equation (4.14) that a gain in sensitivity is obtained if W_{eff} is substantially smaller then X_1. This result is a

simple manifestation of the current deflection principle. The magnitude of the deflection is inversely proportional to the effective width of the current flow.

The effect of increasing the substrate potential V_S is to push the position of the plane X_2 towards the chip surface. This is due to the increase in the depletion width of the substrate base junction. The consequences of this effect is seen in two ways. Equation (4.12) indicates that the collector current decreases as W_{eff} is reduced and equation (4.14) suggests that the sensitivity increases as W_{eff} is reduced. It can be expected that the substrate potential has a greater effect on the operation of the device with additional p^+ stripes, rather than on the LMT, due to the flow of electrons being pushed deeper into the device.

4.2.3 SSIMT operation with stripes biased

The effect of biasing the p^+ stripes to ground, or to a slightly negative voltage, on the operation of the SSIMT is to magnify the previously considered effects of the stripes The application of a potential to the stripes less than that of the emitter potential will reverse bias the p^+/n^+ junction between the stripes and the emitter and also two regions of the emitter/p-well junction adjacent to the stripes. A negative potential applied to the stripes will also cause a potential hill for electrons, to be produced in the base region surrounding each stripe. Electrons injected into the base from the bottom of the emitter will have to flow around this potential hill to the collectors. This lateral flow of electrons will be enhanced by the formation of a strong laterally accelerating electric field, due to the flow of holes from the base contact to the p^+stripe.

As with the LMT and the SSIMT with stripes floating, a theoretical model of the SSIMT can be developed. It is based on the assumption that a magnetic flux

density B causes a linear displacement of the minority carriers in the neutral base region [5] (see Fig. 4-7). This deflection of the minority carriers is due to the action of the Lorentz force. To obtain the magnetic response of the SSIMT we shall only consider the action of the magnetic field on one half of the device. The flow of the minority carriers within half of the device is shown in a cross section of right half of the structure, (Fig. 4-7). We analyze the part of the electron flow which contributes to the collector current, (Fig. 4-8). For simplicity we assume that this flow of electrons from the emitter to the collector, consists of a current tube of constant cross-sectional area. We model this current flow as first a vertical flow and then a lateral flow, (Fig. 4-9a). The vertical flow is a consequence of the negative potential applied to the p+ stripes and the lateral flow is due to the strong lateral electric field in the neutral base region.

To facilitate the analysis of the deflection of the carriers, the L-shaped current flow can be further broken down into two boxes, one vertical and the other horizontal, Fig. 4-9b. The corresponding current densities within these two boxes are J_{nx} and J_{ny} for the vertical and lateral directions respectively. It remains to determine the boundaries of these boxes. The top and bottom edges of the horizontal box are defined by two planes $x = X_1$ and $x = X_2$ as for the previous case of floating stripes. The first plane $x = X_1$ is defined so as to provide a means to analyze the effect of the negative potential V_r applied to the p^+ stripes. The negative potential applied to the stripes will block the injection of electrons from the emitter into the p^+ stripes and also the injection across a small region of the bottom of the emitter next to each stripe. This will have the effect of preventing movement of the injected electrons laterally and forcing the minority current flow down into the device. The plane $x = X_1$ is positioned such that a majority of the laterally flowing electron current will flow below this plane. We also assume that

OA = X_1 (the penetration of the negative potential is equal in all directions). The plane $x = X_2$ is used to analyze the effect of the substrate potential V_S on the electron flow. Electron current above this plane is presumed to be collected by the collector, conversely, electron current below this plane is collected by the substrate. This definition is similar to the one presented in [25]. According to this model all of the electron current flow contributing to the collector current will flow in the region

$$X_1 \leq x \leq X_2. \tag{4.15}$$

The distance between these two planes X_1 and X_2 is defined as $W_{eff} = X_2 - X_1$, and can be thought of as the effective width of the stream of laterally flowing electrons. We assume that all the electrons flowing in the region defined by equation (4.15) that reach the plane $y = W_B$ are collected by the collector and form the collector current.

The length L_1 of the vertical box can be expressed in terms of the two planes defined above as

$$L_1 = X_1 + \frac{W_{eff}}{2} \tag{4.16}$$

With the assumptions given above L_2 can be expressed as

$$L_2 = W_{eff} + X_1 + \frac{W}{2} \tag{4.17}$$

or

$$L_1 = \frac{X_1 + X_2}{2} \qquad (4.18a)$$

$$L_2 = W_B + L_1 \qquad (4.18b)$$

4.2.3.1 Analytical Model

The total current I_{C20} collected by the right collector at zero magnetic field can be expressed in terms of the current density J_{ny} of laterally flowing electrons

$$I_{C2} = \int_{-\frac{W_E}{2}}^{\frac{W_E}{2}} \int_{X_1}^{X_2} J_{ny}(x, y = W_B, z)\, dx\, dz \qquad (4.19)$$

with W_E denoting the emitter width. If we presume that a uniform current distribution exists in the region between the two planes X_1 and X_2 then $J_{ny}(x, y=W_B, z) = J_{ny0}$, and equation (4.19) simplifies to

$$I_{C2} = W_{eff} J_{ny0} W_E \qquad (4.20)$$

To obtain the current change ΔI_C due to a change in the magnetic field ΔB we have to determine the effect of the magnetic field on both the vertical and lateral electron flows. Both flows will be deflected through an angle $\Theta_H = \mu_n^* B$ where μ_n^* is the electron Hall mobility [14]. This is shown in Fig. 4-8b. The change in the vertical current can be calculated by integrating the current density J_{nx} in the plane $x = L_1$ over the area defined by ΔY and the emitter width W_E. It is

$$\Delta I_{C2v} = \int_{-\frac{W_E}{2}}^{\frac{W_E}{2}} \int_{-X_2}^{-X_2+\Delta Y} J_{nx}(x = L_1, y, z)\, dy\, dz \qquad (4.21)$$

where (for small $\emptyset_H$ and $\tan\emptyset_H \approx \emptyset_H$)

$$\Delta Y = L_1 \mu_n^* B \qquad (4.22)$$

If we assume ΔY is small and therefore $J_{nx}(x= L_1, y, z) \approx J_{nx}(x =L_1, y = X_2, z)$ over the region of deflection $y = -X_2$ to $y = -X_2 +\Delta Y$, we obtain from equation (4.21) that

$$\Delta I_{C2v} = \mu_n^* B\, L_1\, J_{nx}(x = L_1, y = X_2, z)\, W_E \qquad (4.23)$$

The change of the lateral current can be calculated by integrating the current density J_{ny} in the plane $y = W_B$ over the area defined by ΔX and the emitter length W_E

$$\Delta I_{C2l} = \int_{-\frac{W_E}{2}}^{\frac{W_E}{2}} \int_{X_2+\Delta X}^{X_2} J_{ny}(x, y = W_B, z)\, dx\, dz \qquad (4.24)$$

where

$$\Delta X = L_2 \mu_n^* B \qquad (4.25)$$

If we assume, as before, a uniform current distribution in the area of integration we have

$$\Delta I_{C2l} = \mu_n^* B L_2 J_{ny}(x = X_2, y = L_2, z) W_E \qquad (4.26)$$

Our analysis presumed a continuous current flow of constant cross-sectional area and if we presume $J_{nx}(x = L_1, y = X_2, z) \approx J_{ny}(x = X_2, y = L_2, z) = J_{ny}(X_2)$ we can then obtain the total current change as the sum of ΔI_{C2l} and ΔI_{C2v}

$$\Delta I_{C2} = \mu_n^* B (L_1 + L_2) J_{yn0} W_E \qquad (4.27)$$

If we also assume a uniform current density in both boxes, then the current density in both boxes must be equal and $J_{nx} = J_{ny} = J_{ny0}$. Using equation (4.20) to express J_{ny0} as a function of I_{C20} we express equations (4.23) and (4.26) as

$$\Delta I_{C2v} = \mu_n^* \frac{L_1}{W_{eff}} I_{C20} B \qquad (4.28a)$$

$$\Delta I_{C2l} = \mu_n^* \frac{L_2}{W_{eff}} I_{C20} B \qquad (4.28b)$$

The total current change is then

$$\Delta I_{C2} = \mu_n^* \frac{L_1 + L_2}{W_{eff}} I_{C20} B \qquad (4.29)$$

Defining the relative sensitivity as

$$S_r = \frac{\Delta I_{C2}}{I_{C20}} \frac{1}{B} \qquad (4.30)$$

and using equation (4.29) we have

$$S_r = \mu_n \frac{L_1 + L_2}{W_{eff}} \qquad (4.31)$$

The above results for the magnetic response of the collector currents and the relative sensitivity were derived for the current flow of half of the device. In the actual device there are, of course, two collector currents I_{C1} and I_{C2} and the relative sensitivity is defined as

$$S_r = \frac{\Delta I_C}{I_{C0}} \frac{1}{B} \qquad (4.32)$$

with $\Delta I_C = \Delta I_{C2} - \Delta I_{C1}$ and $I_{C0} = I_{C10} + I_{C20}$. The structure is symmetrical and we can assume $\Delta I_{C1} = -\Delta I_{C2}$ and $I_{C10} = I_{C20}$. The final expression for sensitivity is therefore unaffected as both the current change and the total current are increased by a factor of two.

We can express the collector currents I_{C1} and I_{C2} as a function of the magnetic field in terms of the zero field current and ΔI_{C1} and ΔI_{C2}, namely

$$I_{C1} = I_{C10} + \Delta I_{C1} \qquad (4.33)$$

and

$$I_{C2} = I_{C20} + \Delta I_{C2} \qquad (4.34)$$

Using $I_{C1} = -\Delta I_{C2}$ and defining $\Delta B = B$ we have

$$I_{C1} = I_{C10}\left(1 - \mu_n \frac{L_1 + L_2}{W_{eff}} B\right) \qquad (W_{eff} > 0) \qquad (4.35a)$$

$$I_{C2} = I_{C20}\left(1 + \mu_n \frac{L_1 + L_2}{W_{eff}} B\right) \qquad (W_{eff} > 0) \qquad (4.35b)$$

The last two equations suggest that both collector currents are linear functions of the magnetic induction and can be expressed as

$$I_{C1} = I_{C10}(1 - S_r B) \qquad (W_{eff} > 0) \qquad (4.36a)$$

$$I_{C2} = I_{C20}(1 + S_r B) \qquad (W_{eff} > 0) \qquad (4.36b)$$

where S_r is defined by equation (4.30). From equations (4.36a) and (4.36b) it is obvious the higher the sensitivity the higher the change in the collector currents.

4.2.3.2 The effect of the bias parameters on sensitivity

Equation (4.31) suggests that in order to obtain high sensitivities W_{eff} should be made as small as possible. The definition of planes X_1 and X_2 used to derive W_{eff} imply that W_{eff} is a function of the applied potential the stripe potential V_r and the substrate potential V_S. It is therefore expected that by

altering these potentials it will be possible to enhance the sensitivity of the device. It can also be expected that the applied base current I_B will also influence the magnitude to W_{eff}. We analyze the influence of each of these parameters when the others are held constant.

4.2.3.2.1 Influence of V_r

The negative potential V_r applied to the p^+ stripes can be expected to influence the positions of both planes X_1 and X_2. The functional dependence of the two planes on V_r should be a linear, as the stripes make an ohmic contact with the neutral base region. This dependence can be expressed as

$$X_1 = X_{10} - c_1 V_r \qquad (4.37a)$$

$$X_2 = X_{20} - c_2 V_r \qquad (4.37b)$$

where X_{10} and X_{20} represent the position of the planes when $V_r = 0$ and c_1 and c_2 are proportionality constants. The magnitudes of X_1 and X_2 therefore increase with an increase in $|V_r|$ (V_r is negative). Using equations (4.37a,b) W_{eff} can be expressed as

$$W_{eff} = X_2 - X_1 = W_{eff0} + K_r V_r \qquad (4.38)$$

where $W_{eff0} = X_{20} - X_{10}$ and $K_r = c_1 - c_2$. From equation (4.38) it is obvious that at some critical value V_{rc} W_{eff} will be reduced to zero, and the collector current is shut off. In that case we have from equation (4.38) that

$$V_{rc} = -\frac{W_{eff0}}{K_r} \qquad (4.39)$$

Then (4.38) can be expressed in terms of V_{rc} as

$$W_{eff} = K_r (V_r - V_{rc}) \qquad (|V_r| < |V_{rc}|) \qquad (4.40)$$

Using equations (4.38) and (4.31) we can express the sensitivity as

$$S_r = \mu_n^* \frac{L_1 + L_2}{K_r (V_r - V_{rc})} \qquad (|V_r| < |V_{rc}|) \qquad (4.41)$$

Equation (4.41) indicates that V_r will have a dramatic effect on the relative sensitivity. It is necessary to note that the sum $L_1 + L_2$ is also a function of V_r and using (4.18a) and (4.18b) as well as (4.37a) and (4.37b) can be expressed as

$$L_1 + L_2 = L_0 - K_r V_r \qquad (4.42)$$

where $L_0 = W_B + X_{10} + X_{20}$ and $K_L = c_1 + c_2$. When V_r approaches V_{rc} the value of W_{eff} approaches zero and the sensitivity tends towards infinity. This is of course physically unsound and the maximum sensitivity attainable with $V_r \approx V_{rc}$ will need to be determined by experiment. However, in the region where V_r is slightly less then V_{rc} the sensitivity will be very high. In this region of V_r, W_{eff} will be reduced for increasing V_r whereas $L_1 + L_2$ will increase slightly. These two results allow us to assume that $L_1 + L_2$ is a constant. Using equations (4.18a) and (4.18b) the sum $L_1 + L_2$ can be expressed as $W_B + 2 L_1$ and we assume for L_1 a likely value of one half of the p-well depth. We can now obtain V_{rc} and K_r from the

experimental data. Once these two parameters are determined we can obtain W_{eff0} from equation (4.39) and W_{eff} as function of V_r from equation (4.38).

A check of the above assumptions can be made by the following procedure. From equation (4.35a) it is obvious that I_{C1} can be driven to zero if B is increased sufficiently to B_c, it is only for $B \leq B_c$ that the device will exhibit linear behavior. If $B = B_c$ then $I_{C1} = 0$ and we have from (4.35a)

$$1 - S_r B_c = 0 \tag{4.43}$$

which gives

$$B_c = \frac{1}{S_r} \tag{4.44}$$

where B_c is a the critical value of the magnetic induction at which I_{C1} approaches zero. From (4.18a) it follows that

$$L_1 + L_2 = W_B + 2 L_1 \tag{4.45}$$

and using equation (4.44) and (4.30) we determine L_1 as a function of W_{eff}, to be

$$L_1 = \frac{W_{eff}}{2 \mu_n^* B_c} - \frac{W_B}{2} \tag{4.46}$$

Once L_1 is determined for a number of stripe potentials L_2 can be determined using (4.18a) and the position of the two planes X_1 and X_2 can be plotted as a function of V_r.

4.2.3.2.2 Influence of V_S

The substrate potential V_S provides for the reverse polarization of the p-well junction. This junction can be approximated by a linear junction. The functional dependence of the two planes X_2 and X_1 on V_S can be expressed through a linear relation with the depletion region of the p-well/n-substrate junction

$$X_2 = X_{2S} - C_{S2}\frac{W_L}{2} \qquad (4.47a)$$

$$X_1 = X_{1S} - C_{S1}\frac{W_L}{2} \qquad (4.47b)$$

where X_{2S} and X_{1S} represent the positions of the two planes for an arbitrary value V_S = Const., C_{S2} and C_{S1} are proportionality constants, and $W_L/2$ is the width of the depletion region on the p-well side of the junction. The p-well/n-substrate junction can be considered as a linearly graded junction and W_L expressed [14] as

$$W_L = \sqrt[3]{\left(\frac{12\varepsilon}{qa}\right)\left(V_{bi} + V_S - V_{Bn}\right)} \qquad (4.48)$$

where ε is the dielectric permittivity for silicon, a is the impurity gradient at the junction, q is the electron charge, V_{bi} is the built in junction voltage and V_{Bn} is the voltage in the neutral base region at the edge of the depletion region. Substituting $V_B = V_{bi} - V_{Bn}$ and $C_W = (12\ \varepsilon/qa)^{1/3}$ into equation (4.48) W_L can be expressed as

$$W_L = C_W \sqrt[3]{(V_S - V_B)} \qquad (4.49)$$

Using equations (4.47a), (4.47b) and (4.49) W_{eff} can be expressed as

$$W_{eff} = X_2 - X_1 = W_{eff0} - K_S \sqrt[3]{(V_S - V_B)} \qquad (4.50)$$

where $W_{effS} = X_{2s} - X_{1s}$ and $K_S = (C_{s2} - C_{s1})\, C_W/2$. Increasing V_S will decrease W_{eff} and at some critical value V_{Sc}, W_{eff} will be reduced to zero and the collector current shut off. We can therefore express W_{eff0} as

$$W_{eff0} = K_S \sqrt[3]{(V_{Sc} - V_B)} \qquad (4.51)$$

Using (4.50) and (4.51) we have that

$$W_{eff} = K_S \left[\sqrt[3]{(V_{Sc} - V_B)} - \sqrt[3]{(V_S - V_B)}\right] \qquad (V_S < V_{SC}) \qquad (4.52)$$

Using equation (4.31) we can express S_r as

$$S_r = \mu_n^* \frac{L_1 + L_2}{K_s\left[\sqrt[3]{(V_{Sc} - V_B)} - \sqrt[3]{(V_S - V_B)}\right]} \qquad (|V_S| < |V_{Sc}|) \qquad (4.53)$$

where V_{sc} is a critical substrate voltage at which W_{eff} reduces to zero, $V_B = V_{Bn} - V_{bi}$ and K_S is a constant. For this case the sum $L_1 + L_2$ can be expected to be relatively insensitive to changes in V_S and the behavior of S_r is dominated by the reduction in W_{eff}. S_r is an increasing function of V_S. K_S can be determined from the experimental data, L_1 from equations (4.45) and (4.46), and L_2 from (4.13a).

4.2.3.2.3 Influence of I_B

A constant base current I_B is used to forward bias emitter base junction of the device. It can be predicted that an increase in the magnitude of I_B will have an effect on W_{eff} that is equivalent to a decrease in the magnitude of the applied potential V_r. The base contacts are laterally placed and we assume that I_B affects both planes X_1 and X_2. A decrease in the base current will bring about an increase in X_1 and correspondingly a decrease in X_2 with the net result of decreasing W_{eff}. The sum $L_1 + L_2$ will be a weak function of I_B if, as we assume, the change in both planes is nearly equal. The functional dependence of the two planes X_1 and X_2 of I_B should be a linear function as the base contact is an ohmic contact in the neutral base region. This dependence can be expressed as

$$X_2 = X_{2B} - C_{B2} I_B \qquad (4.54a)$$

$$X_1 = X_{1B} - C_{B1} I_B \qquad (4.54b)$$

where X_{1b} and X_{2b} represent the positions of the two planes for an arbitrary value of I_B and C_{b1} and C_{b2} are proportionality constants. Using equations (4.54a) and (4.54b) W_{eff} can be expressed as

$$W_{eff} = X_2 - X_1 = W_{effB} + C_B I_B \qquad (4.55)$$

where $W_{effB} = X_{2b} - X_{1b}$ and $C_B = C_{b2} - C_{b1}$. Decreasing I_B will decrease W_{eff} and at some critical value I_{bc} , it will be reduced to zero and the collector current is shut off. We can, in that case, express W_{effB} as

$$W_{effB} = - C_B I_{Bc} \qquad (4.56)$$

Using equations (4.55) and (4.56) W_{eff} can be expressed as

$$W_{eff} = K_B(I_B - I_{Bc}) \qquad (I_B \geq I_{Bc}) \tag{4.57}$$

where I_{Bc} is a critical value of the base current at which the effective width reduces to zero. Therefore in order to "open" up a lateral path for the electrons to the collectors it is necessary to apply a minimal base current Ibc . For all values of $I_B < I_{Bc}$ the collector currents will be zero. Using equations (4.57) and (4.31) we can obtain for the sensitivity as a function of I_B

$$S_r = \mu_n \frac{L_1 + L_2}{K_B(I_B - I_{Bc})} \qquad (I_B \geq I_{Bc}) \tag{4.58}$$

Thus S_r is a decreasing function of I_B. K_B can be determined from the experimental data, L_1 from equations (4.57) and (4.58), and L_2 from (4.18a).

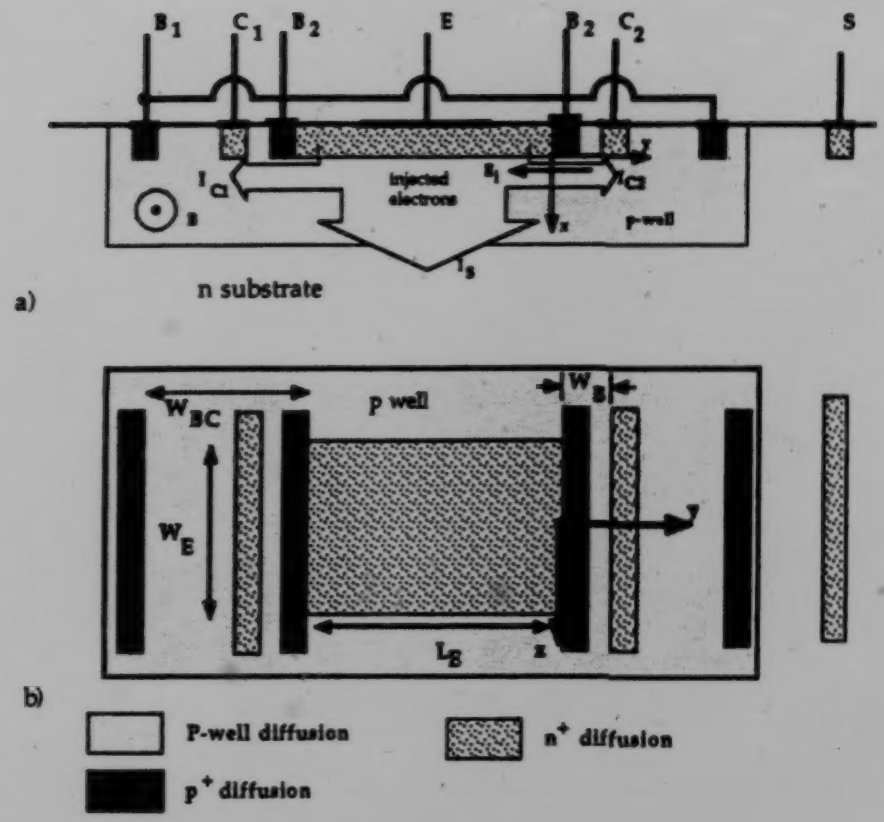

Fig. 4-1 Basic SSIMT structure a) crossection b) plan view

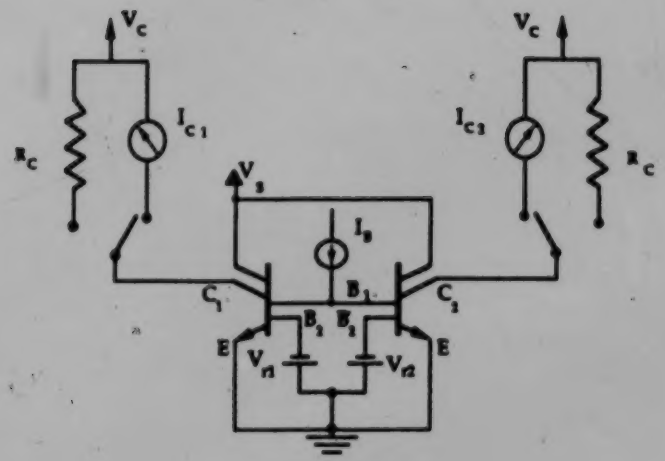

Fig 4-2 Circuit diagram for SSIMT with stripes biased

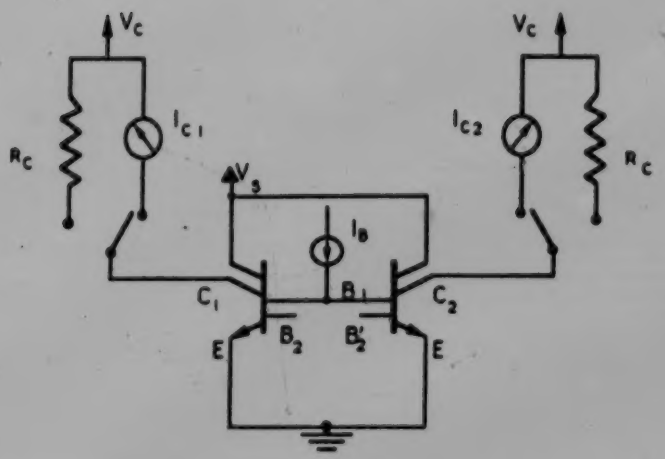

Fig 4-3 Circuit diagram for SSIMT stripes floating

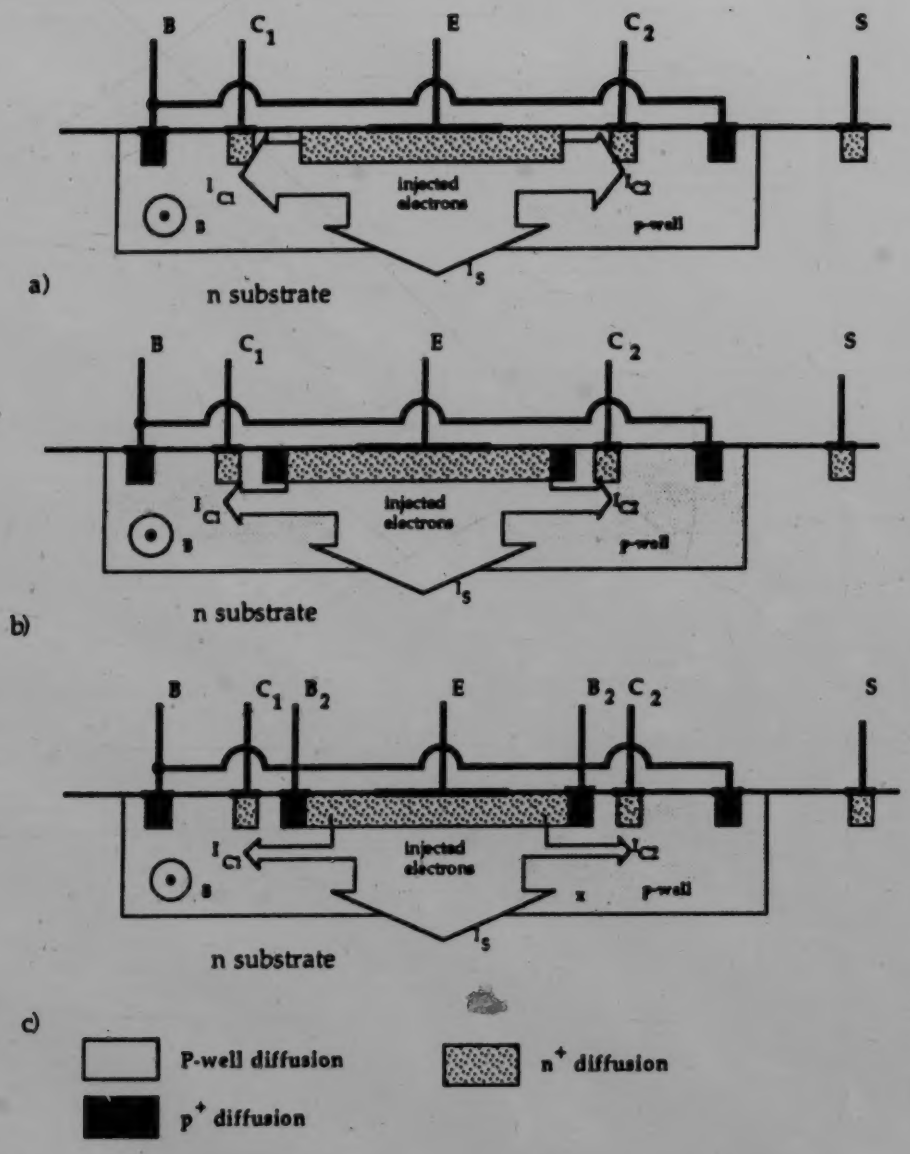

Fig 4-4 Electron flow for a) LMT b) SSIMT stripes floating c) SSIMT with stripes biased

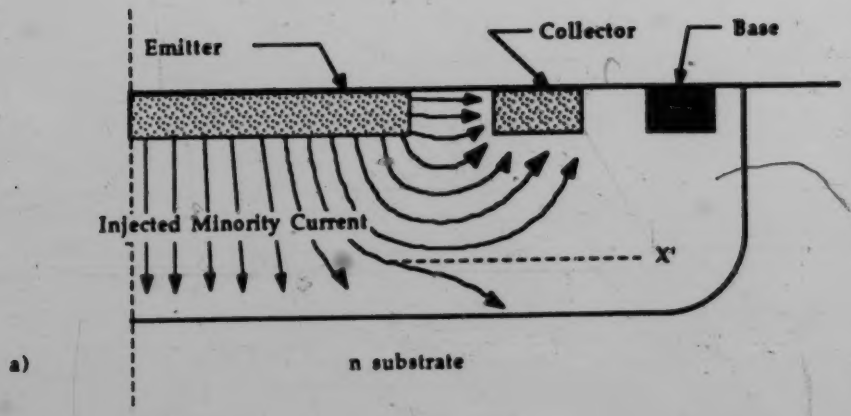

a)

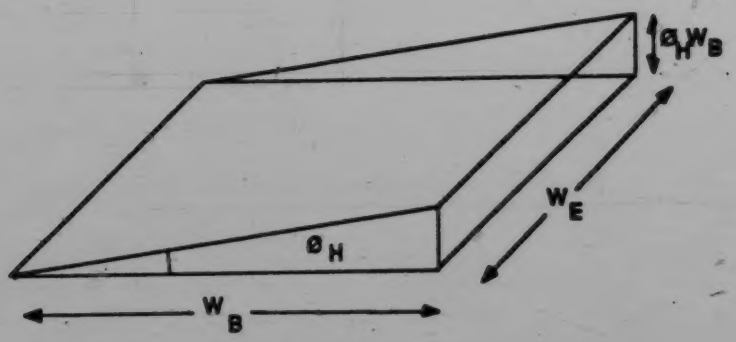

b)

Fig 4-5 a) Electron current flow in base region LMT
b) Area defined by deflection of current through ϕ_H

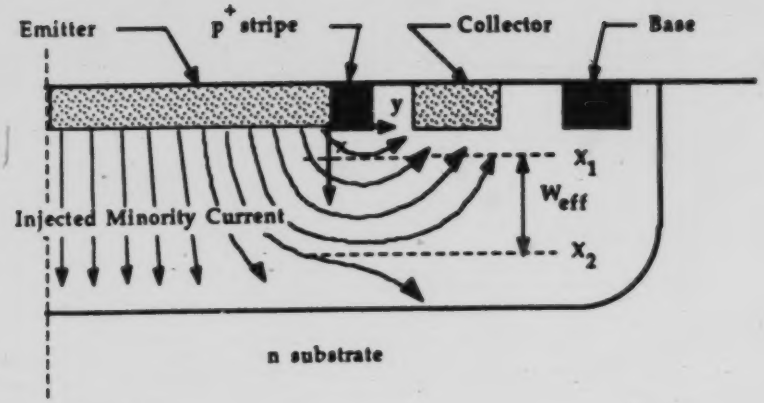

Fig. 4-6 Electron current flow in base region of SSIMT with stripes floating

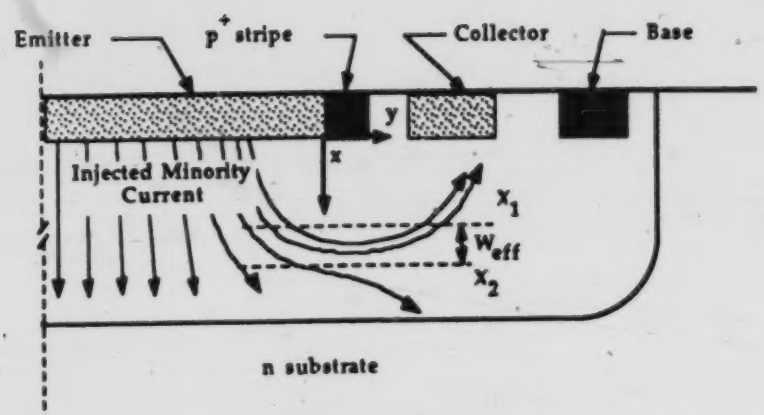

Fig 4-7 Electron current flow in base region of SSIMT with stripes biased

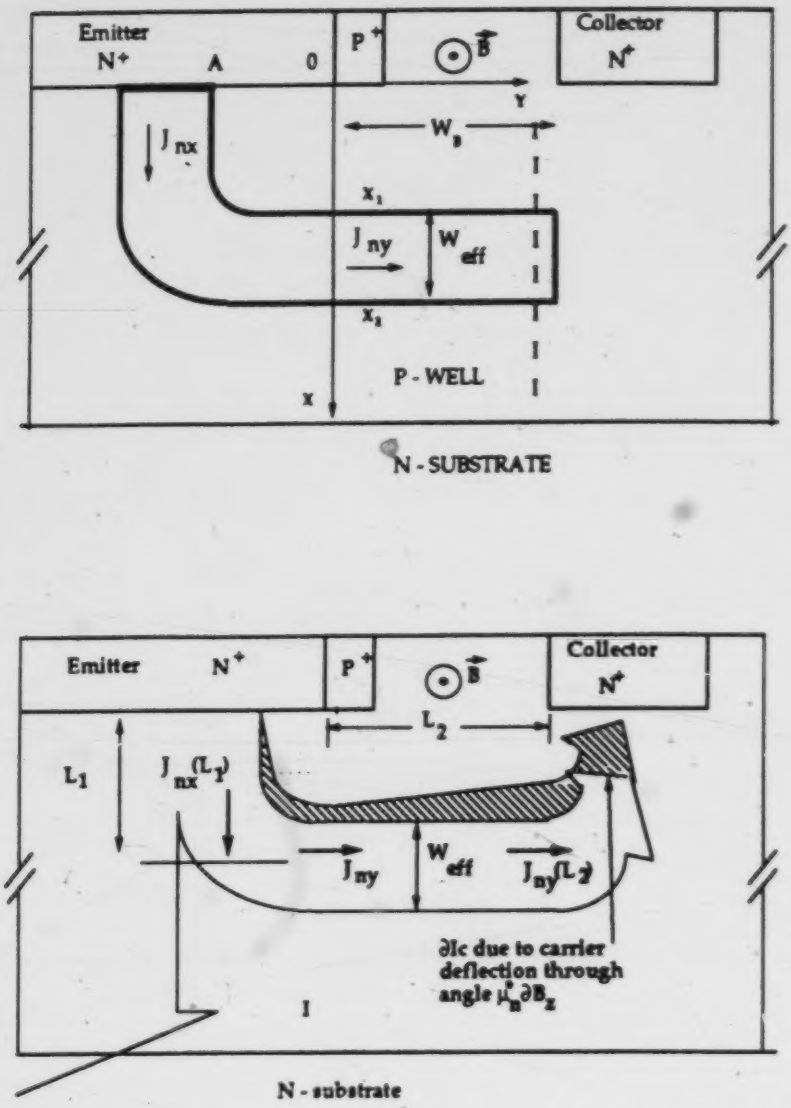

Fig. 4-8 a) Electron flow in base responsible for collector current,
b) magnetic response of this electorn flow.

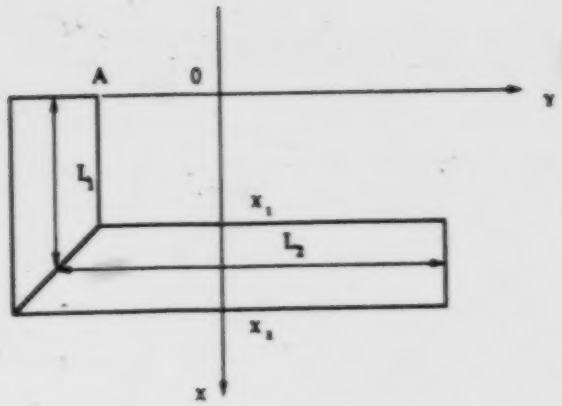

a)

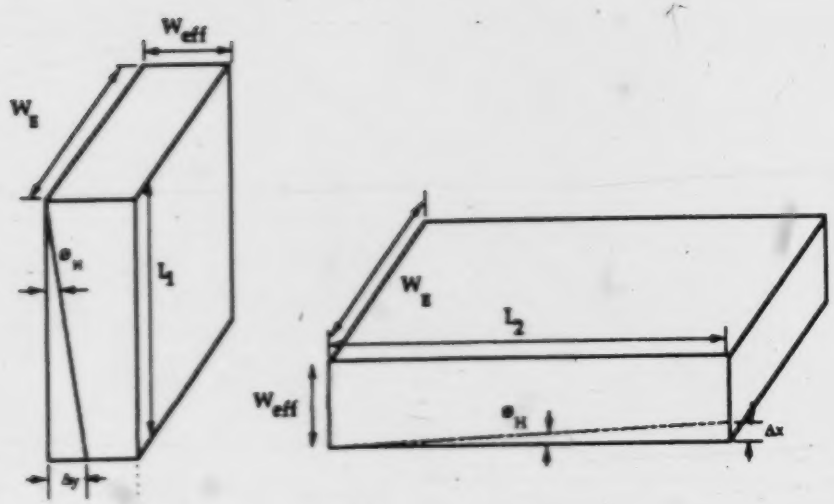

b)

Fig. 4-9 a) L-shaped model of the flow of electrons responsible for the collector current, b) current deflection through the Hall angle of linear current flow.

5.0 Experimental Results

In the first section of this chapter a short description of the CMOS process and the different geometries of the devices designed and tested is given. The second part of the chapter deals with an experimental characterization of the SSIMT in the two bias conditions - biased stripes and floating stripes.

To test the devices they were mounted on a suitable non-magnetic package and a magnetic field was generated by a VARIAN V-4005 four inch electromagnet using a Varian V-2900 regulated current supply. A LDJ-511 Gaussmeter was used to determine the magnetic field present near the the device. The devices were biased and the collector currents measured using a HP-4145A semiconductor parameter analyser.

5.1 Process and Geometrical variations

A large number of CMOS based SSIMTs differing in both geometry and fabrication process were designed in order to investigate the mechanisms of the device operation and optimize the device.

5.1.1 CMOS processes

The initial SSIMT designs were manufactured in a 4 μm Microtel Pacific CMOS process and had a 50X100 μm ($L_E X W_E$) emitter, a 4 μm p^+ stripe and a 8 μm base width, W_B (see Fig. 4-1). Typical diffusion depths for this process are 10 μm for the p-well and 1.5 μm for the source/drain diffusions.

After the initial designs were characterized the Northern Telecom CMOS process, CMOS-1B became available through the Canadian Microelectronic Corporation. A large variety of devices were fabricated using this 5 μm process. Typical diffusion depths for the 1B process were 12 μm for the p-well depth and 1.6 μm for the source/drain diffusions.The p-well doping is 10^{16} cm^{-3}.

5.1.2 Device geometries

5.1.2.1 Basic SSIMT structure

The basic SSIMT was manufactured in both the 4 μm Microtel Pacific process and the 5 μm CMOS-1b Northern Telecom process. The geometries of both these devices (see Fig. 4-1) were essentially the same with a 50X100 μm emitter and p^+ stripe/base contact separation of 40 μm. The only difference between the two devices was the base width, W_B, and the stripe width, W_{p^+}. For the case of the 4 μm process these were respectively 8 μm and 4 μm and for the 5 μm process 10 μm and 5 μm respectively.

In order to fabricate a simple LMT to compare to the SSIMT an identical device without the stripes present was manufactured in both the 4 μm and 5μm processes.

5.1.2.3 Emitter geometries

In order to allow for an analysis of the relative importance of electron injection from various portions of the emitter large variety of devices were fabricated with differing emitter geometries. Devices were fabricated emitter lengths of 80, 60, 40 and 20 μm with all other dimensions as for the standard

Device	Process	L_E	W_E	W_B	W_{BC}
SSIMT	4 µm	100	50	8	85
LMT	4 µm	100	50	8	85
SSIMT	5 µm	100	50	10	85
LMT	5 µm	100	50	10	85
SSIMT	5 µm	100	60	10	85
SSIMT	5 µm	100	40	10	85
SSIMT	5 µm	100	30	10	85
SSIMT	5 µm	100	20	10	85
SSIMT	5 µm	80	50	10	85
SSIMT	5 µm	60	50	10	85
SSIMT	5 µm	40	50	10	85
SSIMT	5 µm	20	5	10	85
SSIMT	5 µm	60	60	10	85
SSIMT	5 µm	50	50	10	85
SSIMT	5 µm	40	40	10	85
SSIMT	5 µm	30	30	10	85
SSIMT	5 µm	20	20	10	85

Table 5.1 emitter geometries

device. The emitter width was varied through the range of 60, 50, 40, 30 and 20 μm

Device	Process	L_E	W_E	W_B	W_{BC}
SSIMT	5 μm	100	60	10	105
SSIMT	5 μm	100	40	20	105
SSIMT	5 μm	100	30	30	105
SSIMT	5 μm	100	20	40	105
SSIMT	5 μm	100	20	50	105

Table 5.2 Base width variation

with the emitter length kept at 100 μm. Also fabricated were devices with square emitters of 60 X 60, 50 X 50, 40 X 40, 30 X 30 and 20 X 20 μm. In all these devices only the emitter dimensions were changed and the position of the collectors and p^+stripes when needed, see Fig. 5-1 and Table 5.1.

5.1.2.4 Base width variation

To analyze the effect of increasing the base width, W_B, a number of devices were fabricated in a large p-well of 130X400 μm and a p^+ stripe/base contact separation of 80 μm. The basic emitter geometry of the devices was that of the standard device, a 50X100 μm emitter. The base width was, however, varied through 10 to 50 μm in 10 μm steps, see Table 5.2. This should allow for an analysis of the carrier deflection effect as the magnitude of this effect should increase roughly linearly with increasing base width. A typical device is shown in Fig. 5-2.

5.2 LMT and SSIMT with stripes floating

In this section experimental results from the operation of the 4 μm LMT and the 4 μm SSIMT with the stripes floating (unless otherwise noted the p^+ stripes are unbiased for this section) are presented. Results are given showing the basic characteristics of both the LMT and the SSIMT. Both the vertical and lateral transistors of each device are analyzed. Magnetic results for both devices are then presented. The current change ΔI_C is plotted as a function of the magnetic field and sensitivities are shown as a function of the bias conditions.

5.2.1 Electrical Characteristics

Fig. 5-3 and Fig. 5-4 present the collector current as a function of the applied base current I_B for LMT and the SSIMT respectively. A general increase in the collector currents is revealed as I_B is increased. This is expected as the collector currents are due to the drift of electrons laterally from the emitter to the collectors and the effectiveness of this drift is proportional to the applied base current. It is interesting to note that the p^+ stripes appear to inhibit the operation of the lateral transistor at low base currents, resulting in a well defined critical base current at which the lateral transistor "turns on".

The variation of the base potential V_B as a function of I_B is shown in Fig. 5-5 for both the LMT and the SSIMT with stripes floating (solid). The most striking feature in this plot is the negative resistance region displayed for all bias conditions as I_B increases past a critical value I_{Bc} at which V_B shows a maximum. This critical base current marks the onset of high injection current conditions. At this point the injection of electrons becomes sufficiently large to modulate the

resistance of the base region resulting in a drop in V_B. A comparison of Fig. 5-5 and Fig. 5-4 illustrates the effect of the p^+ stripes. By suppressing the lateral flow of electrons along the surface of the device the p^+ stripes cause the lateral transistor to only become active after the the onset of the high current conditions and the establishment of a lateral electric field in the base region. It can be seen from these figures that the critical base current increases as the substrate voltage VS is increased.

The relationship between the substrate current I_S and the applied base current is shown for both devices in Fig. 5-6. It is seen that for low base currents that a linear relationship holds between I_S and I_B. This implies normal operation of the vertical transistor with $I_S = \beta_v I_B$, where β_v is the DC gain of the vertical transistor. However, as the base current is increased high current effects dominate and I_S saturates, β_v decreases significantly and I_S becomes relatively insensitive to changes in the base current.

Fig. 5-7 and Fig. 5-8 present an electrical characterization of the LMT and SSIMT with floating stripes with respect to changes in the substrate voltage. In Fig. 5-7 it can be seen that as V_S is increased beyond 5 V I_{C0} drops for the floating SSIMT. This is due to a change in the position of the plane X_2 in the base region of the device. As V_S is increased the depletion region of the n-substrate/p-well junction becomes larger forcing the plane X_2 nearer the chip surface. This results in a redistribution of the electron flow in the base region of the device. More electrons now flow to the substrate and less to the collectors. It would appear that, for the LMT, the lateral flow along the surface dominates the operation of the device, as the collector current is relatively insensitive to the substrate potential. Fig. 5-8 shows the effect of V_S on the vertical transistor. It can

be seen that there is basically no difference in the vertical transistor formed by either the LMT or the SSIMT.

5.2.2 Magnetic characteristics

The magnetic response of both the LMT and the SSIMT with floating stripes is presented in Fig. 5-9a and Fig. 5-9b respectively. In these two figures the collector current difference is shown as a function of the magnetic field. A zero field offset can be seen clearly in both graphs with an effective offset of 125 mT for the LMT and 150 mT for the SSIMT. Around the field at which $\Delta I_C = 0$ both devices exhibit a linear response to the magnetic field and it is also at this point at which the sensitivity is a maximum. However, as B is increased the collector currents become very unbalanced and the collector current response decreases.

The absolute sensitivity S_a as defined by equation (3.30), is directly proportional the current density of the electrons flowing laterally in the base region in the vicinity of the plane X_2 (see equation (4.13)). The effect of I_B on the absolute sensitivity is seen clearly in Fig. 5-10a and Fig. 5-10b which show the absolute sensitivity versus I_B for the LMT and the SSIMT respectively. For both devices S_a rises rapidly to a maximum and then drops off. At low base currents the lateral transistor is turned off for both devices ($I_{C0} \approx 0$), and ΔI_C is effectively 0. As the base current is increased past I_{Bc} a lateral electric field is established in the base region causing a collector current to flow and ΔI_C to increase. Further increasing of the base current causes a rapid rise in absolute sensitivity as the laterally flowing electron current density becomes larger. If the base current is increased even further S_a drops off. The peaked shape of the curves is probably due to nonuniform electron current densities in the base region of the device due to high

current effects. The effect of the substrate voltage on the absolute sensitivity, is also seen clearly in these figures. As the substrate voltage is increased S_a displays an increasingly more peaked shape indicating the presence of a more concentrated electron flow. This is due to the position of the plane X' or X_2 moving towards the chip surface causing a concentration of the laterally flowing electrons. This movement in the plane X' or X_2 is due to the increase in the reverse biased depletion width of the p-well/n-substrate junction as has been explained in chapter 4.0.

The relative sensitivity, according to the definition of equation (3.29), is proportional to S_a and inversely proportional to I_{C0}. S_r is plotted as function of I_B in Fig. 5-11a and Fig. 5-11b for the LMT and the SSIMT respectively. As can be seen for both devices a sharp peak in the relative sensitivity occurs near the onset of the base resistance modulation due to the large S_a at this point and the small value of I_C.

Using the results presented in Fig. 5-11a and equation (4.6) we can calculate a value for the position of the plane X'. At I_B = 2 mA , V_C = 5 and V_S = 10 V we have a sensitivity of 100 %/T which results in a value of 5.25 μm for the position of the plane X'. The plane is therefore positioned near the middle of the p-well. The value of 5.25 μm is physically reasonable and compares well with the values calculated by Popovic and Widmar [25]. In a similar way we can use the results in Fig. 5-11b and equation (4.14) to calculate W_{eff} for SSIMT with floating stripes at maximum sensitivity. We obtain a figure of 1.05 μm for W_{eff} at a sensitivity of 500 %/T. A comparison of these two values provides an indication of the effectiveness of the p^+ stripes in shaping the injected electron flow.

In Fig. 5-11c and Fig. 5-11d S_r is plotted as function of the substrate voltage for the LMT and the SSIMT respectively. With increasing base current the peak in S_r is obtained at larger values of V_S. The magnitude of this peak is an indication that the electron current density increases significantly as V_S is increased and the depletion region of the n-substrate/p-well junction is increased. At the large base currents the high current effects are more dominant, the lateral electric field larger and the area of current concentration more sharply defined . This results in a larger V_S being necessary to obtain a maximum sensitivity.

An investigation of the variation in S_r with respect to collector voltage was also done. A plot of S_r versus the collector voltage V_C is shown for both devices in Fig. 5-11e and Fig. 5-11f. It is expected that S_r will change little with respect to V_C and this is indeed the case. However, a small drop in S_r can be seen and this can be attributed to the Early effect. As V_C is increased the depletion region width of the reverse biased collector/base junction increases. This causes a drop in the effective base width of the device. As S_r is proportional to this length (see equation (4.14)) we can expect a drop in it as well.

5.3 SSIMT with stripes biased

In this section basic electrical and magnetic characteristics are presented for both the 4 μm and 5 μm devices with biased stripes [5, 54-56]. The fundamental difference of this bias configuration and that of the stripes floating is presence of a small negative potential V_r applied to the p^+ stripes. This voltage is essential for the operation of the SSIMT at very high sensitivities.

5.3.1 Electrical Characteristics

In Fig. 5-12 through 5-15 the basic electrical characteristics of the 4 μm SSIMT with biased stripes is shown. In Fig. 5-12 we present the variation of the laterally collected current I_C as a function of V_C, the collector voltage. As can be seen for all three base currents the device is in the forward biased operating regime. I_C displays a slight response to changes in V_C due to initially the Early effect and then break down effects.

The dramatic effect on the device operation of applying a potential V_r to the stripes can be seen in Fig. 5-13. The grounding or application of a small negative potential to the stripes has completely suppressed the operation of the lateral transistor below a critical voltage. The operation of the device can, therefore, be broken into two distinct modes. One is for base currents less then a critical base current I_{Bc} at which the lateral transistor turns on and a collector current is measured. Although presence of a critical base current was apparent for the LMT and the SSIMT with stripes floating, it is much more clearly defined when the stripes are biased and the device operates in two completely different ways below and above this critical current. Below the critical base current the lateral transistor is completely turned off and the collector current is very small (see Fig. 5-13). Under this condition the device is basically off. Above the critical base current the lateral transistor turns on and the device is in the forward active region.

The effect of increasing the negative potential V_r on I_{Bc} can clearly be seen in Fig. 5-13, with I_{Bc} increasing as V_r is made more negative. This is easily understood as applying a more negative voltage to the stripes forces the base region near the stripes to a lower potential and in order to turn on the device a

larger base current is needed. The collector current for $I_B > I_{Bc}$ displays a fairly linear behavior with respect to I_B as expected. The collector current as a function of the stripe potential is shown in Fig. 5-14. The collector current is seen to drop as $|V_r|$ is increased. This is expected as increasing the magnitude of V_r causes the plane X_1 to move away from the chip surface reducing W_{eff} and therefore decreasing I_C (equation (4.22)).

In Fig. 5-15a and Fig. 5-15b the base voltage and substrate current are shown as a function of I_B. Both of these figures clearly show the distinctive bimodal operation of the device. It is clear, from Fig. 5-13 and Fig. 5-15a that when I_B is increased past I_{Bc} the emitter/base junction becomes forward biased, electrons are injected into the base and a current flow is established to the collectors and the substrate. From Fig. 5-15a it can be seen that high injection effects become manifest for $I_B > I_{Bc}$ and the base voltage falls due to the injected electrons modulating the conductivity of the base region. The base voltage displays a linear relationship to the base current for $I_B < I_{Bc}$. This is an indication of an ohmic relationship between I_B and V_B and in fact a measurement of the current passing through the p^+ stripes for $I_B < I_{Bc}$ this suggests that almost all of the base current is passing directly from the base contact to the stripes under this condition.

A plot of the substrate current I_S versus the base current is shown in Fig. 5-15b. It reveals that even for $I_B < I_{Bc}$ there would appear to be some injection of electrons into the base, however these electrons are collected entirely by the substrate. For $I_B < I_{Bc}$ but greater then that required to turn on the vertical transistor I_S is a linear function of the base current indicating normal operation of the vertical transistor. As I_B is increased past I_{Bc}, the lateral transistor turns on,

high injection effects become dominant and there is an initial sharp increase of I_S after which I_S saturates.

In Fig.5-15c a plot of I_C with respect to increasing V_S is presented. Increasing V_S causes the plane X_2 to push closer to the chip surface, due to the increase in the depletion region of the p-well/n-substrate junction, this in turn causes a reduction in W_{eff} and a consequent drop in I_C. The drop in I_C can be seen clearly, in Fig. 5-15c, as V_S is increased from the point at which the p-well/n-substrate junction is reverse biased to the point at which the lateral transistor turns off.

5.2.2 Magnetic characteristics

The basic magnetic response of the SSIMT is shown in Fig. 5-16. The variation of the collector current, $\Delta I_C = I_{C2} - I_{C1}$, is shown in Fig. 5-16a. In order to minimize the zero field offset slightly different potentials were applied to the p^+ stripes. The device exhibits a very linear behavior with respect to the magnetic field. This figure shows the symmetrical nature of the SSIMT with respect to the magnetic field. Fig. 5-16b shows the effect of altering the stripe potential on the sensitivity of the device. As can be seen from this figure, the larger the negative potential applied to the stripes the higher the magnetic sensitivity. Very large sensitivities were measured for V_r close to V_{rc}. In fact critical magnetic fields B_c were displayed at which one collector current could effectively turned off. If the magnetic field is increased beyond this magnitude the sensitivity of the device decreases as only the remaining collector current is affected. It was noted that by the use of different biasing conditions critical magnetic fields from 30 mT to 1 T were obtainable [5].

The absolute sensitivity S_a is shown as a function of V_r in Fig. 5-17. The dramatic increase in S_a as V_r approaches V_{rc} and W_{eff} is made very small, by pushing the plane X_1 near the plane X_2 indicates the presence of high current densities in the base region near X_2.

The relative sensitivity S_r as a function of V_r is presented in Fig. 5-18 and equation (4.41) is shown in solid. It can be seen the agreement between theory and experiment is good. The values of K_r and V_{rc} were 5.66 μm/ V and -212 mV respectively. These measurements clearly show the crucial role of V_r for the attainment of high sensitivity. An additional insight into the effect of V_r can be seen in Fig. 5-19 where results for W_{eff}, $L_1 + L_2$ and the planes X_1 and X_2 are presented. It can be seen, that W_{eff} decreases to zero as V_r approaches V_{rc} At the same time $L_1 + L_2$ slightly increases, Fig. 5-19b. This confirms our assumption that the sum $L_1 + L_2$ is almost constant and the reduction of W_{eff} is the dominant geometric influence on S_r. Corresponding values for X_1 and X_2 are shown in Fig. 5-19b. It is interesting to note that X_2 is almost unaffected by changes in V_r and positioned at ≈ 5 μm . The reduction of W_{eff} is therefore brought about only by a shift in the position of the plane X_1.

The variation in S_a with V_S is shown in Fig. 5-20. As with the variation of S_a with V_r, maximum sensitivities are obtained when V_S is near the critical value at which the lateral transistor turns off. The rapid increase in S_a as V_S increases is due to W_{eff} being reduced and the increasing of current densities in the base

The influence of V_S on the relative sensitivity is presented in Fig. 5-21. Experimental results are in good agreement with equation (4.53). It is of special interest to note the reduction of V_{Sc} with the increasing of V_r. This is expected as

the plane X_1 is positioned deeper within the device for larger negative stripe potentials. For the case of V_r = -180 mV (K_s = 6.56 μm/ $V^{1/3}$), W_{eff}, and $L_1 + L_2$ are plotted in Fig. 5-22. As the sum $L_1 + L_2$ changes only slightly, it is obvious that, as before with variations in V_r, the dominant geometric influence on S_r is the reduction of Weff.

The variation of S_a with the applied base current is presented in Fig. 5-23a. As with the other bias parameters as I_B approaches I_{Bc} and W_{eff} tends to zero the absolute sensitivity increases sharply. The influence of I_B on S_r is presented in Fig. 6-24. These results are in agreement with equation (5.58) (K_B = 1.0), and confirm the existence of I_{Bc}, with S_r being at a maximum at $I_B \approx I_{Bc}$ and decreasing as I_B is increased. It is apparent that as a larger negative potential is applied to the p^+ stripes it is necessarily to have a larger I_B to open up a path for the lateral flow of electrons. W_{eff} and $L_1 + L_2$ are plotted in Fig. 6-25 as a function of I_B and again there is little variation in the sum $L_1 + L_2$ and W_{eff} governs the behavior of S_r.

In Fig. 5-26 the variation in the relative and absolute sensitivities with V_C is shown respectively. Fig. 5-26a shows S_a to be a slightly increasing function of V_C. The increase in S_a follows the increase in I_C In Fig. 5-26b S_r displays a slight drop as V_C is increased. This indicates that the increase in ΔI_C is not as great as that of increase in I_C due to the Early effect.

The results presented above reveal the SSIMT to be a highly sensitive magnetic sensor with a linear response to the magnetic field. The analytical model developed in chapter 4 appears to describe the operation of the device well and the

theoretical dependance of S_r on the bias conditions compares well with the measured data.

5.4 Device geometry variation

In order to optimize the operation of the SSIMT a variety of devices were manufactured in a 5 μm process. A number of devices with differing emitter geometries were fabricated to analyze the geometrical aspects of the electron injection into the base. Devices were also fabricated with increasing base widths to facilitate an analysis of the deflection mechanism in the magnetic operation of the SSIMT.

5.4.1 Emitter geometry variation

To provide a basis of comparison with the 4 μm device presented in the previous section an almost identical device was fabricated using the 5 μm process. The electrical and magnetic characteristics of this device are presented in the Fig. 5-27. A comparison of these figures with the comparable ones in section 5.2.2 shows that the device operates in the same manner. As before two modes of operation are evident, with the lateral transistor turning on at a particular base current, I_{Bc}. The base voltage (Fig. 5-27b) displays the same dramatic drop as electrons start to be injected into the base region. Fig. 5-27a shows I_S as a function of I_B and it would appear that for this device the vertical transistor turns on at the same base current as the lateral transistor. This is in contrast to the 4 μm device where the vertical transistor turned on before the lateral one.

Magnetic characteristics are shown in Fig. 5-27c and 5-27d. Both the absolute and relative sensitivities display a very similar behavior to that measured

for the 4 μm devices, with a strongly peaked response being observed at the critical base current.

Fourteen devices were manufactured of differing emitter geometries varying in size from a 20X20 μm emitter to a 100X60 μm emitter. The measured collector current, I_{C0}, at a particular bias point showed little variation with the emitter geometry. This is expected as the magnitude of the collector current is basically determined by the base width and the positions of the planes X_1 and X_2.

The critical base current at which the device turns on I_{Bc} did, however, show a strong dependance on the emitter geometry. In Fig. 5-28 I_{Bc} is presented as a function of the area A_E of the emitter. There would appear to be a strong correlation between A_E and I_{Bc}. This can be explained as consequence of the following fact. As A_E is reduced the effective resistance of the base increases, due to the reduction in the volume through which the base current flows. This increase in base resistance means that a larger base current is required to produce the potential needed to forward bias the emitter/base junction.

The effect of the emitter geometry on the magnetic response of the SSIMT was also analyzed. In Fig. 5-29 the absolute sensitivity is shown as a function of the emitter length, L_E, for both the square emitter devices and the devices where W_E was kept constant. It is clearly seen that S_a drops off sharply for the larger emitter devices and a peak in S_a is observed with an emitter of approximately 30 μm long. An example of the collector current response of the devices with varying L_E is presented in Fig. 5-30. In this figure ΔI_C is shown as function of B for devices with emitters varying in length from 100 μm to 20 μm. All devices exhibit a linear behavior with respect to the magnetic field. The smaller the emitter length the

larger the current response to the magnetic field. The absolute sensitivity of the device was found to be relatively unaffected by changes in W_E.

In Fig. 5.31 and Fig. 5.32 the relative and absolute sensitivities of all the devices are shown as a function of the emitter area. These graphs indicate a general trend of increasing sensitivity as the emitter size is decreased. This implies the presence of a higher current density of the laterally flowing electron current for smaller geometries.

To analyze the effect of increasing the base width of the SSIMT, devices were fabricated with base widths of 10, 20, 30, 40 and 50 μm. S_a is found to be an increasing function of W_B as is expected from equation (4.14).

5.5 DC zero field offset control

An important aspect of the performance of magnetic field sensors is DC resolution, the minimum DC magnetic field that can be detected. The zero field offset B_{off} of the magnetic sensor determines this resolution and the ability to minimize this offset is desirable. The SSIMT, when operated with stripes biased, offers the possibility of annulling B_{off} by applying slightly different potentials to each of the p^+ stripes [56]. This procedure allows for the compensation of asymmetries in the device due the fabrication process.

The investigation of the current offset when both of the p^+ stripes are at the same potential V_r shows that the offset increases with V_r increasing (see Fig. 5-33). This can be explained as follows: when the negative value of V_r increases, the effective width of the current flow out to each collector is reduced, the collector

currents I_{C10} and I_{C20} decrease and the influence of imperfections in the device structure on the offset becomes more pronounced.

A graph of the potential difference $\Delta V_r = |V_{r2} - V_{r1}|$ needed to eliminate B_{off} is presented in Fig. 5-34. These results show that a smaller potential difference is needed to annul the offset as V_r is increased, indicating that as W_{eff} is forced smaller changes in V_r have a greater effect.

The minimum detectable magnetic field is determined by the sensitivity of the device and the zero field offset, ΔI_{C0}. The exploitation of the very high sensitivities of the SSIMT and the ability to annul the zero field offset allow for the reduction of the minimum detectable DC field to the order of 200 μT.

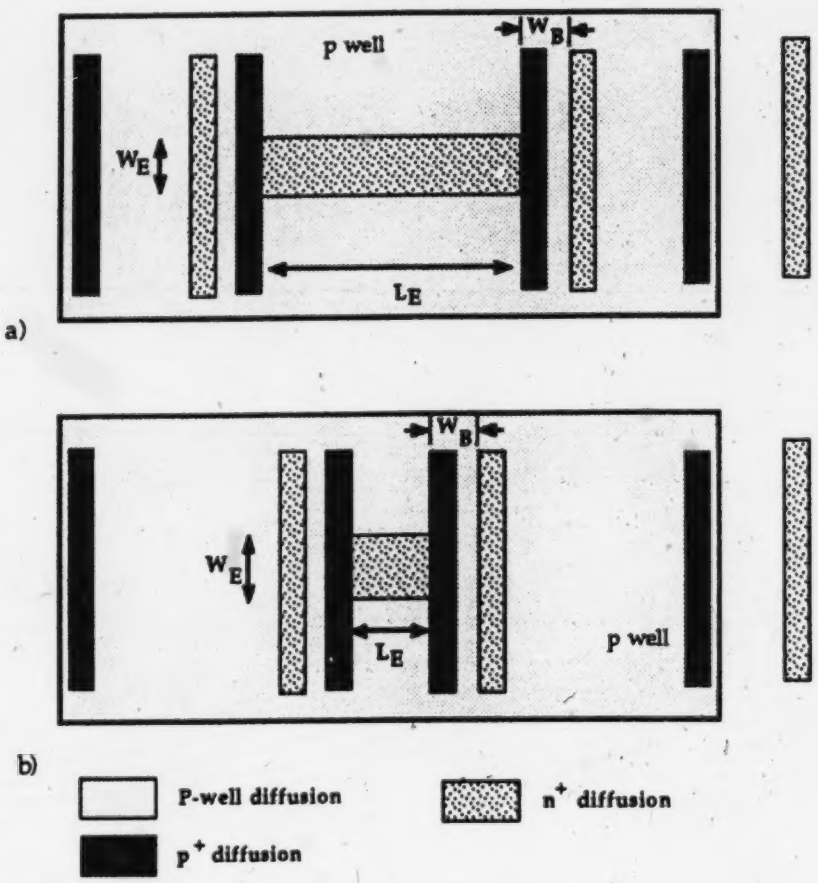

Fig. 5-1 SSIMT emitter structure a) 30X100 μm
b) 30 X 30 μm

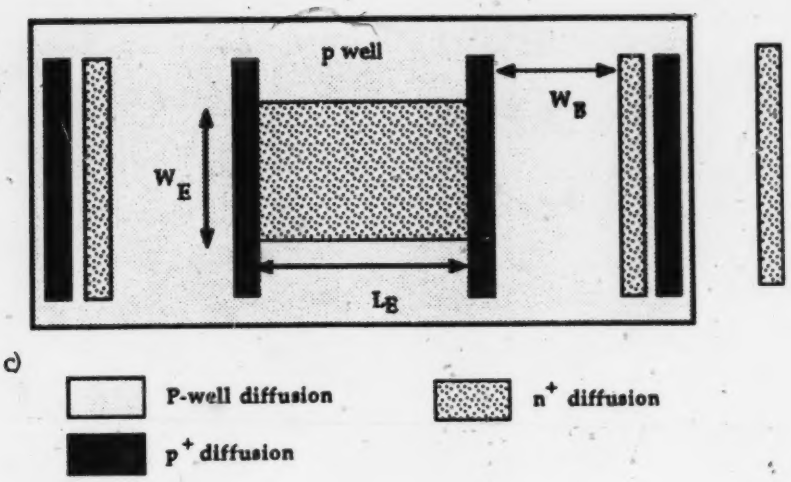

Fig. 5-2 SSIMT 50 μm base width

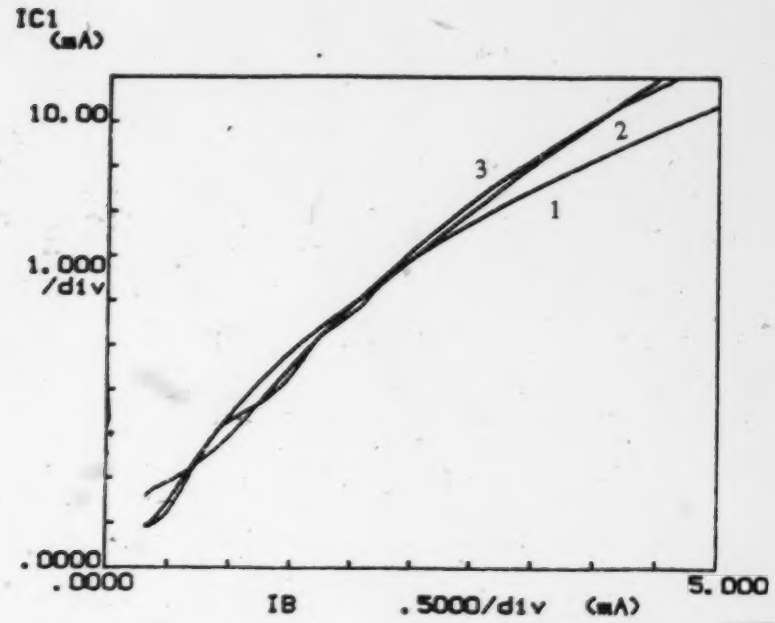

Fig. 5-3 I_C as a function of I_B for the LMT with stripes floating and $V_C = 5$ V. 1) $V_S = 5$ V. 2) $V_S = 10$ V. 3) $V_S = 15$ V.

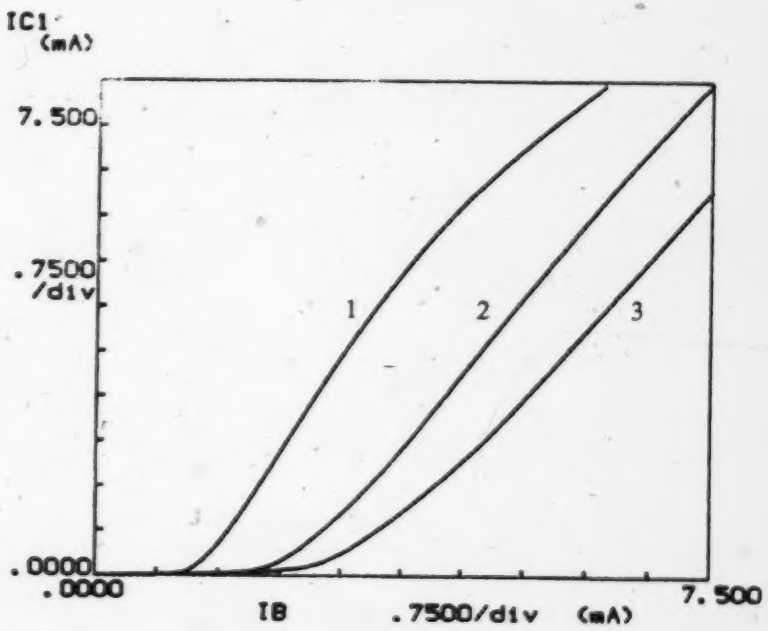

Fig. 5-4 I_C as a function of I_B for the SSIMT with stripes floating and $V_C = 5$ V. 1) $V_S = 5$ V. 2) $V_S = 10$ V. 3) $V_S = 15$ V.

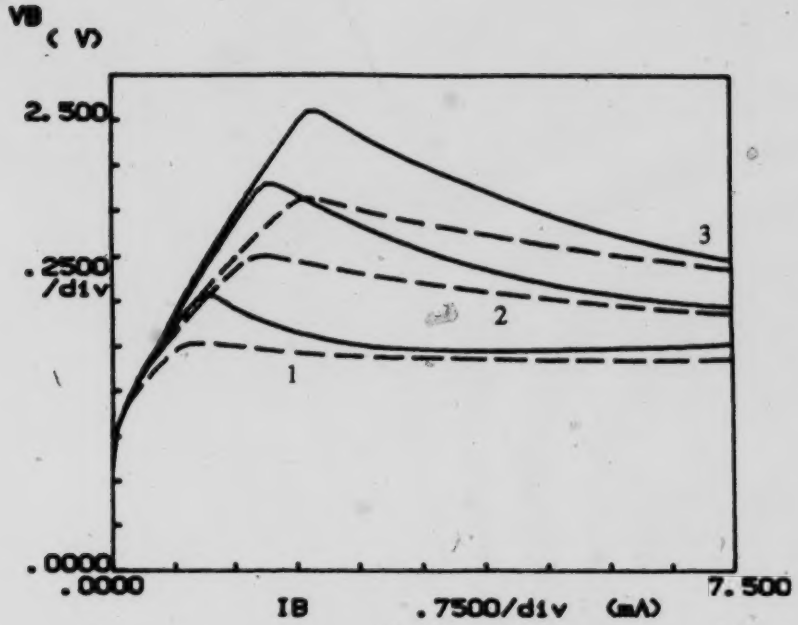

Fig. 5-5 V_B as a function of I_B for both the LMT (dashed) and the SSIMT with stripes floating (solid) V_C = 5 V. 1) V_S = 5 V. 2) V_S = 10 V. 3) V_S= 15 V.

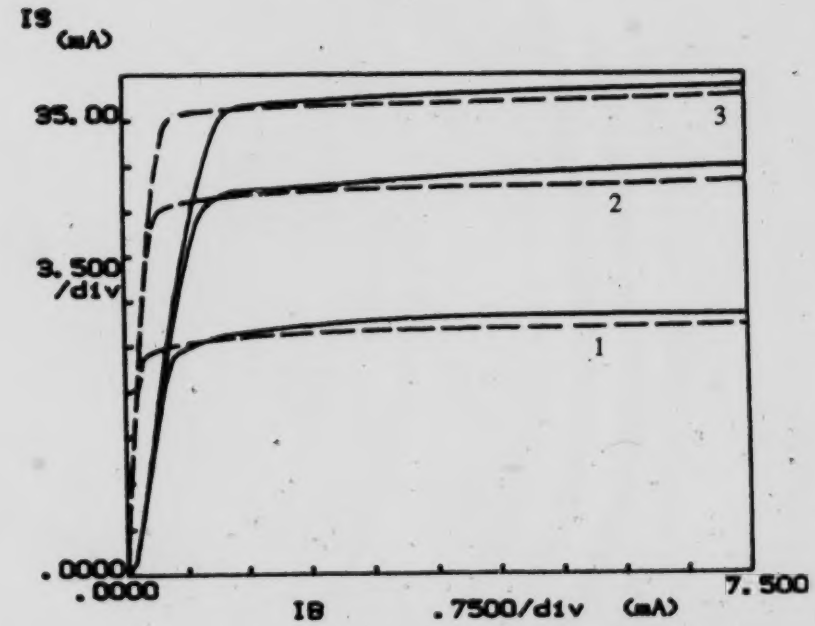

Fig. 5-6 I_S as a function of I_B for both the LMT (dashed) and the SSIMT with stripes floating (solid) V_C = 5 V. 1) V_S = 5 V. 2) V_S = 10 V. 3) V_S = 15 V.

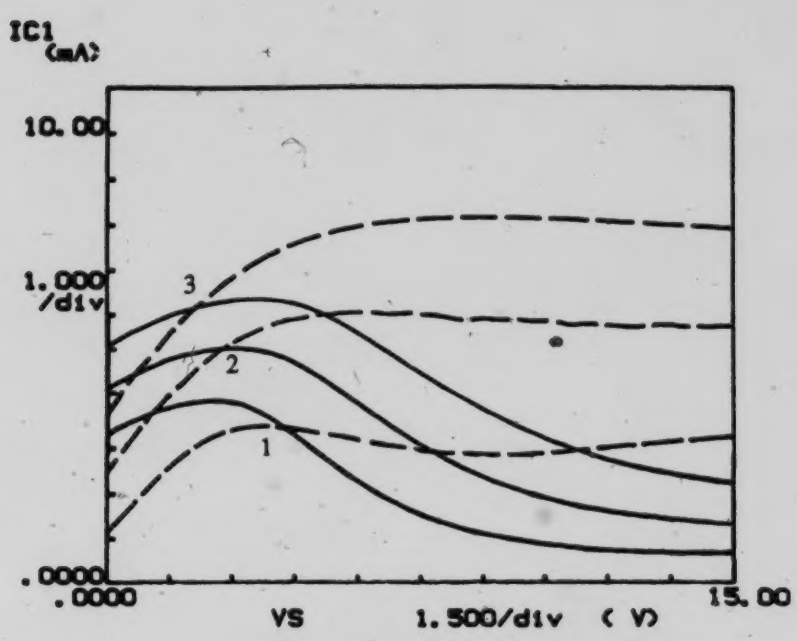

Fig. 5-7 I_C as a function of V_S for both the LMT (dashed) and the SSIMT with stripes floating (solid) V_C = 5 V. 1) I_B = 1 mA. 2) I_B =2 mA. 3) I_B =3 mA.

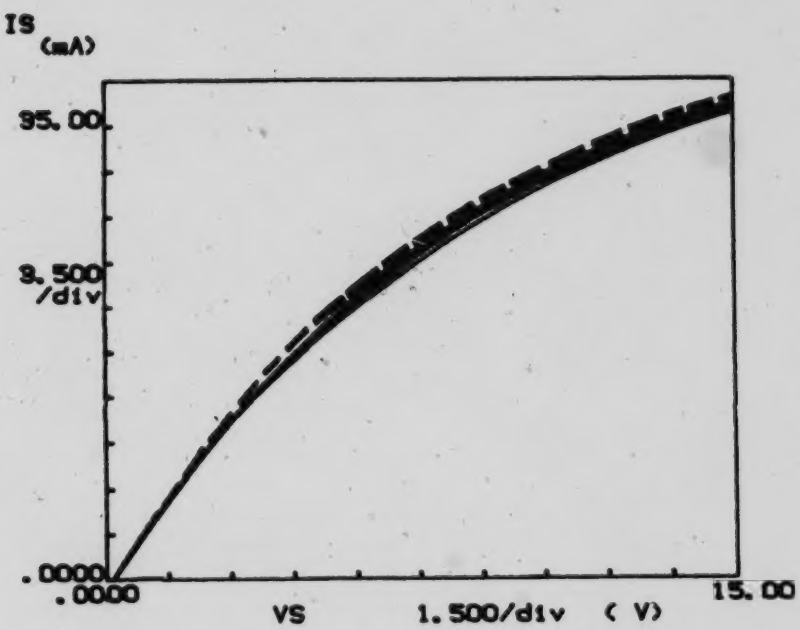

Fig. 5-8 I_S as a function of V_S for both the LMT (dashed) and the SSIMT with stripes floating (solid) V_C = 5 V. 1) I_B = 1 mA. 2) I_B =2 mA. 3) I_B = 3 mA.

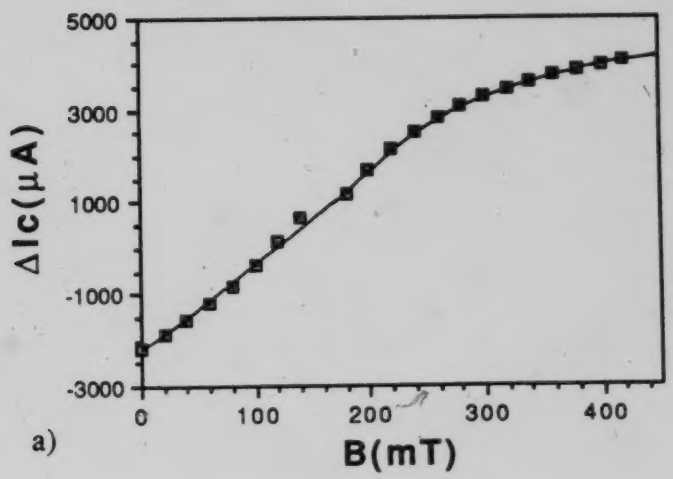

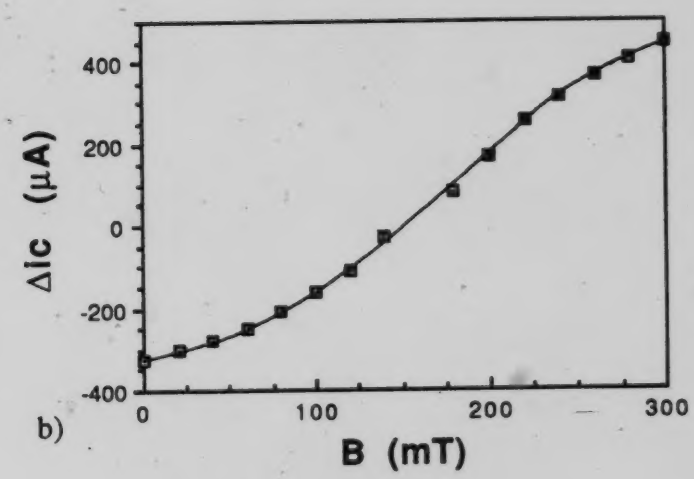

Fig 5-9 a) Current response, ΔI_C, of LMT as a function of B V_C = 5 V, I_B = 1 mA, V_S = 15 V. b) Current response, ΔI_C - ΔI_{C0}, of SSIMT with stripes floating as a function of B V_C = 5 V, I_B = 1 mA, V_S = 15 V.

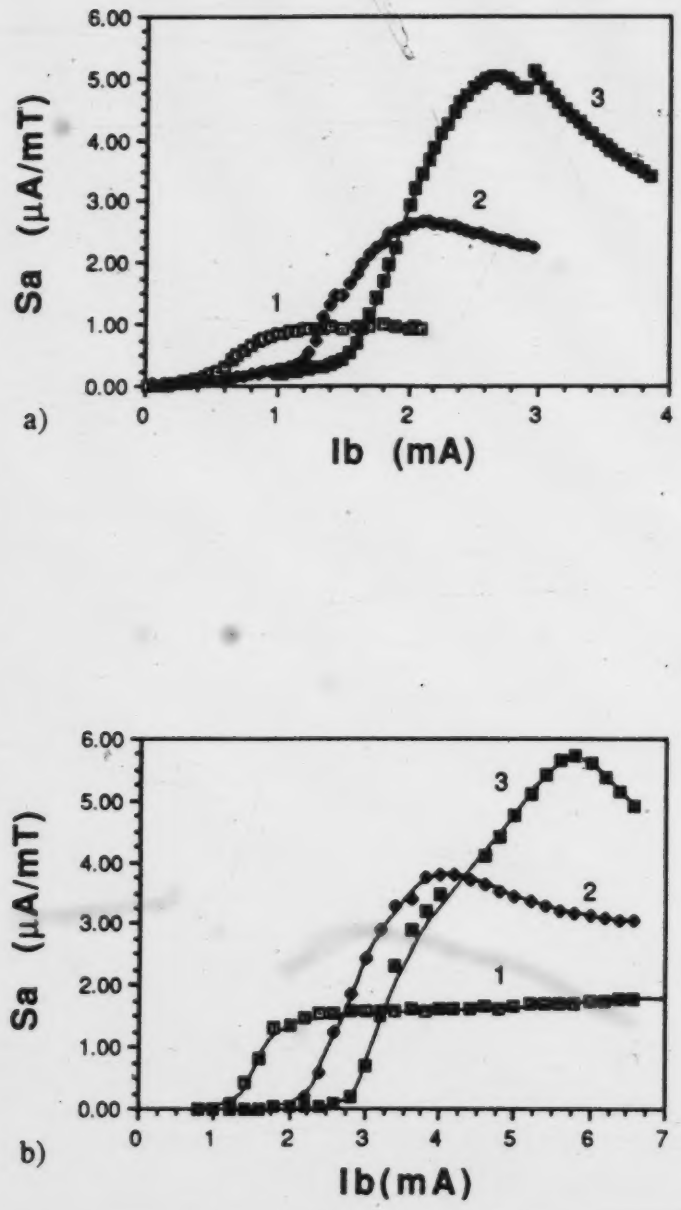

Fig. 5-10 Absolute sensitivity versus I_B, B= 30 mT, V_C = 5 V a) LMT b) SSIMT. 1) V_S = 5 V, 2) V_S = 10 V, 3) V_S = 15 V.

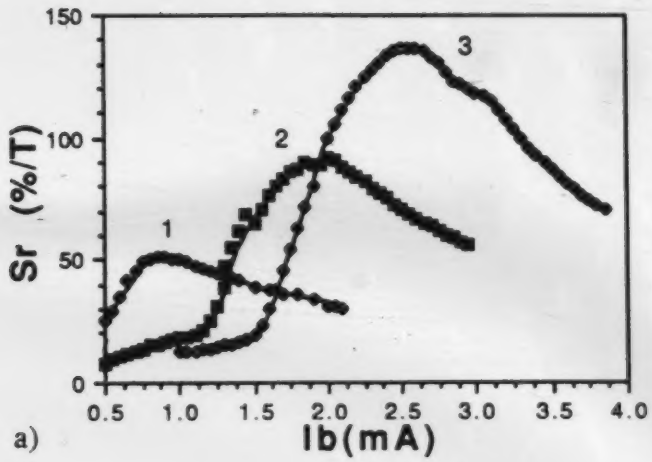

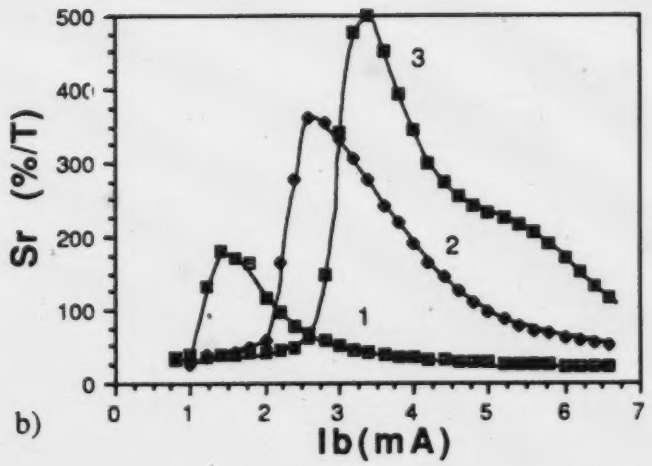

Fig. 5-11 Relative sensitivity versus I_B, V_C = 5 V
a) LMT V b) SSIMT. 1) V_S = 5 V, 2) V_S = 10 V, 3) V_S = 15 V.

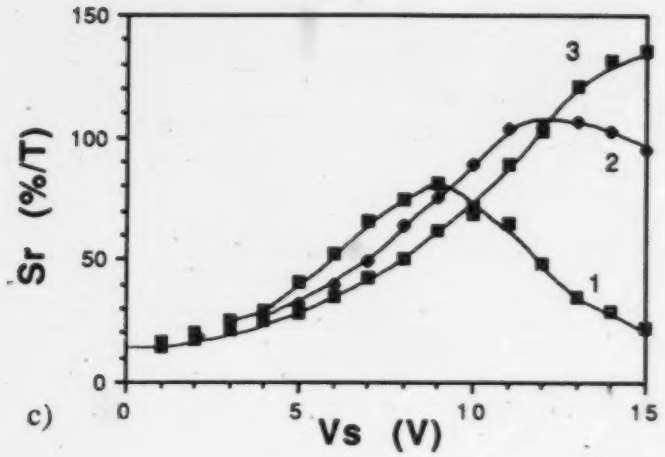

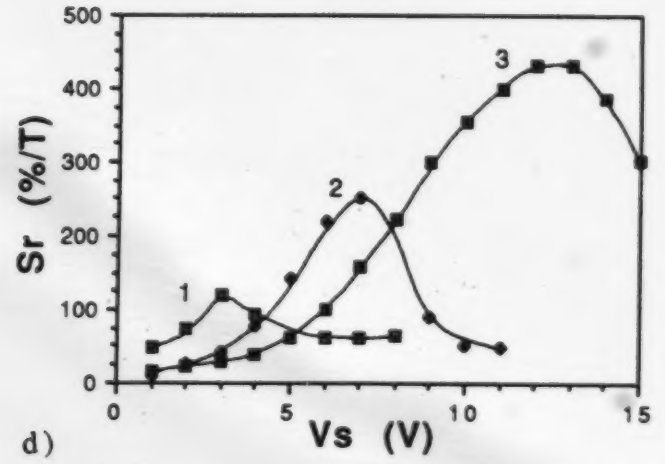

Fig. 5-11 Relative sensitivity versus V_S, V_C = 5 c) LMT V
d) SSIMT. 1) I_B = 1 mA, 2) I_B = 2 mA 3) I_B = 3 mA.

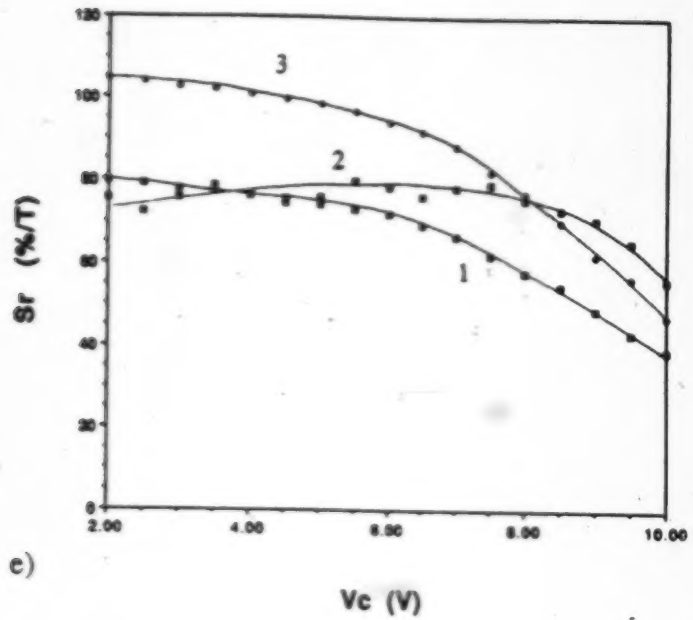

e)

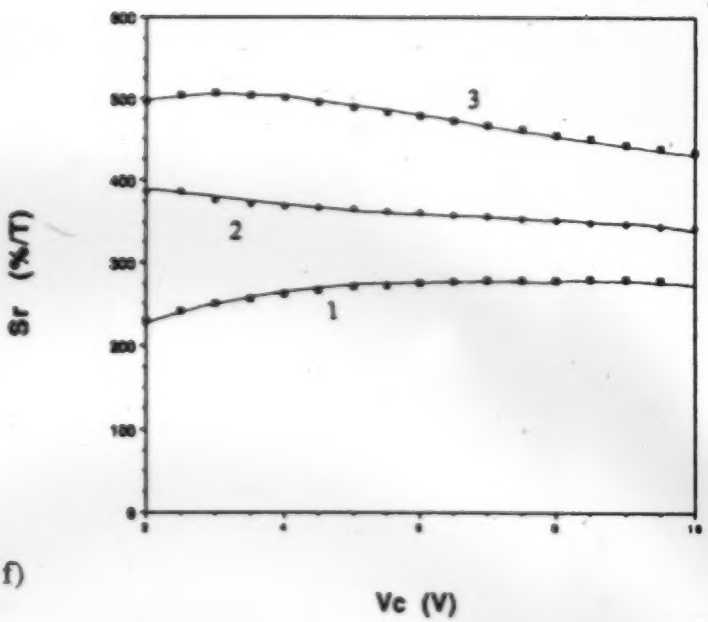

f)

Fig. 5-11 Relative sensitivity versus V_C, V_S = 10 e) LMT
f) SSIMT. 1) I_B = 1 mA, 2) I_B = 2 mA 3) I_B = 3 mA.

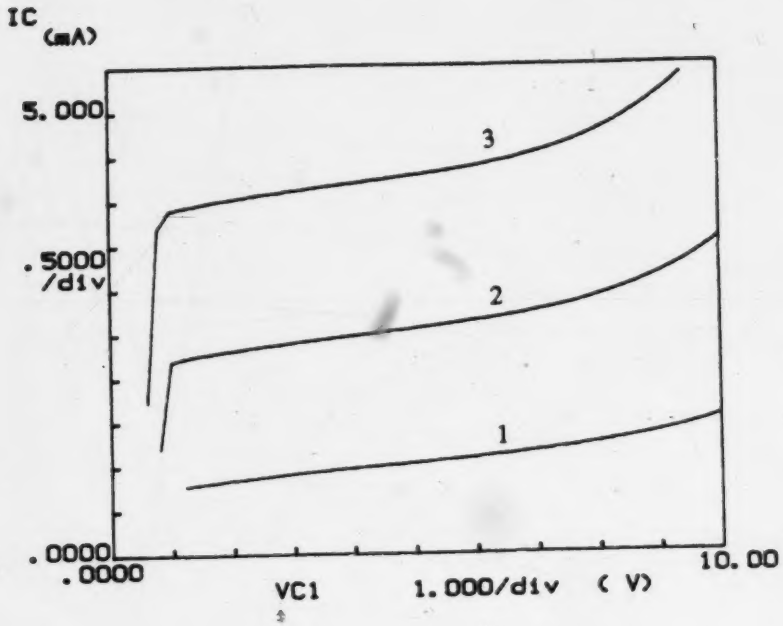

Fig. 5-12 I_C as a function of V_C, V_S = 5 V, V_r = 0 V:
1) I_B =6 mA, 2) I_B = 8 mA, 3) I_B = 10 mA.

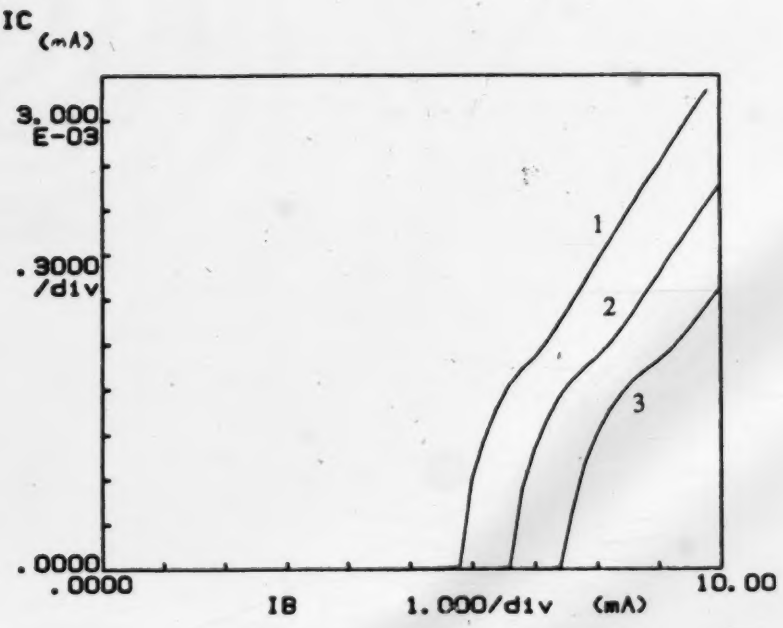

Fig. 5-13 I_C as a function of I_B, V_S = 5 V, V_C = 5 V:
1) V_r = 0.0 V, 2) V_r = -0.2 V, 3) V_r = -0.4 V.

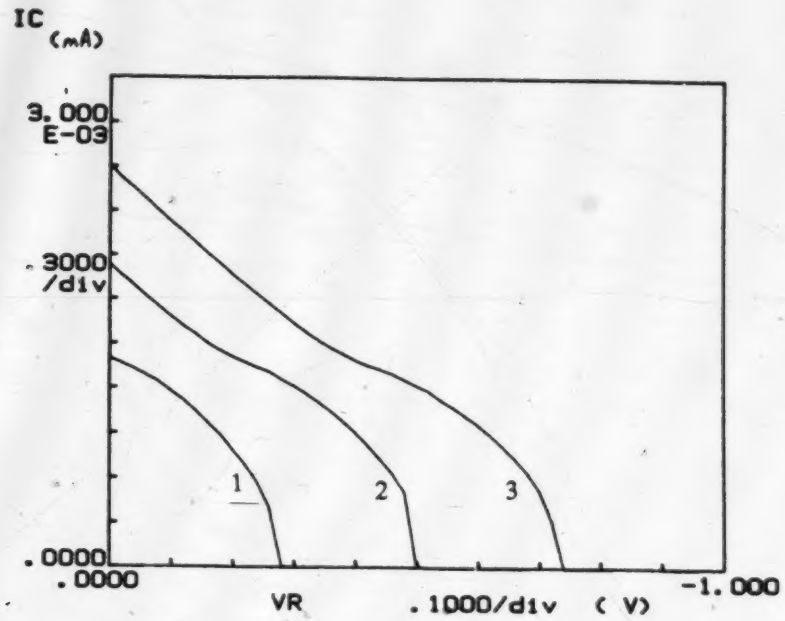

Fig. 5-14 I_C as a function of V_r, V_S = 5 V, V_C = 5 V: 1) I_B =7 mA, 2) I_B = 8 mA, 3) I_B =9 mA.

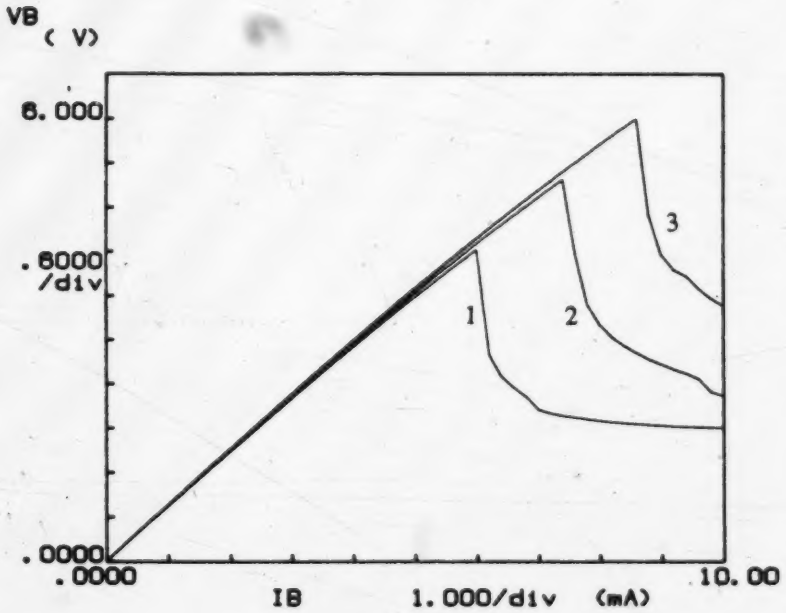

a)

Fig. 5-15 a) V_B as a function of I_B, V_r = 0 V, V_C = 5 V: 1)V_S = 5 V, 2) V_S = 10 V, 3) V_S = 15 V.

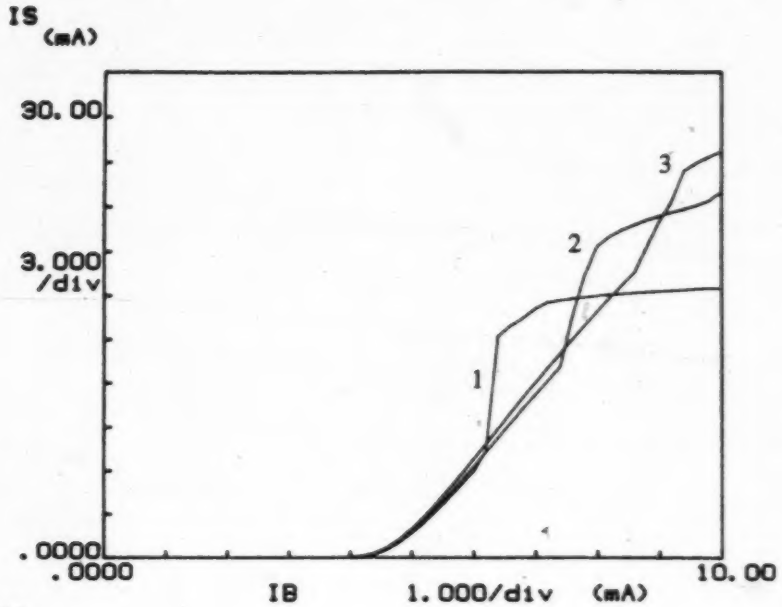

b)

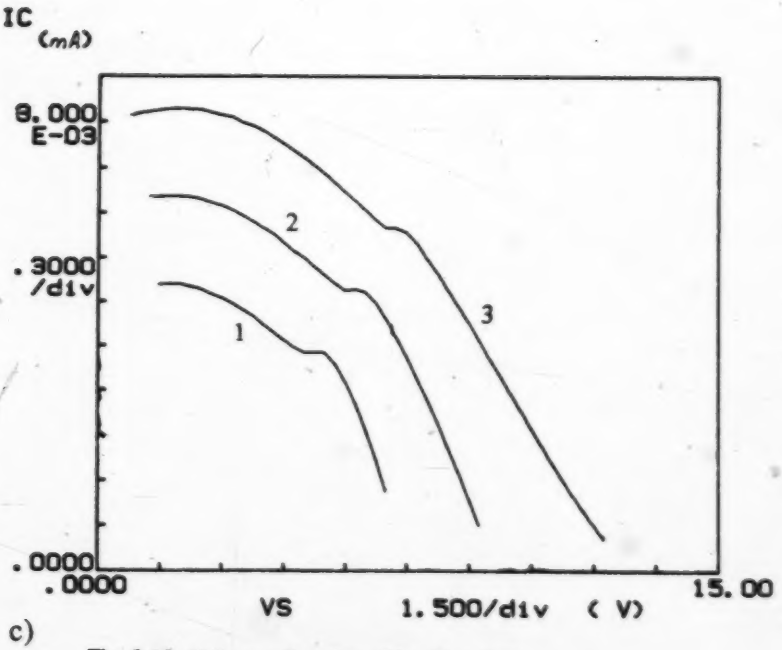

c)

Fig. 5-15 b) I_S as a function of I_B, $V_r = 0$ V, $V_C = 5$ V: 1) $V_S = 5$ V, 2) $V_S = 10$ V, 3) $V_S = 15$ V.
c) I_C as a function of V_S, $V_r = 0$ V, $V_C = 5$ V: 1) $I_B = 7$ mA, 2) $I_B = 8$ mA, 2) $I_B = 9$ mA.

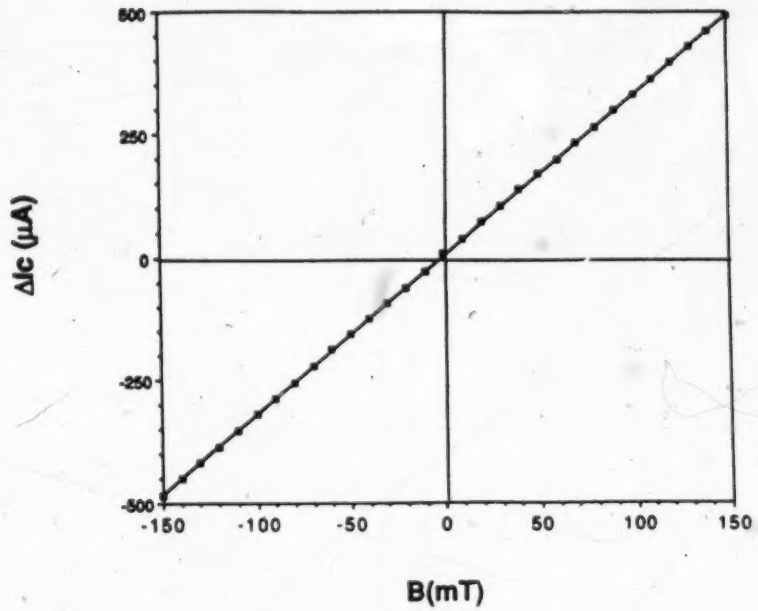

a)

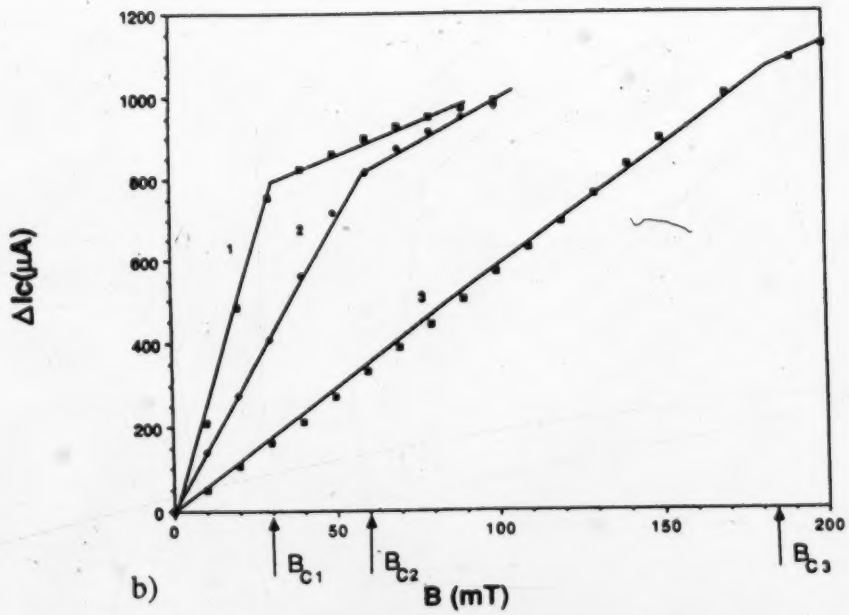

b)

Fig. 5-16 Collector current response as a function of the applied magnetic field. a) V_S = 5 V, V_r = -0.25 V, I_B = 8.5 mA, V_C = 5 V. b) V_S = 5 V, I_B = 7 mA, V_C = 5 V: 1) V_r = -198 mV, 2) V_r = -193 mV, 3) V_r = -150 mV.

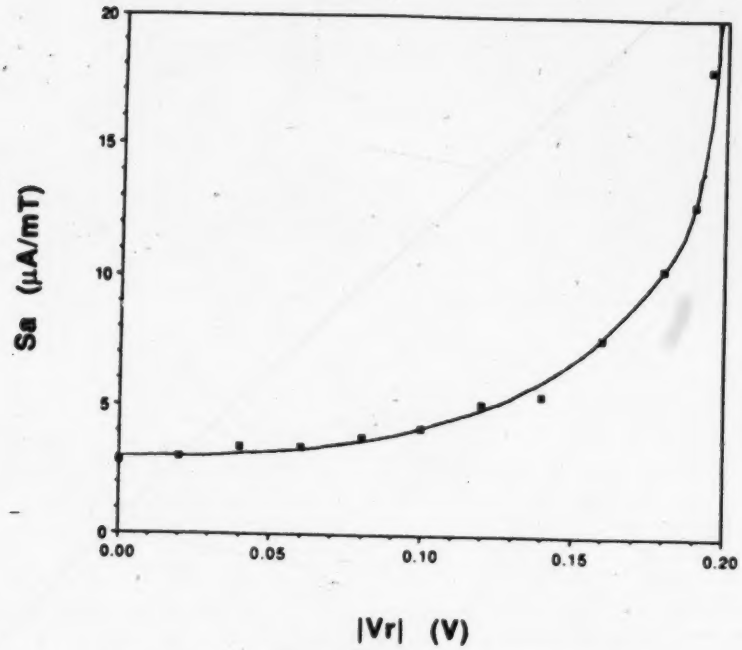

Fig 5-17 Absolute sensitivity versus stripe potential, $V_S = 5$ V, $I_B = 7$ mA, $V_C = 5$ V, B = 30 mT.

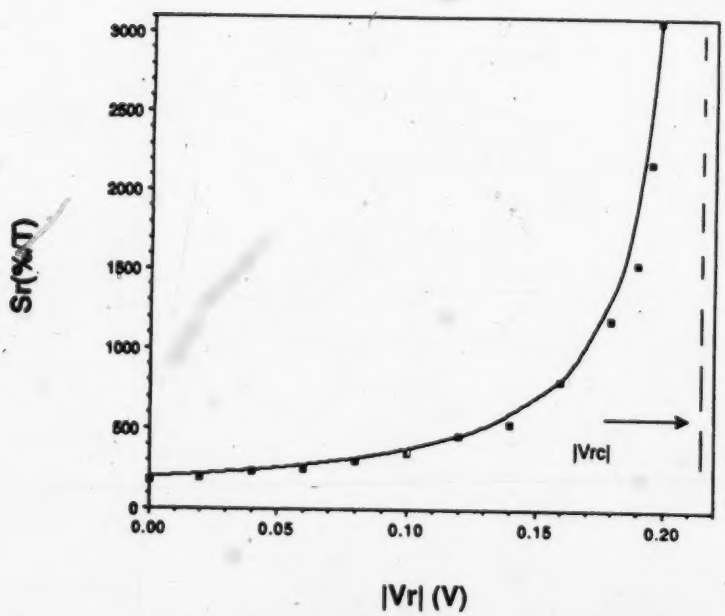

Fig 5-18 Relative sensitivity versus stripe potential, $V_S = 5$ V, $I_B = 7$ mA, $V_C = 5$ V, B = 30 mT. Theory shown in solid.

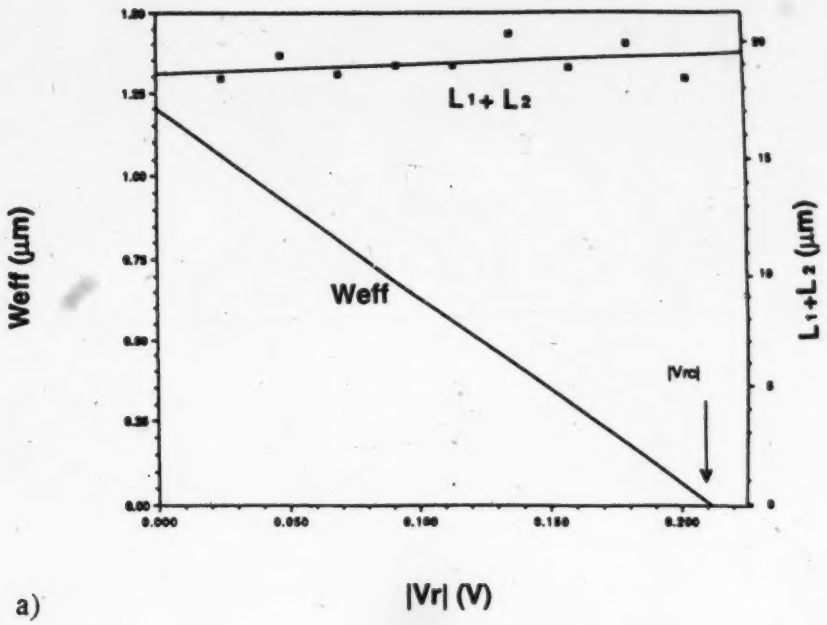

a)

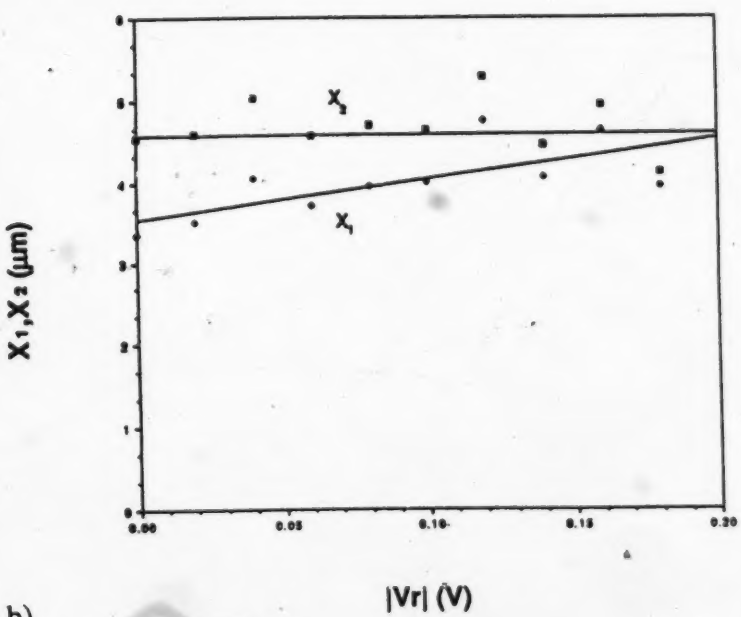

b)

Fig. 5-19 a) W_{eff} and $L_1 + L_2$ as a function of V_r. b) X_1 and X_2 as a function of V_r. Bias conditions as in Fig. 6-18.

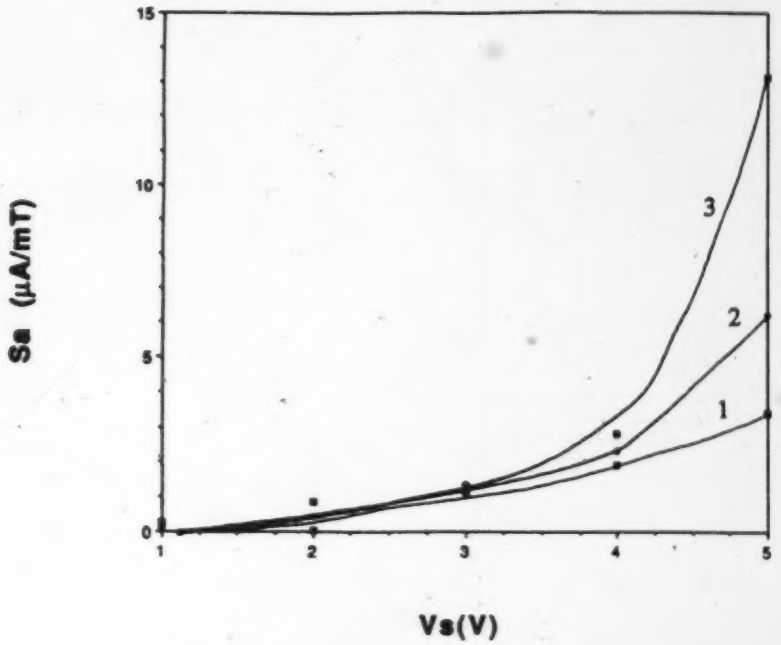

Fig 5-20 Absolute sensitivity versus V_S , I_B = 7 mA, V_C = 5 V, B = 30 mT. 1) V_r = 0.0 mV, 2) V_r =-50 mV, 3) V_r =-100 mV.

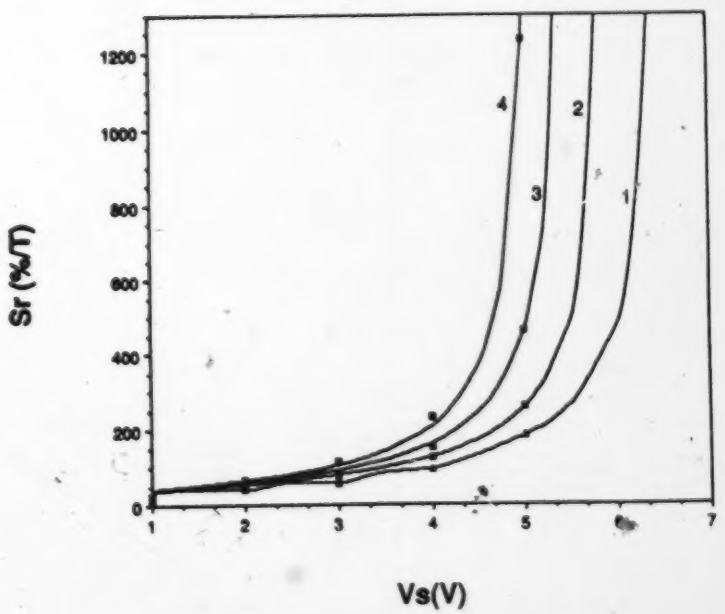

Fig 5-21 Relative sensitivity versus V_S , I_B = 7 mA, V_C = 5 V, B = 30 mT. 1) V_r = 0.0 mV, 2) V_r =-50 mV, 3) V_r =-100 mV, 4) V_r = -180 mV. Theory shown in solid

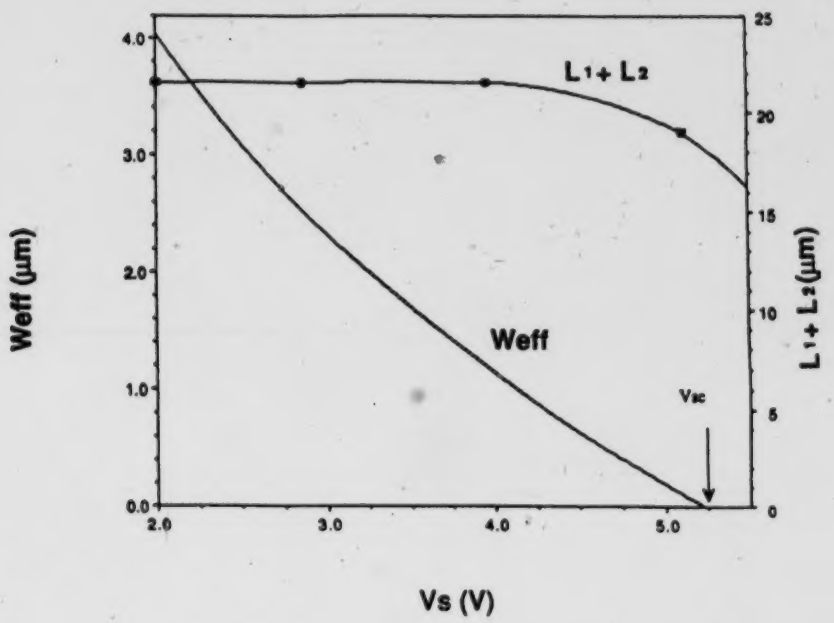

Fig. 5-22 a) W_{eff} and $L_1 + L_2$ as a function of V_r. I_B = 7 mA, V_C = 5 V, V_r = -180 mV.

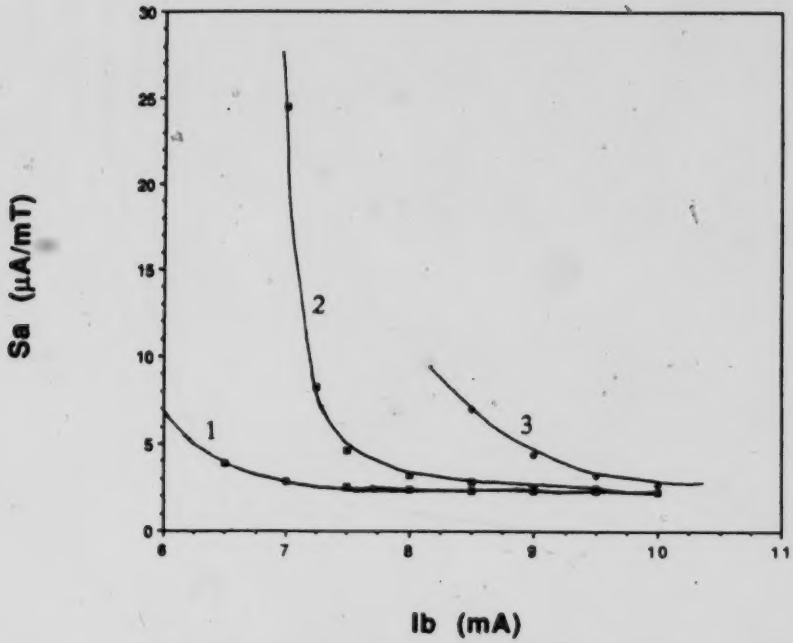

Fig 5-23 Absolute sensitivity versus I_B , V_S = 5 V, V_C = 5 V, B = 30 mT. 1) V_r = 0.0 mV, 2) V_r =-198 mV, 3) V_r =-460 mV

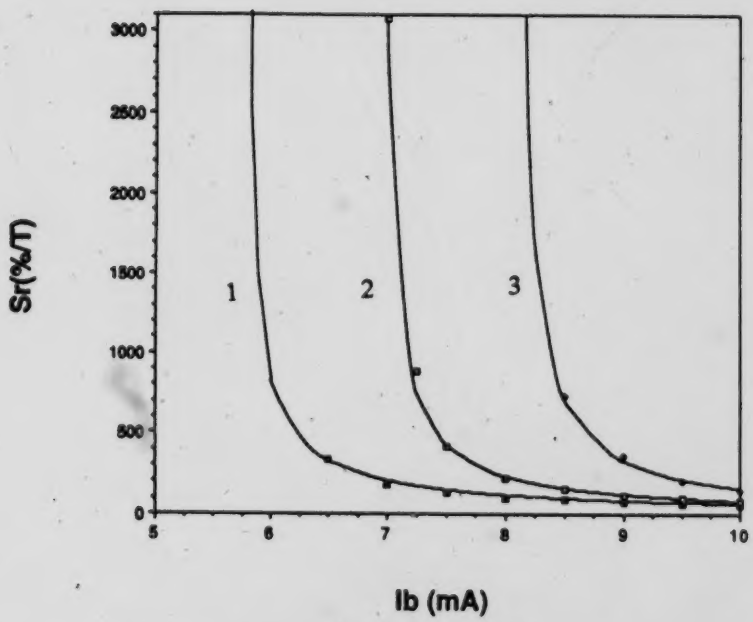

Fig 5-24 Relative sensitivity versus I_B , V_S = 5 V, V_C = 5 V, B = 30 mT. 1) V_r = 0.0 mV, 2) V_r =-198 mV, 3) V_r =-460 mV. Theory shown in solid.

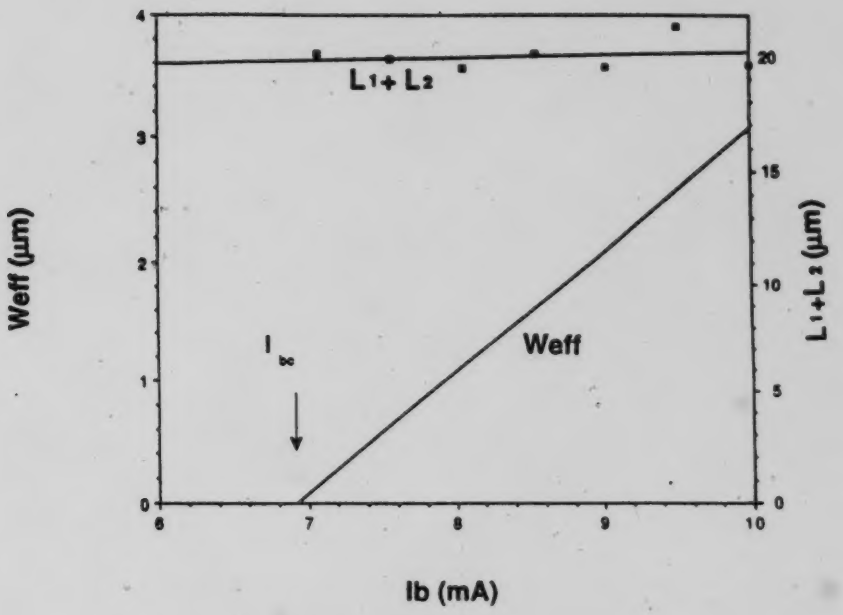

Fig. 5-25 a) W_{eff} and $L_1 + L_2$ as a function of I_B. V_S = 5 V, V_C = 5 V, V_r = -198 mV.

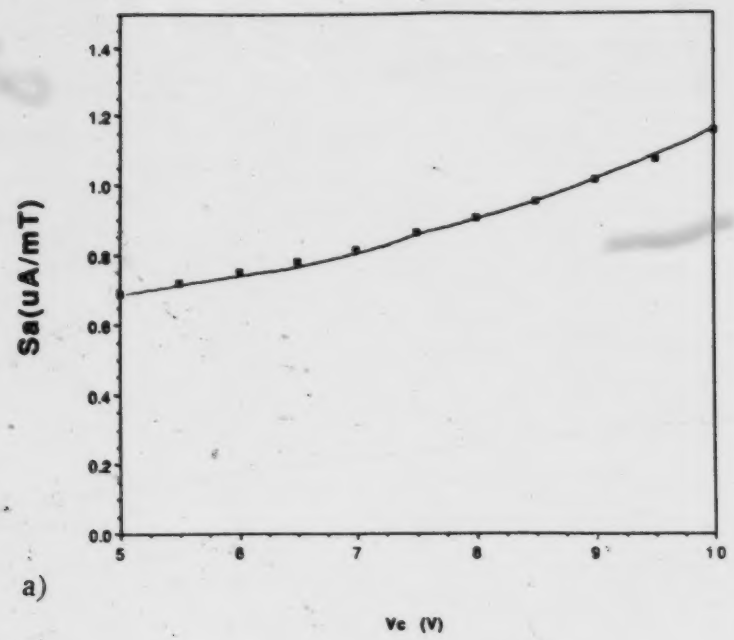

a)

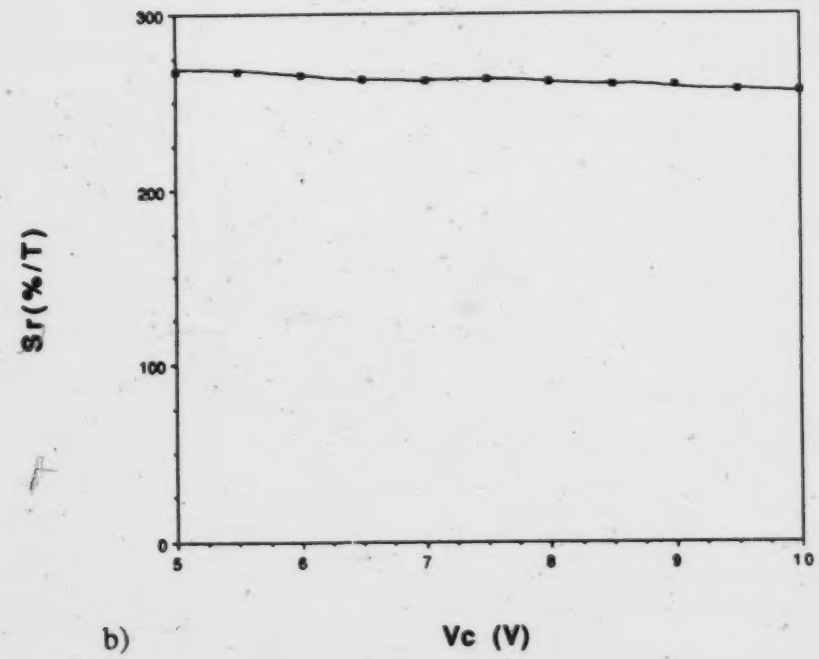

b)

Fig 5-26 a) Absolute sensitivity versus V_C. b) Relative sensitivity versus V_C. $V_S = 5$ V, $V_r = 0$ V, B = 30 mT, $I_B = 8$ mA.

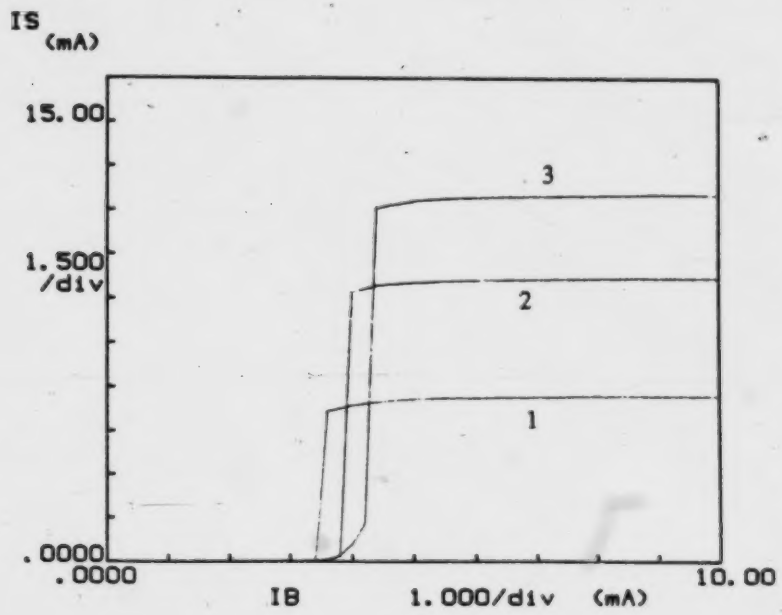

a)

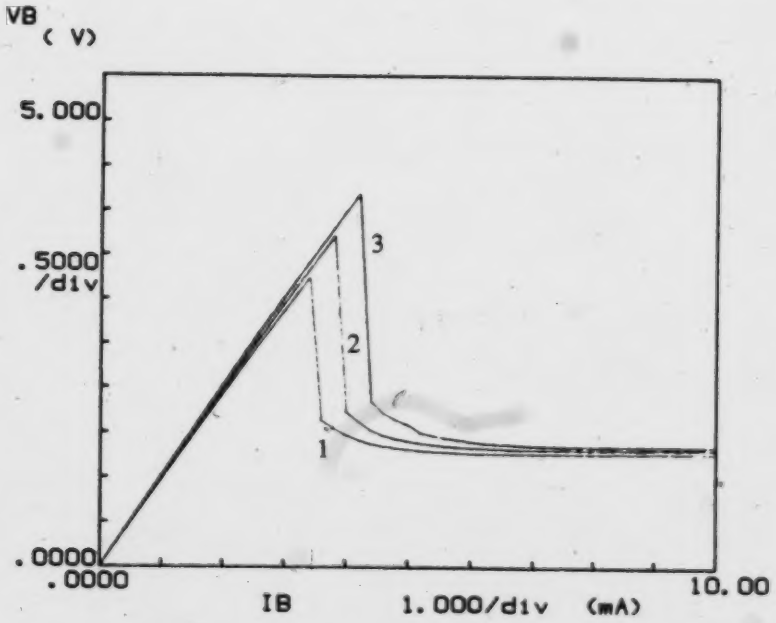

b)

Fig. 5-27 Electrical and magnetic characteristics of 5 μm SSIMT
a) I_S versus I_B, b) V_B versus I_B, c) S_r versus I_B, d) S_a versus I_B, V_r = 0 V, V_C = 5 V, 1) V_S = 5 V, 2) V_S = 10 V, 3) V_S = 15 V.

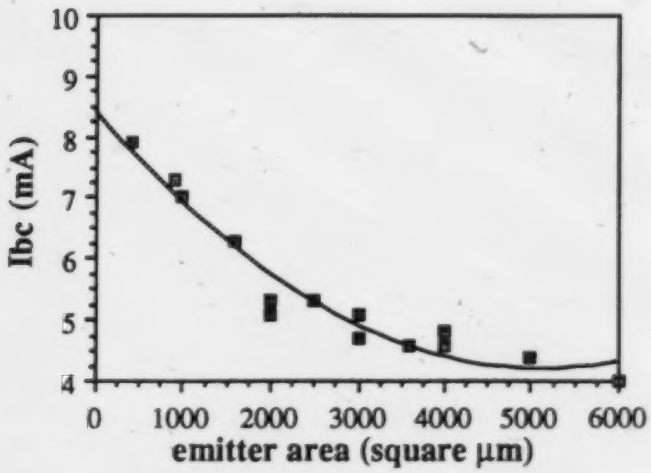

Fig. 5-28 I_{Bc} as a function of A_E V_S = 15 V, V_C = 5 V, I_B = 10 mA, V_r = 0.0 V

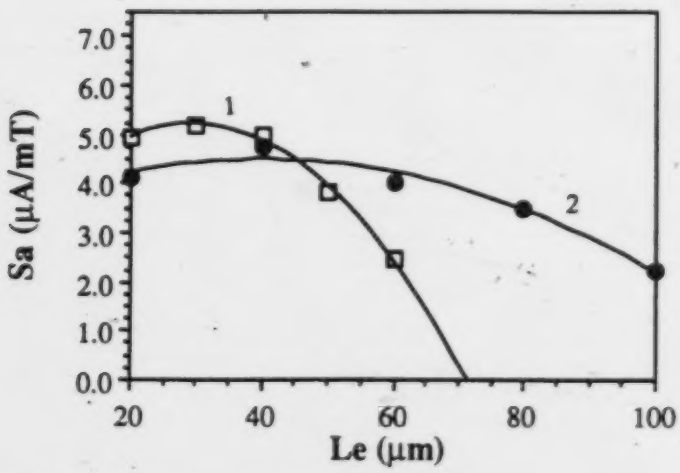

Fig. 5-29 S_a as a function of L_E, V_S = 15 V, V_C = 5 V, I_B = 10 mA, V_r = 0.0 V 1) square devices 2) devices for which W_E is a constant.

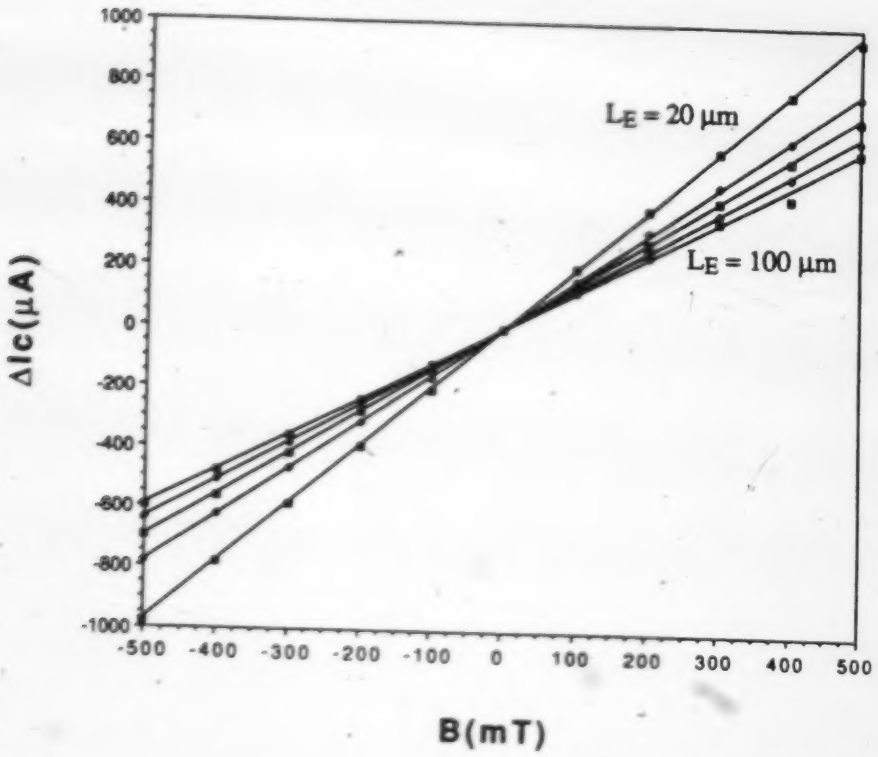

Fig. 5-30 ΔI_C as a function of B, V_S = 5, I_B = 1 mA, stripes floating, V_S = 5 V. L_E = 20, 40, 60, 80 and 100 μm.

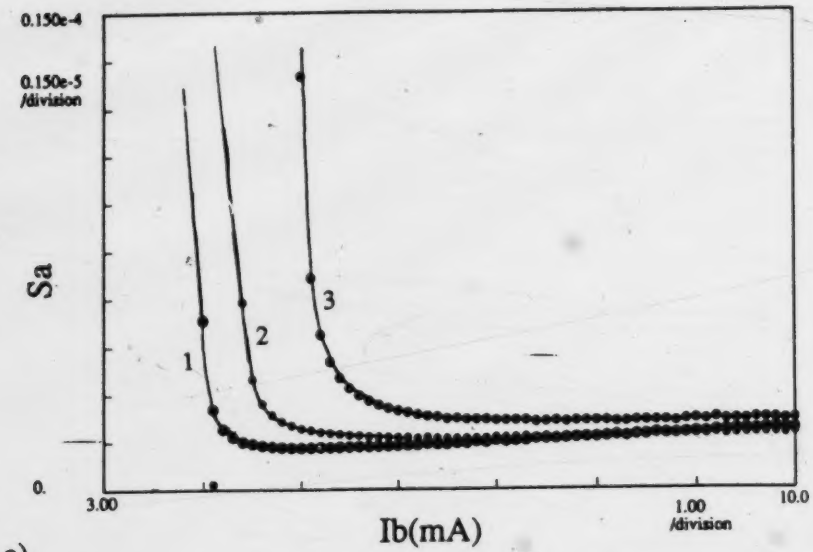
0.150e-4
0.150e-5
/division
Sa
0.
1
2
3
3.00
10.0
1.00
/division
Ib(mA)

c)

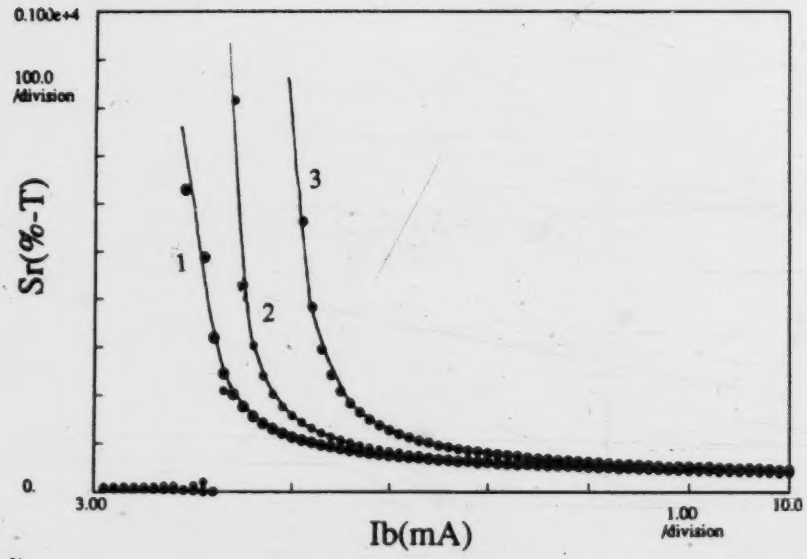
0.100e+4
100.0
/division
Sr(%-T)
0.
1
2
3
3.00
10.0
1.00
/division
Ib(mA)

d)

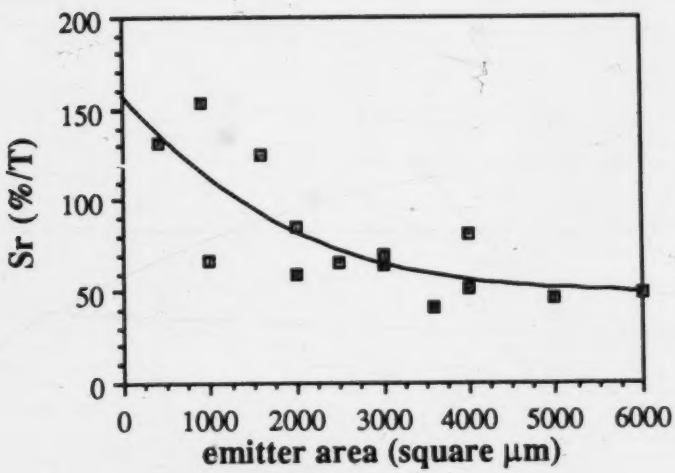

Fig. 5-31 S_r as a function of A_E V_S = 15 V, V_C = 5 V, I_B = 10 mA, V_r = 0.0 V

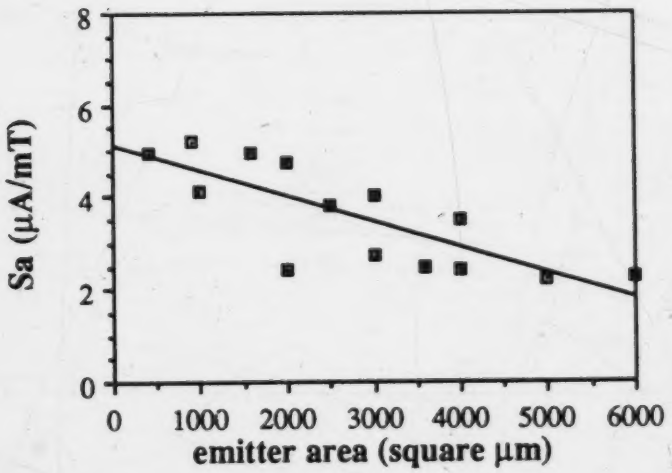

Fig. 5-32 S_a as a function of A_E V_S = 15 V, V_C = 5 V, I_B = 10 mA, V_r = 0.0 V

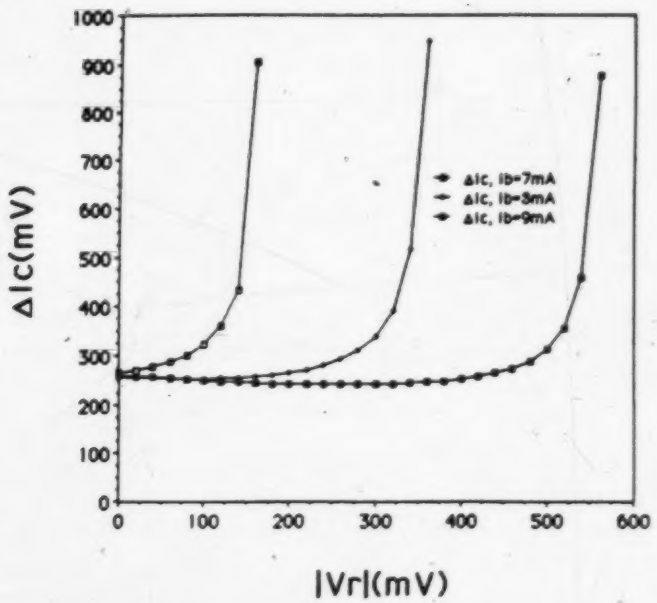

Fig. 5-33 The offset as a function of V_r when both p^+ stripes are at the same potential. $V_C = 5$ V, $V_S = 5$ V.

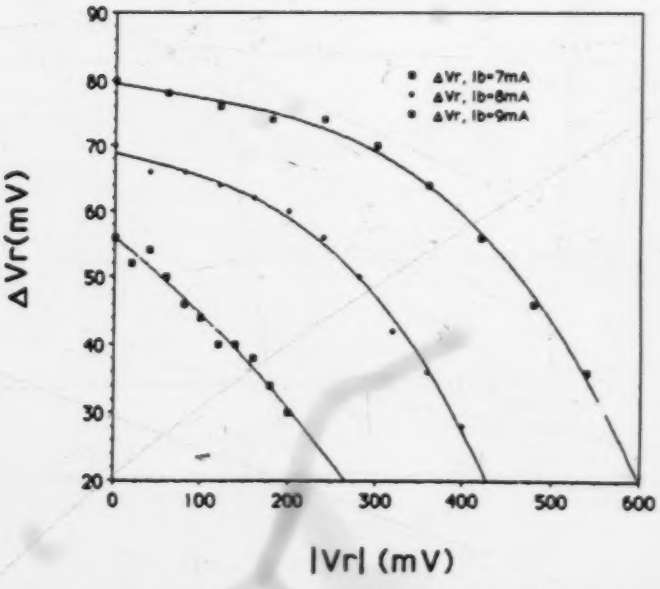

Fig. 5-34 The potential difference as a function of V_r for offset elimination. $V_C = 5$ V, $V_S = 5$ V.

6.0 On the injection modulation effect

The complicated nature of magnetotransistor operation has lead to some disagreement about the relative roles of the mechanisms outlined in sections 3.1, 3.2 and 3.3. In particular the magnitude of the emitter modulation effect has been questioned [13, 32, 33]. The theory of SSIMT operation given in chapter 4 presumed that carrier deflection of the minority carriers was the dominant mechanism and confirmation of this assumption is needed. The presence of the p^+ stripes in the SSIMT provides the opportunity of testing this assumption and analyzing the relative roles of the two mechanisms [6].

In order to estimate the importance of emitter modulation in the device operation the SSIMT is operated with stripes floating, and the voltage difference between the two p^+ stripes is measured as a function of the magnetic field. This voltage essentially gives us an indication of the value of the Hall field produced in the base region along the emitter/base junction due to the flow of holes across the emitter junction. We can then calculate the approximate current change due to this asymmetrical injection and compare it to the actual measured change in current.

The first two sections of this chapter develop expressions for the Hall voltage produced in the base region of the floating SSIMT (see Fig. 4.1) and the collector current response of the SSIMT, if emitter modulation is assumed to be the dominant mechanism. In the last two sections of the chapter an experimental analysis of the role of emitter modulation is presented.

6.1 Injection modulation effect

For simplicity, in this section, our analysis will focus on the device operation with the substrate disconnected. The basic electrical operation is as presented in chapter 4 for the SSIMT with floating stripes. Electrons are injected from the emitter into the base region of the device and then flow laterally to the collectors. An applied magnetic field parallel to the chip surface will cause an imbalance in the two collector currents.

6.1.1 Hall voltage generation

As shown in section 3.2 the Hall voltage produced in the base region of the SSIMT (Fig. 4-1) can be approximated by

$$V_H = K R_H I_E B_x \tag{6.1}$$

where I_E is the emitter current, R_H is the Hall coefficient and B_x the applied magnetic field. K is a geometric factor which will be a function of both the geometry and operating conditions of the device. As with the single collector LMT analyzed in section 3.2 it is difficult to evaluate K due to the complicated geometry of the base region of the device. The Hall voltage can be expected to directly relate to the emitter current, the applied field and the Hall coefficient.The Hall coefficient is defined [14] as

$$R_H = \frac{r}{q}\left(\frac{p - nb^2}{(p + nb)^2}\right) \tag{6.2}$$

and will be a strong function of the injection carrier concentrations in the base region of the device [34].The Hall voltage produced along the emitter/base junction will therefore be a function of the magnitude of the minority current density injected into the base.

In order to express R_H as a function of the injection level in the base we introduce the parameter α defined as the ratio of n over p. At low injection $\alpha \approx 0$ as n is much smaller then p which in turn is equal to the p-well doping, N_A. At higher injection levels n will approach p in magnitude and α will approach 1. Using the quasi-neutral equation for the base region, $p + N_A = n + N_D$ and $\alpha = n/p$, One can obtain that, $p = N_A/(1-\alpha)$ for the case of $N_A >> N_D$. This enables us to express R_H as a function of α

$$R_H = \frac{r(1-\alpha)}{qN_a}\left(\frac{1-\alpha b^2}{(1+\alpha b)^2}\right) \qquad (6.3)$$

A plot of this function is shown in Fig. 6-2. Values of 1.1 and 3 were used for r and b respectively [35,36]. An examination of Fig. 6-2 shows the presence of a critical $\alpha_c = 1/b^2$. Beyond α_c the Hall coefficient is negative. We can identify three distinctive regions of injection: low injection ($\alpha \approx 0$), high injection with $\alpha < \alpha_c$ and high injection for which $\alpha > \alpha_c$. Under low injection ($n << p$) we have $\alpha \approx 0$ and $R_H = r/qN_A$. For these conditions the device is in the normal forward biased operating mode and therefore I_E is a linear function of I_B, related by the DC gain β, and we can write equation (3.21) in the form of

$$V_H = K R_H (1+\beta) I_B B_x \qquad (6.4)$$

If β is constant, which is usually the case at low level injection, then V_H is an increasing function of the biasing current I_B. As the injection level is increased n will approach p in magnitude and α will approach α_c. Taking the value of β as approximately equal to 3 [3] we can calculate that for n and p at the critical injection level α_c the values of $1/8N_A$ and $9/8N_A$ respectively. These values indicate a high level of injection and we can no longer assume a linear variation of V_H with I_B. Namely, it is known that the current gain of a lateral transistor decreases due to high injection effects [37]. Therefore an exact expression for the Hall voltage is unattainable. However, we can predict the general trend of V_H as a function of I_B. As I_B increases, a high injection level will be reached, the current gain of the transistor decreases, and the magnitude of R_H will fall. These two effects counteract the consequences of increasing I_B. We can therefore expect a slow moderation and then dropping off of V_H towards zero with increasing base current. If the injection level is increased beyond α_c the Hall coefficient will switch sign and become negative, and of course V_H will also be negative. At the limit of very high injection levels $n \approx p$, $\alpha \approx 1$ and the Hall coefficient is still negative as will be the Hall voltage.

The net result is that V_H linearly increases with I_B at low injection. As the injection level increases the Hall voltage will saturate, then start to drop eventually passing zero and changing sign at extremely high injection conditions.

6.1.2 Collector currents response

For the simple case of two collectors with a disconnected substrate we can, given that a Hall voltage is produced in the base region near the emitter, derive the variation in the collector currents due to the injection modulation effect. According to Vinal and Masnari [30], the Hall potential along the emitter junction will be a function

of position. With a magnetic field as applied in Fig. 4-1, this potential will be a monotonically increasing function, (Fig. 6-2). We assume that this function is symmetrical with respect to the center of the emitter. Differing from previous authors, whose results imply the assumption of a step function for V_H [34], we assume a linear variation of the Hall potential. Physically this is a more reasonable approximation, see Fig. 6-2.

The collector current flowing to the right collector can then be represented as

$$I_{C2}=\int_0^{L_E/2} J_S e^{\frac{V+V_H(y)}{mV_t}} W_E dy \qquad (6.5)$$

where J_S is the saturation current density, V_t is the thermal voltage, V is the base emitter voltage under zero magnetic field, $V_H(y)$ is the Hall potential along the base emitter junction as a function of position, and m is an empirical constant. If we define V_{H21} as $V_{H21}=V_{H2}-V_{H1}$, we can express the collector current as

$$I_{C2}=J_S W_E \frac{mV}{V_{H21}} \frac{L_E}{2} e^{\frac{V}{mV_t}}\left(e^{\frac{V_{H21}}{mV_t}}-1\right) \qquad (6.6)$$

Defining the collector current I_{C20} for zero magnetic field

$$I_{C20}=J_S W_E \frac{L_E}{2} e^{\frac{V}{mV_t}} \qquad (6.7)$$

and the injection modulation coefficient

$$K_{MI} = V_{H21} / 2mV_t \tag{6.8}$$

we obtain for that

$$I_{C2} = I_{C20} \frac{e^{K_{MI}} - 1}{K_{MI}} \tag{6.9}$$

In a similar fashion we can obtain that

$$I_{C1} = I_{C10} \frac{1 - e^{-K_{MI}}}{K_{MI}} \tag{6.10}$$

These two equations differ in form from equations derived by previous authors [30,34] due to our use of a linearly varying Hall potential. As with previous derivations, the collector currents exhibit an exponential variation with the Hall voltage but in in addition there is an added nonlinearity due to the collector currents being inversely proportional to the hall voltage. Using the two equations (6.9) and (6.10) and assuming $I_{C20} = I_{C10} = I_{C0}/2$, from symmetry we can calculate the current difference $\Delta I_C = I_{C2} - I_{C1}$

$$\Delta I_C = I_{C0} \frac{\cosh(K_{MI}) - 1}{K_{MI}} \tag{6.11}$$

This equation indicates that the magnetic response of the device due to the injection modulation effect will be nonlinear with respect to the magnetic field. The relative sensitivity of the device is then

$$S_r = \frac{\cosh(K_{MI}) - 1}{K_{MI}} \frac{1}{B_x} \qquad (6.12)$$

6.2 Experimental results

The theory in chapter 4 and the analysis of the results in chapter 5 presumed the dominance of carrier deflection as an operating mechanism over the emitter modulation effect. The SSIMT structure allows us to analyze the relative roles of the two mechanisms by means of the Hall voltage produced on the stripes when the SSIMT is operated with the stripes floating [6].

In order to analyze the relative importance of the injection modulation described above, 5 sets of devices were use. Each set having a different emitter length varying from 20 μm to 100 μm. Our purpose was to investigate the Hall voltage V_H produced along the emitter base junction as function of the biasing conditions and the emitter geometry. The p^+ stripes placed at both edges of the emitter parallel to the collectors allow for the detection of the base potential near the emitter edge.

The devices were operated in a common emitter configuration, a constant base current I_B was supplied to the base contact, B_1, the collector voltages were 5 V. The p^+ stripes were unbiased and the potentials at the points V_{H1} and V_{H2} were measured using a high impedance voltmeter.

To determine the effect of isolating the devices, by the reverse biasing of the p-well, on the Hall voltage two bias configurations were used. In the first configuration a simple two collector transistor configuration was used and for this case the substrate was disconnected. In the second configuration the substrate was connected

to a 5 V constant voltage source. Under these conditions the substrate is effectively a third collector.

6.2.1 Hall Voltage

In Fig. 6-3 we present typical results for the variation $V_{H21} = V_{H2} - V_{H1}$ of the measured Hall voltage at an applied magnetic field of 500 mT as a function of I_B for both bias configurations, (100 μm device). At low injection there is a steep rise in V_{H21} as I_B increases, which is in agreement with equation (6.4). As the injection level is further increased this rise is moderated (as discussed in section 6.1) by a decrease in R_H and the current gain. The configuration with the substrate connected produces a higher Hall voltage at low and medium injection levels. This can be attributed to a higher current gain measured in this configuration. However, at high injection levels there would appear to be a larger degradation in current gain causing V_H to drop below that of the simple configuration. For neither configuration was the injection level high enough to cause a sign change of V_H.

The variation of the Hall voltage as a function of B for the 100 μm device, for both configurations is shown in Fig. 6-4. It can be seen that the variation is a linear and symmetric function of B which is in agreement with equation (6.4). The configuration with the substrate connected exhibits a larger Hall voltage due to a larger current gain.

The geometric dependance of V_H is shown in Fig. 6-5. The Hall voltage was measured with a field of 500 mT at a base current of 5 mA. It is interesting to note that both configurations exhibited a maximum in the Hall voltage at an L_E of 80 μm. The drop of V_H as L_E increased from 80 μm to 100 μm could be explained by a variation in the geometric constant K in equation (6.1). Emitter crowding effects will become more

significant as the emitter length increases, causing a change in the distribution of electron flow in the base.

6.2.2 Collector current response

The main impetus for these measurements was to determine the relative importance of the injection modulation effect on the magnetic response of the collector currents. Equation (6.11) was used in order to provide a comparison between the actual change in the collector currents and that due to injection modulation. The value for the Hall voltage was obtained from Fig. 6-4 and the parameter I_{C0} obtained experimentally. If injection modulation is the dominant mechanism of magnetic operation the values of ΔI_C determined experimentally should follow the theoretical curves.

Typical results are shown in Fig. 6-6. The curves designated IM1 and IM2 are the result of equation (6.11) for the two bias configurations. In order to obtain these plots the values of 6.6 mA and 7.7 mA were used respectively. The DC operating point chosen was I_B = 5 mA so as to be in the region where V_H is maximal (Fig. 6-6). As can be seen from Fig. 6-6 the actual change in current is substantially larger then the prediction of equation (6.11) for both configurations. The current change is larger then in theory by an order of magnitude and shows a linear variation with the applied magnetic field. These results would seem to strongly indicate that the magnetic operation of the SSIMT is dominated by carrier deflection.

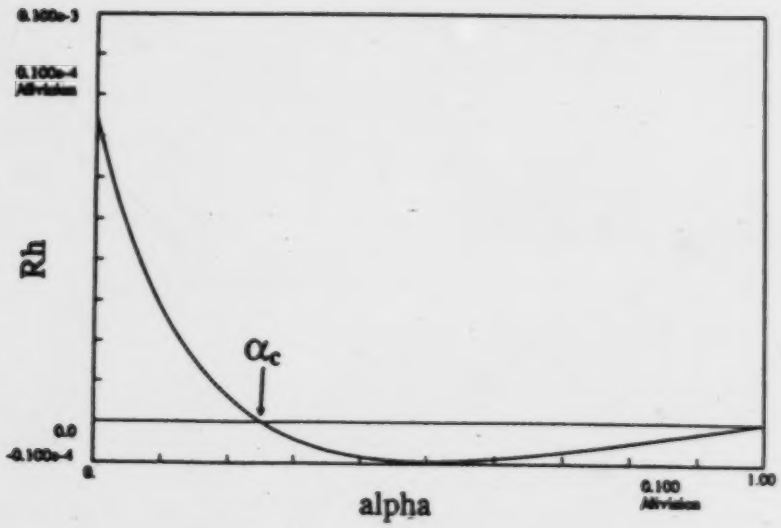

Fig. 6-1 R_H as a function of the injection level, b=3, $N_A = 10^{16}\,cm^{-3}$, r = 1.2.

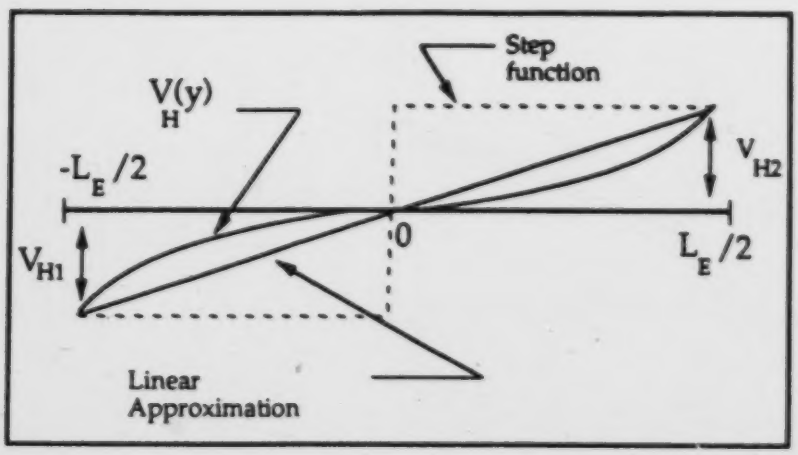

Fig. 6-2 Hall voltage distribution along emitter/base junction

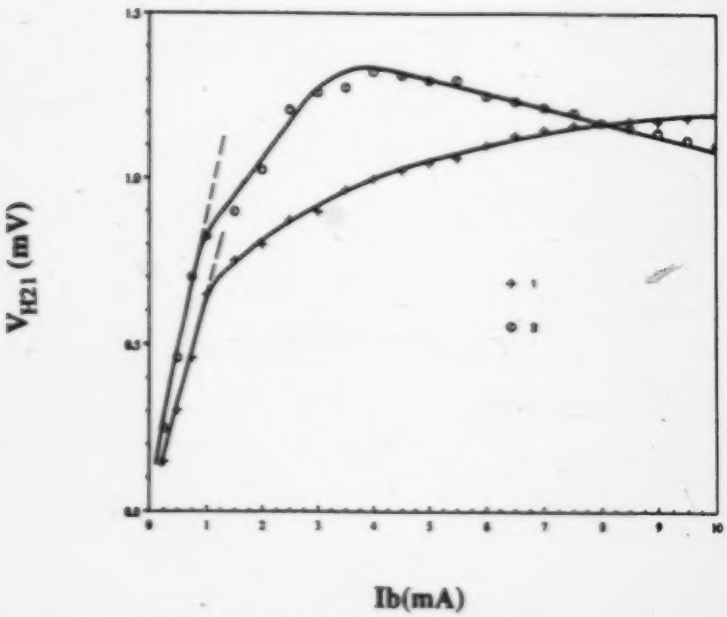

Fig. 6-3 Hall voltage versus applied base current at a magnetic field of 500 mT, L_E = 100 µm, 1) substrate disconnected, 2) V_S = 5 V.

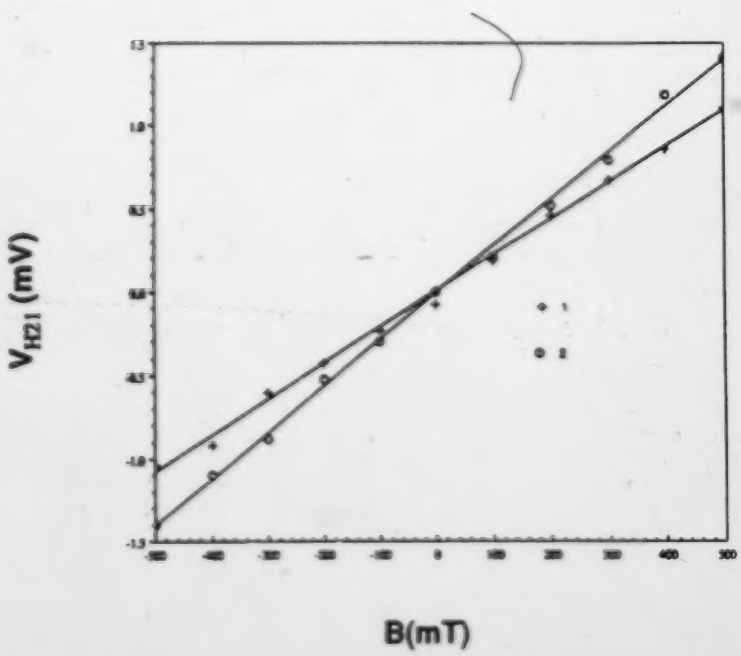

Fig. 6-4 Hall voltage versus magnetic field, I_B = 5 mA, L_E = 100 µm, 1) substrate disconnected, 2) V_S = 5 V.

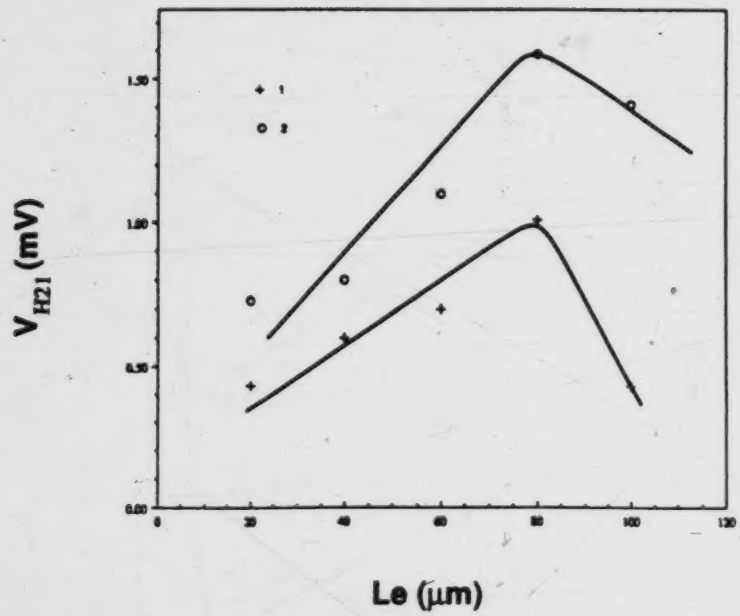

Fig. 6-5 Hall voltage versus emitter length I_B = 5 mA, B = 500 mT, 1) substrate disconnected, 2) V_S = 5 V.

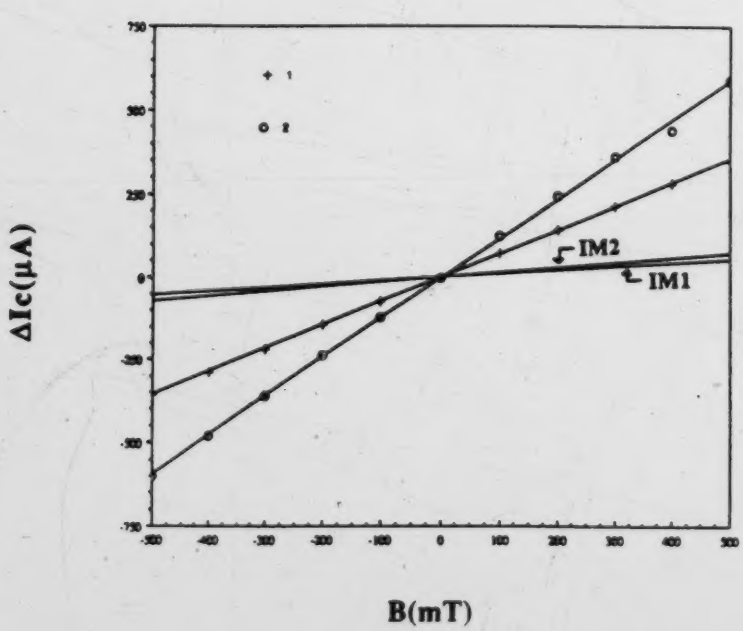

Fig. 6-6 ΔI_C as a function of B, I_B = 5 mA, L_E = 100 μm, 1) substrate disconnected, 2) V_S = 5 V. IM1 and IM2 correspond to equation 3.29 for conditions 1) and 2) respectivly

7.0 Conclusion

The aim of the work behind this thesis was to both provide a good analytical model of SSIMT operation and to provide a thorough experimental characterization of the SSIMT under a wide variety of operating conditions. The device model was outlined in chapters 4 and the basic aspects of the model confirmed by the experimental results presented in chapter 5. Experimentally a wide variety of devices were investigated over their full range of operation, with both electrical and magnetic characteristics being reported.

The structure of the SSIMT enabled a comprehensive study of the operating mechanisms of the device and particular emphasis was placed on the relative roles of carrier deflection and emitter modulation. The effect of the p^+ stripes was determined for two bias conditions (stripes biased and stripes floating) and compared to a simple device with no stripes. The stripes were found to increase both the absolute and relative sensitivities. Biasing the stripes slightly negative, with respect to the emitter was found to amplify the fundamental effects of the stripes and further increase the sensitivity.

The operation of the SSIMT with stripes biased is very complex. A distinctive aspect of SSIMT operation was the presence of critical bias conditions delineating the presence of two different modes of operation. In the first mode the lateral transistor is effectively turned off and acts as a simple resistor with no transistor action present. However, at the critical bias conditions the device dramatically turns on and both the lateral and vertical transistors become active.

The operation of the device under normal conditions was modeled in chapter 4. The device operation was assumed to be dominated by carrier deflection of the minority carriers in the base. The minority flow in the base was analyzed. The effect of the stripes was proposed to be a concentration of the electron flow within the device resulting in a "beam" of electron current flowing laterally to the collectors. The deflection of this flow was assumed to be the result of the Lorentz force deflection of the electrons. The sensitivity of the SSIMT was found to be determined by the effective width of this electron "beam" and the approximate variation of the width of this beam with variable bias conditions was determined. The variation of the sensitivity was then calculated with respect to the bias conditions and compared to experiment in chapter 5.

The SSIMT exhibited very large sensitivities, larger than any previously reported for a magnetotransistor with a linear response to the magnetic field. The geometrical variations of the SSIMT indicated that large sensitivities are obtained for devices with smaller emitter geometries.

Maximum sensitivities were obtained at the critical bias conditions at which the SSIMT just turned on. Very high sensitivities could be obtained for all the SSIMTs by using the stripes to balance the collector currents and then lowering the base current to just above the critical base current at which the device turns off. The largest maximum sensitivities were measured for the devices with the smallest emitters and values in the order of 5000 %/T and 100 μA/mT were measured for the relative and absolute sensitivities respectively. Also presented in chapter 5 were results pertaining to the control of the zero field offset through the use of different stripe potentials. A minimum zero field offset equivalent to a magnetic field of the order of 200 μT was shown to be obtainable

In chapter 6 experimental measurements were presented which, when incorporated into a theoretical structure of the emitter injection effect, indicate the dominance of carrier deflection as the mechanism of magnetic operation of the SSIMT. These results justify the primary assumption of the models in chapter 4.

The results presented in this work suggest that the SSIMT is a promising device. The high sensitivities of the SSIMT, and the use of standard CMOS, prompted an attempt to use it in an application previously performed by small coils. This application involved the measurement of a 200 Hz magnetic field of the order of 100 mG. The SSIMT performed as well as expected under these conditions and research into the use of the SSIMT is still being undertaken. There would appear to be a considerable number of practical applications for a small, inexpensive, mass-produced magnetic sensor and the SSIMT would appear to be a strong contender for this role.

To achieve this role a number of characteristics need further investigation For example, the noise characteristics of the device need to be characterized with respect to both geometry and bias. The determination of the noise correlation between the collector currents will be important in determining the minimum resolvable AC magnetic field. Results presented in chapter 5 indicate that the emitter geometry is important in the operation of the device and further study into this would be constructive. The spatial response of the device as a function of geometry is of considerable practical interest as well as the AC magnetic response of the SSIMT. A study of the temperature characteristics of the collector currents and the turn on point of the device will need to be done. Finally, a study of the reliability of the device and uniformity of different device samples will have to be undertaken.

References

[1] H.P. Baltes and R.S. Popovic, "Integrated Semiconductor Magnetic Field Sensors," Proc. IEEE, vol. 74, pp. 1107-1132, 1986.

[2] S. Kordic, "Integrated Circuit Magnetic Field Sensor," Sensors and Actuators, vol. 10, pp.347, 1986.

[3] W.G. Wolber and K.D. Wise, "Sensor development in the microcomputer age", IEEE Trans. Electron Devices, vol. ED-26, pp. 1864-1874, 1979.

[4] T. Smy, Lj. Ristic and H. Baltes, "An analytical model of a new magnetotransistor: the SSIMT" IEDM Tech. Digest, , Dec. 1987

[5] Lj. Ristic, T. Smy and H.P. Baltes, "A lateral magneto-transistor structure with a linear response to the magnetic field", IEEE Trans. Electron Devices, vol. ED-36, p. 1076, 1989.

[6] T. Smy and Lj. Ristic, "On the injection modulation effect", Sensors and Materials, vol. 1, p. 18, 1989.

[7] G. Bosch, "A Hall Device in an Integrated Circuit," Solid State Electron., vol.22, pp.712-714, 1968.

[8] R.S. Popovic, " The Vertical Hall Effect Device," IEEE Electron Device Lett., vol. EDL-5, pp. 357-358, 1984.

[9] E.I. Karakushan and V.I. Stafeev, "Magnetodiodes," Sov. Phys.-Solid State, vol. 3, p. 493, 1961.

[10] R.S. Popovic, "A MOS Hall Effect Device Free From Short -Circuit Effect," Sensors and Actuators, vol. 5, pp. 253-262, 1984.

[11] R.S. Hemmert, "Invariance of the Hall Effect MOSFET to Gate Geometry," Solid State Electron., vol. 17,pp. 1039-1043, 1974.

[12] V. Zieren and B. P. M. Duyndam, "Magnetic-Field-Sensitive Multicollector N-P-N Transistors," IEEE Trans. Electron Devices, vol. ED-19, pp. 83-90, 1982.

[13] A. W. Vinal and N. A. Masnari, "Magnetic Transistor Behaviour Explained by Modulation of Emitter Injection, Not Carrier Deflection," IEEE Electron Device Lett., vol. EDL-3, pp. 203-205, 1982.

[14] S. M. Sze, Physics of Semiconductor Devices, 2nd ed. New York, NY: Wiley, 1981.

[15] H. H. Wieder, Hall Generators and Magnetoresistors. London, England: Pion Ltd., 1971.

[16] P. W. Fry and S. J. Hoey, "A Silicon MOS Magnetic Field Transducer of High Sensitivity," IEEE Trans. Electron Devices, vol. ED-16, pp. 35-39, 1969.

[17] J. L. Berchier and R. S. Popovic, "Sensitivity of the Vertical-Hall Effect Device," presented at the 14th European Solid-State Device Research Conf. ESSDERC '84, Lille, France, 1984, also in Europhysics Conf Abstracts, vol. 8F, pp. 265-266, 1984.

[18] R. S. Hemmert, "Invariance of the Hall Effect MOSFET to Gate Geometry," Solid-State Electron., vol. 17, pp. 1039-1043, 1974.

[19] A. Yagi and S. Sato, "Magnetic and Electrical Properties of N-Channel MOS Hall-Effect Device," Jap. J. Appl. Phys., vol. 15, pp. 655-661, 1976.

[20] S. Takamiya and K. Fujikawa, "Differential Amplification Magnetic Sensors," IEEE Trans. Electron Devices, vol. ED-19, pp. 1085-1090, 1972.

[21] H. Suhl and W. Shockley, "Concentrating holes and electrons by magnetic fields", letter to the editor, Phys. Rev, July 1962

[22] I.M. Mitnikova, T.V. Persiyanov, G.I. Relakova and G. Shtyubner, "Investigation of the characteristics of silicon lateral magnetotransistors with two measuring collectors," Sov. Phys. - Semicond., vol. 12, pp. 26-28, 1978.

[23] O. S. Lutes, P. S. Nussbaum, and O. S. Aadland, "Sensitivity Limits in SOS Magnetodiodes," IEEE Trans. Electron Devices, vol. ED-27, pp. 2156-2157, 1980.

[24] R. S. Popovic, H. P. Baltes, and F. Rudolf, " An Integrated Silicon Magnetic Field Sensor Using the Magnetodiode Principle," IEEE Trans. Electron Devices, vol. ED-31, pp. 286-291, 1984.

[25] R. S. Popovic and R. Widmer, "Magneto-Transistor in CMOS Technology," IEEE Trans. Electron Devices, vol. ED-33, 1986.

[26] L. W. Davies and M. S. Wells, "Magneto Transistor Incorporated in a Bipolar IC," in Proc. ICMCST (Sidney, Australia, 1970) pp. 34-35.

[27] J. I. Goicolea, R. S. Muller, and J. E. Smith, "Highly Sensitive Silicon Carrier Domain Magnetometer," Sensors and Actuators, vol. 5, pp. 147-167, 1984.

[28] L. Halbo and J. Haraldsen, "The Magnetic Field Sensitive Transistor: A New Sensor for Crankshaft Angle Position," Trans. ASE, vol. 89, p. 701, 1981.

[29] R. S Popovic and H. P. Baltes, " Dual-collector magneto-transistors optimized with respect to injection modulation", Sensors and Actuators, vol. 4, p. 155, 1983.

[30] A. W. Vinal and N. A. Masnari, "Bipolar Magnetic Sensors," in IEDM Tech. Dig., pp. 308-311, Dec. 1982.

[31] A. W. Vinal and N. A. Masnari, "Operating Principles of Bipolar Transistor Magnetic Sensors," IEEE Trans. Electron Devices, vol. ED-31, pp. 1486-1494, 1984.

[32] V. Zieren, S. Kordic, and S. Middelhoek, "Comment on 'magnetic transistor behaviour explained by modulation of emitter injection, not carrier deflection'," IEEE Electron Device Lett., vol. EDL-3, pp. 394-395, 1982.

[33] A. W. Vinal and N. A. Masnari, "Response to "Comment on 'Magnetic Transistor Behavior Explained by Modulation of Emitter Injection, not Carrier Deflection'," IEEE Electron Device Lett., vol. EDL-3, pp. 396-397, 1982.

[34] R. S. Popovic, and H.P. Baltes, "An investigation of the sensitivity of lateral transistors", IEEE Electron Dev. Lett, vol. EDL-4, pp. 51-53, 1983.

[35] J. F. Lin, S. S. Li, L. Linares and K. W. Teng, :Theoretical Analysis of Hall Factor and Hall Mobility in P-Type Silicon," Solid State Electronics, vol. 24, p. 827, 1981.

[36] A. S. Grove, Physics and Technology of Semiconductor Devices, New York: Wiley, 1967.

[37] S. Chou, "An Investigation of Lateral Transistors - DC Characteristics," Solid-State Electronics, vol. 14, p. 811, 1971.

[38] A. M. J. Huiser and H. P. Baltes, "Numerical Modelling of Vertical Hall-Effect Devices," IEEE Electron. Device Lett., vol. EDL-5, pp. 482-484, 1984.

[39] A. Nathan, W. Allegretto, H. P. Baltes, and Y. Sugiyama, "Numerical Modelling of Hall Devices for Nonuniform Magnetic Induction," in Proc. 6th Sensor Symp., 1986, S. Kataoka Ed. [Toyko, Japan, Inst. Elect. Eng of Japan].

[40] W. Allegretto, A. Nathan and H.P. Baltes, "Two-dimensional numerical analysisof silicon bipolar magnetotransistors", Proc. NASECODE V Conf, June 17-19, J.J.H Miller, Ed., pp. 87-92, 1987.

[41] A. Nathan, W. Allegretto, W.B. Joerg and H.P. Baltes, "Numerical modeling of bipolar magnetotransistors", Tech. Dig. Transducer's 87, Tokyo, June 2-5, 1987.

[42] R.S. Popovic and R. Widmar, "Sensitivity and noise of a lateral magnetotransistor in CMOS technology", IEDM 1984, Tech. Dig., IEEE, pp. 568-571, 1984.

[43] M.J. Buckingham, Noise in Electronic Devices and Systems, Ellis Horward LTD., Chichester, Eng.and, 1983.

[44] D.R. Briglio, Characterisation of CMOS Magnetic Field Sensors, M.Sc. Thesis, University of Alberta, Canada, 1988.

[45] G. Bjorklund, "Improved Design of Hall Plates for IC's," IEEE Trans. on Electron Devices, vol. ED-25, p.541, 1978.

[46] Y. Kanda and M. Migitoka, "Effect of the Mechanical Stress on the Offset Voltages of Hall Devices in Si," Phys. Stat. Sol. [a], vol. 35, p. K115, 1981.

[47] R. J. Braun et al., "FET Hall Transducers With Control Gates," IBM Techn. Discl. Bull., vol. 17, p. 7, 1979.

[48] J. T. Maupin and M. L. Gaske, "The Hall Effect in Silicon Circuits," The Hall Effect and its Applications, ed. C. L. Chien and C. R. Westgate, New York: Plenum, p.241, 1980.

[49] S. Kordic, V. Zieren, and S. Middelhoek, "A Magnetic-Field-Sensitive Multicollector Transistor with Low Offset," IEDM Techn. Dig., p. 631, Washington, DC, 1983.

[50] S. Kordic and P. C. M. Van Der Jagt, "Theory and Practice of Electronic Implementation of the Sensistivity-Variation Offset-Reduction Method," Sensors and Actuators, vol. 8, p. 197, 1985.

[51] P.L. Hower and W.G. Einthoven, " Emitter current-crowding in High voltage Transistors", IEEE Trans. Elec. Dev., Vol ED-25, p. 465, 1978

[52] H.C.Poon, H.K. Gummel and D.L. Sharfetter, "High injection in Epitaxial transistors", IEEE Trans. Elec. Dev., Vol ED-16, p. 455, 1969

[53] G.C. Ebner and P.E. Gray, " Static V-I relationships in transistors at high injection levels", IEEE Trans. Elec. Dev., Vol ED-13, p. 692, 1966

[54] Lj. Ristic, T. Smy, H.P. Baltes and I. Filanovsky, "A highly sensitive magnetic field sensor based on magnetotransistor action with suppressed sidewall injection", in Proc. Yugoslav Conf. Microelectronics(Banja Luc, May 13-15, 1987), p.25.

[55] Lj. Ristic, T. Smy, H.P. Baltes and I. Filanovsky, "Suppressed sidewall injection magnetotransistor in CMOS technology", in Dig. Transducers '87 4th Int. Conf. Solid-State sensors .

[56] Lj. Ristic, T. Smy, H.P. Baltes and I. Filanovsky, "Suppresed Sidewall injection magnetotransistor with focused emitter injection and double deflection", IEEE Elec. Dev. Lett., vol EDL-8, p. 395, 1987.

[57] Lj. Ristic, T. Smy and H.P. Baltes, "A magnetotransistor with offset elimination", Sensors and Materials, vol. 1, no. 2, p. 83, 1988.